


1-1-2005

Effect of DNA Base Modification on Polymerase Chain Reaction Efficiency and Fidelity

Jan A. Sikorsky
jsikorsky@lead-america.org

Follow this and additional works at: <http://mds.marshall.edu/etd>

 Part of the [Biological Phenomena, Cell Phenomena, and Immunity Commons](#), [Medical Cell Biology Commons](#), [Medical Genetics Commons](#), and the [Medical Microbiology Commons](#)

Recommended Citation

Sikorsky, Jan A., "Effect of DNA Base Modification on Polymerase Chain Reaction Efficiency and Fidelity" (2005). *Theses, Dissertations and Capstones*. Paper 179.

**EFFECT OF DNA BASE MODIFICATION ON
POLYMERASE CHAIN REACTION
EFFICIENCY AND FIDELITY**

by

Jan A. Sikorsky

**Dissertation submitted to
the Graduate College
of
Marshall University
in partial fulfillment of the requirements
for the degree of**

**Doctor of Philosophy
in
Biomedical Sciences**

Approved by

**Terry W. Fenger, Ph.D., Committee Chairperson
Elizabeth C. Bryda, Ph.D.
Donald A. Primerano, Ph.D.
Vernon E. Reichenbecher, Ph.D.
Jeffrey D. Wells, Ph.D.**

Microbiology, Immunology, and Molecular Genetics

ABSTRACT

EFFECT OF DNA BASE MODIFICATION ON POLYMERASE CHAIN REACTION EFFICIENCY AND FIDELITY

by Jan A. Sikorsky

Polymerase stop assays, used to quantify DNA damage, assume single lesions are sufficient to block thermostable DNA polymerase progression. To explore this assumption, 90 base oligonucleotides containing normal or modified DNA bases were amplified using real-time PCR. Data implied that the PCR efficiency was influenced to differing degrees depending on which base lesion was present on the input oligonucleotide; specifically, while reactions with templates containing a single 8-oxo-7,8-dihydro-2'-deoxyguanosine (8-oxodG) were not noticeably altered, the presence of a single 8-oxo-7,8-dihydro-2'-deoxyadenosine, an abasic site, or a *cis-syn* thymidine dimer (TT dimer) dramatically delayed amplification. In addition, the presence of two tandem 8-oxodGs substantially hindered amplification when compared with two 8-oxodGs separated by 13 bases which indicated that the position of lesions also influenced the PCR. To quantify variations in amplification, novel mathematical formulae were developed which report differences in exponential amplification as rates of damage bypass. These treatments assume each template in the PCR is damaged to the same degree. Quantification of damage to cellular DNA, which is a mixture of damaged and undamaged template, required further refinement of real-time PCR mathematics; differences in amplification were defined in terms of damage probability (*lesion frequency*) rather than lesion bypass rate. The validity of these formulae was determined using DNA samples quantified previously using current polymerase stop methods. In addition to impacting reaction efficiency, DNA base modifications decreased reaction fidelity. In reactions with templates containing 8-oxodGs, both the normal Watson/Crick association with dCMP as well as the incorporation of dAMP occurred at the lesion site. Despite similar structural characteristics, the existence of 8-oxodA resulted in a pronounced n-1 deletion in addition to the normal association with dTMP. Sequence data from abasic and TT dimer modifications were inconclusive but suggested the presence of multiple nucleotide incorporation events opposite the modifications. The present work enabled the adaptation of real-time PCR for DNA damage quantification, identified DNA base lesions as potential PCR mutagens, and provides the basis for further refinement of polymerase stop assays as research and clinical tools to monitor DNA damage and repair.

DEDICATION

I would like to dedicate this dissertation to my wife: Julie Conover Sikorsky.

Your love, faith, patience, and understanding provided me the strength to overcome the numerous hurdles involved in an undertaking of this magnitude. Without you, I could have never come this far.

Know that this compilation and my love are forever yours.

ACKNOWLEDGMENTS

This project was supported by Grant No. 2001-RC-CX-K002 awarded by the National Institute of Justice, Office of Justice Programs, US Department of Justice. Points of view in this document are those of the author and do not necessarily represent the official position or policies of the US Department of Justice.

I would like to thank my parents, Richard and Theodora Sikorsky, for providing me the building blocks with which to work and develop the critical thought necessary to thrive in a scientific research setting.

I would like to thank the members of the Department of Microbiology, Immunology, and Molecular Genetics for their constant support as both friends and colleagues.

I would like to thank the members of my committee, Drs. Bryda, Fenger, Fet, Primerano, Reichenbecher, and Wells, for being patient with the development of my scientific mind and for their guidance throughout the course of this research project.

Special thanks needs to go to Dr. Terry W. Fenger for his support from both financial and intellectual standpoints. Thank you for believing in me and for providing me with the creative freedom necessary to complete a non-traditional project such as this.

Finally, special recognition needs to be given to Drs. Donald A. Primerano and James Denvir; my collaborators, mentors, and friends. Without your guidance, your patience, and your willingness to expand your responsibilities to include our work, I would have never completed this undertaking.

Thank you all from the bottom of my heart.

TABLE OF CONTENTS

ABSTRACT	ii
DEDICATION	iii
ACKNOWLEDGMENTS	iv
LIST OF FIGURES	vi
LIST OF TABLES	viii
LIST OF SYMBOLS/NOMENCLATURE	x
CHAPTER I	1
INTRODUCTION.....	1
CHAPTER II	4
REVIEW OF LITERATURE.....	4
DNA DAMAGE.....	4
DNA POLYMERASES AND TRANSLESION SYNTHESIS.....	18
MONITORING DNA DAMAGE AND REPAIR.....	24
MODELING THE POLYMERASE CHAIN REACTION IN REAL-TIME.....	27
SUMMARY.....	31
CHAPTER III	32
MATERIALS AND METHODS.....	32
CHAPTER IV	56
RESULTS.....	56
QUANTIFICATION OF DNA DAMAGE.....	56
CHARACTERIZATION OF LESION INDUCED PCR MUTATION.....	98
CHAPTER V	108
SUMMARY AND CONCLUSIONS.....	108
QUANTIFICATION OF DNA DAMAGE.....	108
LESION INDUCED PCR MUTATION.....	118
FUTURE DIRECTIONS.....	120
BIBLIOGRAPHY	122
APPENDIX A	136
PCR PRIMERS.....	136
APPENDIX B	137
AMPLICON SIZE IMPACTS CYCLE THRESHOLD VALUE.....	137
APPENDIX C	138
DISSOCIATION CURVES AND PRODUCT GELS FROM LONG TEMPLATES.....	138
APPENDIX D	140
SIMULATED LESION BYPASS AND LESION FREQUENCY CALCULATIONS.....	140
APPENDIX E	142
SIMULTANEOUS CALCULATION OF LESION FREQUENCY AND RATE OF BYPASS.....	142
APPENDIX F	145
CURRICULUM VITAE.....	145

FIGURES

FIGURE 2.1.	DNA base lesions.	9
FIGURE 2.2.	Formation of 8-oxodG.	9
FIGURE 2.3.	Base pairing of 8-oxodG.	11
FIGURE 2.4.	Multiple factors influence polymerase fidelity.	20
FIGURE 2.5.	Mechanism of nucleotide insertion.	21
FIGURE 2.6.	Fragment analysis of DNA from electron beam irradiated envelopes	25
FIGURE 2.7.	Exponential modeling of real-time PCR.	28
FIGURE 2.8.	Early reaction cycles influence template quantification.	29
FIGURE 3.1.	Purified 90-mer oligonucleotides	35
FIGURE 3.2.	Failure products from 90-mer oligonucleotide synthesis	35
FIGURE 3.3.	Maldi-TOF analyses of 90-mers	36
FIGURE 3.4.	Amplification of mitochondrial DNA by primer walking.	44
FIGURE 4.1.	Model of oligonucleotide amplification.	56
FIGURE 4.2.	Polyacrylamide gel electrophoresis of 90-mer oligonucleotides.	57
FIGURE 4.3.	Auto-sequencing of 90-mer oligonucleotides.	58
FIGURE 4.4.	Product gels from PCRs with 90-mer oligonucleotides templates.	59
FIGURE 4.5.	Product formation is delayed in PCRs with tandem 8-oxodGs.	60
FIGURE 4.6.	Amplification of unmodified Oxo CONTROL oligonucleotide in real-time.	61
FIGURE 4.7.	Amplification of oligonucleotides containing modified bases.	62
FIGURE 4.8.	Amplification of oligonucleotides containing a <i>cis-syn</i> thymidine dimer modification.	63
FIGURE 4.9.	Predicted secondary structures of 90-mer Oxo CONTROL oligonucleotide sequence.	67
FIGURE 4.10.	Predicted secondary structures of 90-mer Dimer CONTROL oligonucleotide sequence.	67
FIGURE 4.11.	Kinetic analysis of raw PCR data.	80
FIGURE 4.12.	Real-time PCR raw data fit to a logistic curve.	82

FIGURE 4.13.	RTC efficiencies from PCRs using AmpliTaq Gold and Restorase.....	85
FIGURE 4.14.	Creation of long templates containing controlled DNA base modification.....	87
FIGURE 4.15.	Amplification of mitochondrial DNA by primer walking.....	89
FIGURE 4.16.	Dissociation curves of PCR products from modified oligonucleotides.....	99
FIGURE 4.17.	Sequence analysis of PCR product from Oxo CONTROL oligonucleotide.	100
FIGURE 4.18.	Sequence analysis of PCR product from oligonucleotides containing 8-oxodG base modifications.	101
FIGURE 4.19.	Sequence analysis of PCR product from oligonucleotides containing 8-oxodA and abasic base modifications.	102
FIGURE 4.20.	Sequence analysis of PCR product from oligonucleotides containing a <i>cis-syn</i> Thymine-Thymine dimer.....	103
FIGURE 4.21.	Sequence analysis of PCR product from modified oligonucleotides amplified by Restorase DNA polymerase.....	106
FIGURE 5.1.	Observed PCR curves from modified and unmodified templates..	109
FIGURE 5.2.	DNA base lesions create a delay in early exponential phase.	110
FIGURE 5.3.	Different base modifications affect amplification to different degrees.....	112
FIGURE 5.4.	The positioning of multiple 8-oxodGs relative to one another alters modified reaction efficiency.	114
FIGURE 5.5.	Mutations opposite 8-oxodA lesions are reduced with Restorase.....	119
FIGURE D.1.	Product gel of long templates PCRs.....	138
FIGURE D.2.	Dissociation profiles of long PCR products.....	139

TABLES

TABLE 3.1.	90-mer oligonucleotides used as templates for the PCR.....	34
TABLE 4.1.	Relative input template amounts from ICR amplification data.	64
TABLE 4.2.	Relative input template amounts from 90-mer amplification data.	65
TABLE 4.3.	RTC amplification efficiencies of templates with non-adjacent lesions.	69
TABLE 4.4.	RTC amplification efficiencies of templates with adjacent lesions.	70
TABLE 4.5.	RTC amplification efficiencies of templates with <i>cis-syn</i> TT dimers.....	71
TABLE 4.6.	PCR efficiencies from oligonucleotide templates.....	72
TABLE 4.7.	Input template fluorescence.	73
TABLE 4.8.	Mean modified efficiencies of templates with non-adjacent lesions.	75
TABLE 4.9.	Mean modified efficiencies of templates with adjacent lesions. ..	76
TABLE 4.10.	Mean modified efficiencies of templates with <i>cis-syn</i> TT dimers.	77
TABLE 4.11.	Inherent template efficiencies.	78
TABLE 4.12.	Comparison between $2^{-\Delta CT}$ and curve-fit calculations.	81
TABLE 4.13.	Curve-fit calculations from reactions with differing primer amounts.	83
TABLE 4.14.	RTC efficiencies from PCRs with Restorase DNA polymerase...	85
TABLE 4.15.	Mean modified efficiencies from long templates.	88
TABLE 4.16.	Input template fluorescence at different amplicon sizes.....	90
TABLE 4.17.	Mean modified efficiencies from UV irradiated DNA.	92
TABLE 4.18.	Lesion frequencies from UV irradiated DNA.	93
TABLE 4.19.	Lesion frequencies calculated using real-time QPCR.....	96
TABLE 4.20.	Influence of lesion bypass (E_D) on lesion frequency (p) estimation.....	97
TABLE 4.21.	Summary of PCR derived mutation as a result of lesion bypass.	104
TABLE 4.22.	Restorase lesion bypass products.....	107

TABLE B.1.	Oligonucleotide primer sequences.	136
TABLE C.1.	Amplicon sizes and threshold cycle values.	137

SYMBOLS / NOMENCLATURE

8-oxodA- 8-oxo-7,8-dihydro-2' deoxyadenosine

8-oxodG- 8-oxo-7,8-dihydro-2' deoxyguanosine

BER- base excision repair

bp- base pair

C_T - threshold cycle

CuZnSOD- copper-zinc superoxide dismutase

dA- 2' deoxyadenosine

dC- 2' deoxycytosine

dH₂O- deionized water

dG- 2' deoxyguanosine

DNA- deoxyribonucleic acid

dNMP- deoxynucleoside monophosphate

dNTP- deoxynucleoside triphosphate

ds- double stranded

dT- 2' deoxythymidine

E.coli- *Escherichia coli*

EDTA- ethylenediaminetetraacetic acid

Exo⁻- exonuclease deficient

H₂O₂- hydrogen peroxide

H⁺- hydrogen ion

hr- hour

kb- kilo base

LBR- lesion bypass rate

LF- lesion frequency

LIM- lesion induced mutagenesis

min- minute

MnSOD- manganese superoxide dismutase

NADP⁺- oxidized nicotinamide adenine dinucleotide phosphate

NADPH- reduced nicotinamide adenine dinucleotide phosphate

NER- nucleotide excision repair

O₂- diatomic oxygen
O₂^{*} - superoxide radical
OH^{*}-hydroxyl radical
OPC- oligonucleotide purification column
PCR- polymerase chain reaction
pol- polymerase
QPCR- quantitative polymerase chain reaction
ROS- reactive oxygen species
s- second
ss- single stranded
Taq- Thermus aquaticus
TBE- tris-borate-EDTA
TE- tris-EDTA
TLS- translesion synthesis
TT Dimer- *cis-syn* thymine-thymine dimer
UV- ultraviolet

CHAPTER I

1.1. Introduction

DNA in living cells can be damaged by chemical and physical processes. Biological defenses such as the superoxide dismutase, catalase, and peroxidase enzyme families protect against these hazardous insults (1). DNA modifications alter base pairing properties between complementary sequences along the length of dsDNA and can lead to substitution mutations (2). Inherited defects, reducing the efficiency of DNA base lesion repair, confer susceptibility to certain cancers and developmental disorders (3). Together, these observations suggest that DNA damage is a preliminary step in carcinogenesis. In addition, DNA base modifications may play a role in the aging process (4). Assays for DNA damage are therefore needed for experimental monitoring of DNA repair pathways and clinical diagnosis of DNA repair defects (5).

1.2. Purpose of the Research

The objective of this dissertation is to characterize the influences of specific DNA base modification on *Thermus aquaticus* (*Taq*) DNA polymerase progression and fidelity during the polymerase chain reaction (PCR) and to design methods to quantify damage to DNA. Previous work demonstrates that aggregate amounts of DNA damage can be detected using radiolabeling and long extension PCR protocols (5-11). The purpose of the work presented here is 1) to determine if fluorescent detection in real-time can be used to advance existing PCR based methods for detecting DNA damage; 2) to experimentally validate the current assumption that all lesions block thermostable DNA polymerase progression; 3) to characterize the mutational spectrum of defined DNA base lesion bypass by *Taq* DNA polymerase; and 4) to adapt real-time PCR mathematics to define observed changes in amplification between samples as differences in amounts of damage to DNA.

1.3. Significance of the Research

Novel mathematical treatments and protocols were developed permitting the use of real-time PCR as a method to quantify damage to synthetic and cellular DNA templates. The real-time PCR method presented here has the potential to act as a screen for DNA damage in a clinical setting and could be used to further diagnose late-onset diseases that cause or are caused by accumulated damage to DNA.

In addition, as stated in *Free Radicals in Biology and Medicine*: “An important question, to which little attention has been given, is the effect of DNA base damage on the behavior of *Taq* DNA polymerase, especially as PCR is being increasingly used to amplify DNA isolated from preserved or fossilized organisms (ancient DNA) (12).” Since its advent in the mid 1980s, PCR has revolutionized clinical and basic science research, allowing large amounts of DNA to be copied from small inputs (13). As the limits of the PCR are pushed in disciplines such as ancient DNA study and forensic science, where degraded and modified DNA is encountered, the need to ensure the accuracy of collected data becomes imperative. Through the use of synthetic DNA as PCR template, a model is provided here with which the influences of specific base lesions on *Taq* polymerase fidelity can be tested. Four common DNA damage products were found to impact nucleotide insertion and extension kinetics during the PCR. Because of this demonstration of base modification induced PCR mutagenesis, sequence data from damaged DNA samples should be interpreted with increased caution.

1.4. Organization of the Dissertation

Emphasis is placed on characterizing the rate of lesion bypass, the calculation of lesion frequencies in cellular DNA, and the impact of DNA base lesions on the fidelity of the PCR. An overview of this work, including the purpose and significance to the scientific community, can be found in Chapter I. Relevant literature on oxidative and ultraviolet stresses, types of DNA damage and their subsequent repair, real-time PCR including the mathematical basis for the calculation of template abundance, and the use of the quantitative polymerase chain reaction (QPCR) to estimate DNA damage, which allowed the formulation of hypotheses, experiments, and subsequent conclusions

presented within, is described in Chapter II. Chapter III describes the development of real-time PCR assays for the quantification of lesion bypass rate (LBR) in synthetic DNA and the calculation of lesion frequency (LF) in cellular DNA, and a complete description of methods used in the characterization of lesion induced mutagenesis (LIM). Chapter IV illustrates the LBRs of four common DNA base lesions, the LIM from each, and the validation of real-time polymerase stop assays for use in LF within ultraviolet irradiated DNA. A summary of the work, including a discussion of the author's conclusions drawn from the data and their potential significance to the scientific community are presented in chapter V. The appendices contain a complete table of oligonucleotide primer sequences used throughout these experiments, a comparison of PCR product sizes and their impact on SYBR Green dye incorporation and threshold cycle values, a discussion of dissociation curve profiles of long amplicons and how different regions on a unique template can produce multiple peaks during melt curve analysis, the derivation of formulae to simultaneously calculate lesion frequency and lesion bypass rates, and the author's curriculum vitae.

CHAPTER II

REVIEW OF THE LITERATURE

2.1. DNA Damage

‘DNA damage’ is defined by the National Library of Medicine (NLM) as drug- or radiation-induced injuries in DNA that introduce deviations from its normal double-helical conformation. These changes include structural distortions which interfere with replication and transcription, as well as point mutations which disrupt base pairs and exert damaging effects on future generations through changes in DNA sequence (14). DNA itself is very stable; without the introduction of outside influence, the DNA molecule undergoes minimal change (12).

DNA bases are altered by exogenous and endogenous insults. For example, reactive oxygen species (ROS) can interact with 2'-deoxyguanosine to form 8-oxo-7,8-dihydro-2'-deoxyguanosine (8-oxodG) or with 2'-deoxyadenosine to form 8-oxo-7,8-dihydro-2'-deoxyadenosine (8-oxodA) (2, 15-17). Regardless of the reactive species, repair systems are in place to prevent assault on nucleic acid and eliminate altered DNA if damage occurs (1). These defenses are not perfect; damage products are found in most biological systems. For example low levels of ROS-induced damage products are present in DNA extracted from aerobic cells (12). *In vivo* evidence for the removal, and therefore the presence, of oxidative DNA damage products exists in humans, as 8-oxodG is excreted in urine and can be used as a marker for monitoring oxidative stress and subsequent repair within cellular DNA (3). 8-oxodG and other modified bases have altered base pairing properties which can lead to substitution mutations (18). Defects in DNA repair confer susceptibility to certain cancers and developmental disorders (3, 19-20). In addition, due to an accumulation of DNA damage products in aging populations, the build up of DNA damage has been implicated as a component in the aging process (4,

21-28). In 1956, Denham Harman proposed the free-radical theory of aging which states that normal aging results from random deleterious damage to tissues by free radicals (29-30). Since Harman's seminal work, a large body of knowledge has accumulated which implicates these damaging events as a unifying link between many of the theories of aging.

The following sections provide a comprehensive review of literature pertaining to DNA damage with an emphasis placed on work influencing the experiments presented in subsequent chapters.

2.1.1. Oxidative stress

Oxidative stress is defined as “a disturbance in the pro- and antioxidant balance in favor of the former, leading to potential cellular damage” (12, 31). Given that definition, it is natural to assume that stress would be caused by either an increase in the production of oxidants or a reduction in antioxidants. Increased oxidant production can result from elevated O₂ levels (12), the prevalence of toxins, such as those in cigarette smoke that are metabolized to form reactive agents (free radicals) (12), or the elevated induction of natural defenses, such as phagocytes, whose function is to generate radicals to protect against pathogenic invasion but may ultimately lead to diseases such as rheumatoid arthritis (12). Depletion of antioxidant defense enzymes such as copper-zinc superoxide dismutase (CuZnSOD), manganese superoxide dismutase (MnSOD), and peroxidases by genetic mutation or exogenous factors tip the balance in favor of oxidative stress (12). In addition, depletion of dietary antioxidants may play a role in the increase of oxidative stress and damage (12).

2.1.1.1. Biologically significant free radicals

In order to discuss oxidative stress, it is important to define the underlying cause of the damage associated with elevated stress levels: the free radical. Halliwell *et al.* (1999) define the ‘free radical’ in simple terms: “a free radical is any species capable of independent existence that contains one or more unpaired electrons (12).” Although the majority of this discussion will concentrate on oxygen-derived radical species, free

radicals can be generated from a wide variety of sources. Some examples of non-oxygen derived radical species are thiyl, sulphur-centered, chlorine, carbon-centered, and nitrogen radicals (12). In addition, many transition-metals (12), such as iron, can qualify as free radicals under the broad definition provided above.

Radicals generated with oxygen as their center (oxygen free radicals) include superoxide (O_2^*) and the hydroxyl radical (OH^*). The superoxide radical is formed when a single electron is added to ground-state oxygen (12). The chemical formation of the hydroxyl radical is more complicated and can be a product of numerous reactions; Fenton chemistry, a reaction catalyzed by transition metals, and homolytic bond fission of H_2O_2 or H_2O induced by ultraviolet or gamma radiation respectively, are two examples (12).

2.1.1.2. Endogenous production of superoxide radicals

Some biologically important reactions rely on the production of superoxide; others generate superoxide as an unfortunate byproduct. During bacterial phagocytosis, NADPH is oxidized producing $NADP^+$, H^+ , and two O_2^{*-} molecules in an activated enzyme complex on the plasma membrane (32). This process is triggered when a foreign body encounters a phagocyte, becomes wrapped up in the plasma membrane, and is engulfed into the phagocyte cytoplasm where it is in close proximity to superoxide production. It is unlikely, given the low reactivity of O_2^* in aqueous solution (12), that bacterial killing is a result of direct exposure to superoxide. Given that intra-vacuolar pH rises in human neutrophils following bacterial phagocytosis (33), the dismutation of superoxide to H_2O_2 may occur which can readily cross cell membranes and may be converted to the highly reactive OH^* (12). Certain strains of bacteria are killed by exposure to hydrogen peroxide which may, in fact, be an underlying mechanism involved in phagocytosis (12).

The mitochondrial electron transport chain is a large producer of O_2^{*-} *in vivo*. It is estimated that, under normal conditions, as much as 3% of the total O_2 reduced in the mitochondria forms O_2^{*-} (34). This superoxide production is directly related to oxygen concentration. Mammalian cytochrome oxidase becomes O_2 saturated at low O_2 tensions, presumably at which point the prior complexes in the electron transport chain

stall, allowing electron leakage to occur which can then associate directly with O₂ forming superoxide (34). While the overall hypothesis that superoxide is produced as a byproduct of electron transport is generally accepted, the precise point at which this occurs in the transport chain is hotly debated. Evidence implicates *b*-type cytochromes, parts of complex I and coenzyme Q, as producers of O₂^{*-} (34). Other reports implicate complex III (ubiquinol cytochrome c reductase) in addition to complex I (NADH dehydrogenase) as a major source of electron transport-derived reactive oxygen species (35).

2.1.1.3. Antioxidant defenses

In order to adapt and survive in an oxygen rich environment, aerobes have evolved antioxidant defense mechanisms. Antioxidant defenses can be broken down into categories such as defense enzymes (e.g. superoxide dismutases), low-molecular mass agents (e.g. ascorbic acid), and agents that sequester potentially harmful metal ions (e.g. iron metabolism); all having the common goal to protect against free radical formation (36-38).

2.1.1.4. Biological consequences of free radical production

The presence of lipid peroxidation, carbonyl and amino acid modification, and oxidative base damage products in DNA isolated from aerobic cells suggests that antioxidant defense systems are not 100% efficient (2, 12, 15-17, 39-40). The primary target of oxygen radical insult on a cell depends on the type of cell and the type and amount of radical assault. For example, when H₂O₂ is administered to mammalian cells grown in culture, DNA strand breakage occurs prior to any detectable lipid peroxidation or protein modification (41-42). This is in contrast to compounds like carbon tetrachloride whose primary cellular target is lipid peroxidation (43-45). Regardless of the source or target, a cell enduring oxidative stress can adapt to or be killed by radical insult.

Adaptation can involve the up-regulation of antioxidant defense mechanisms in an attempt to overcome the increased oxidative stress. For example, *E. coli* can be

preconditioned to endure high levels of H₂O₂ (46). If *E. coli* cells are gradually exposed to low levels of H₂O₂, they become resistant and can survive when exposed to levels that are lethal to normal cells. Genetic adaptation can occur at the transcriptional level; decreased transcription of cytochrome p450 results from the exposure of isolated hepatocytes to elevated oxidative stress levels (47).

The ultimate consequence if adaptation to stress does not happen is that ATP production in cells decreases below a critical threshold and the cells die either by apoptosis or necrosis (12, 48). The mechanism by which a cell expires depends largely on the type and amount of radical inducer; millimolar levels of H₂O₂ exposure causes cells to swell and rupture (death by necrosis) whereas lower levels trigger the apoptotic cascade (49).

2.1.1.4.1. Oxidative DNA damage

Reactive oxygen species can damage DNA through direct and indirect mechanisms. The direct mechanisms by which ROS damage DNA are a primary focus, but it is worth mentioning that ROS insults can influence DNA indirectly by such means as interrupting enzymes responsible for DNA replication or DNA repair (2). Some examples of direct damage to DNA by ROS are strand breakage, hydroxyl addition, and the opening of the imidazole ring (2). Superoxide by itself, at physiologically relevant levels, does not appear to directly react with either DNA bases or the deoxyribose sugars (50). If, however, the hydroxyl radical is formed in close proximity to DNA, a multitude of products result (Figure 2.1; (2, 50)). The most studied of these damage products, 8-oxodG, is formed when a hydroxyl group is added to C-8 on the purine ring of guanine (forming the C-8 OH-adduct radical) and the intermediate compound is reduced (Figure 2.2; (50)). Hydroxyl additions are not limited to guanine. If the OH^{*} attacks adenine, it may add to the C-8 and undergo reductions to form 8-oxodA (2). Pyrimidine bases are also attacked by the hydroxyl radical forming additional base modifications (2).

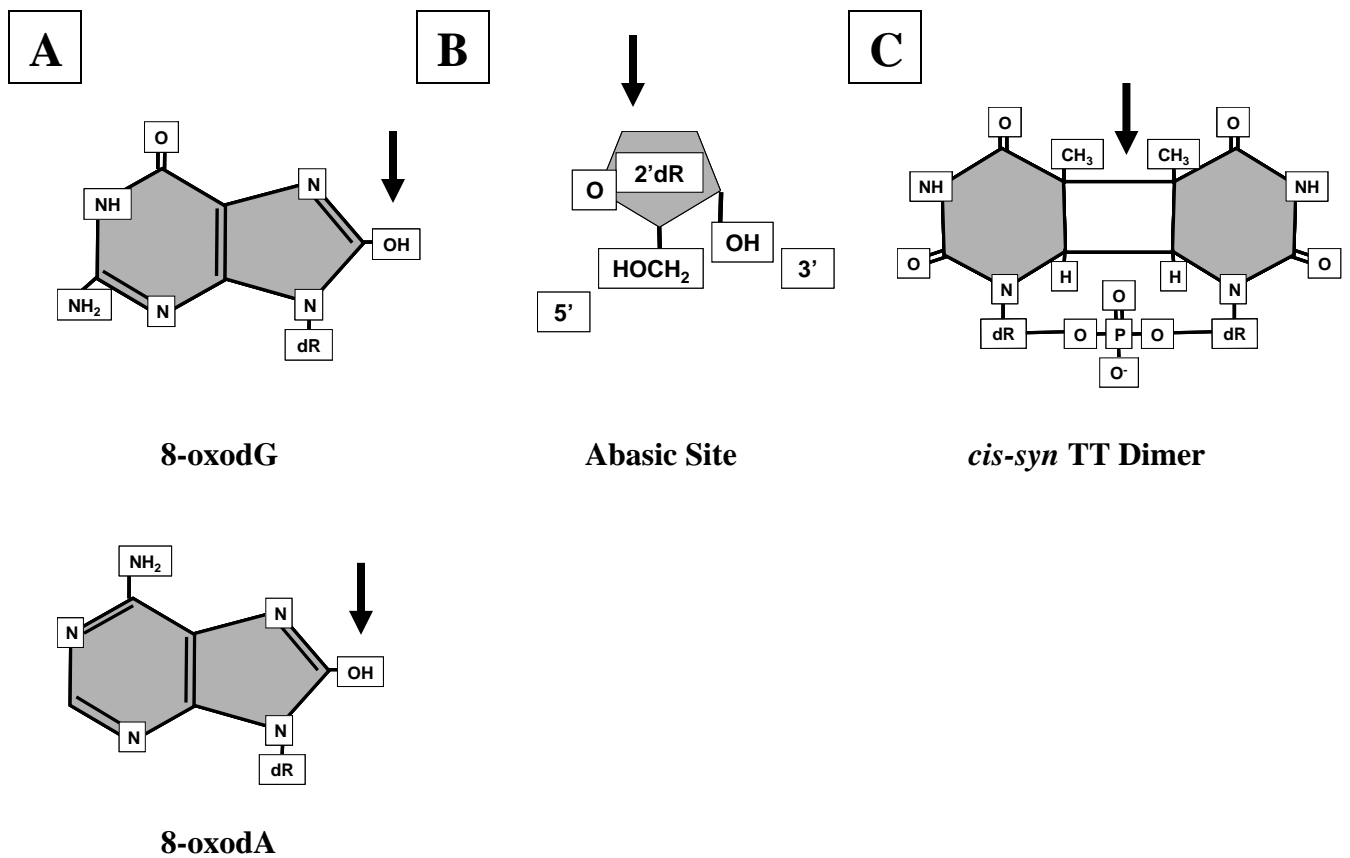


Figure 2.1 DNA base lesions. Lesions occur on DNA resulting from A) direct exposure to increased oxidative stress (adapted from Wang *et al.* (1998) (15)), B) spontaneous base loss or base removal by DNA glycosylase (adapted from Takeshita *et al.* (1987) (51)), or C) direct exposure to ultraviolet light (adapted from Taylor *et al.* (1990) (52)). dR represents deoxyribose. Arrows in panels A and B indicate addition of hydroxyls on the C-8 of each purine; in panel C, arrow points to the lack of DNA base; in panel C, arrow highlights crosslinking between adjacent thymidine bases.

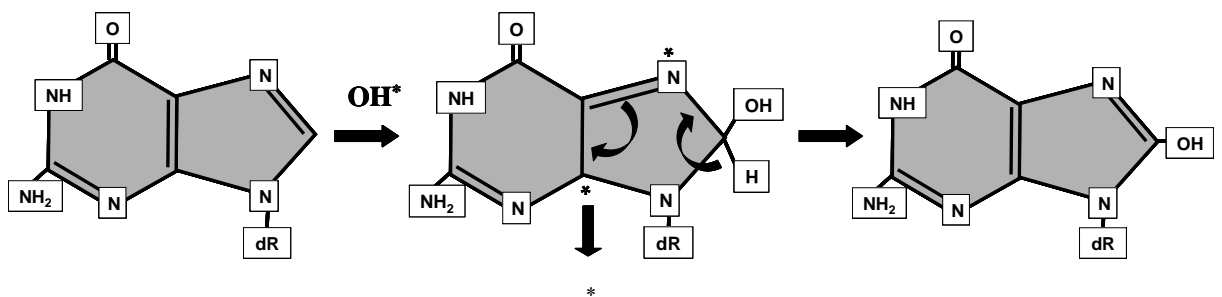


Figure 2.2 Formation of 8-oxodG. The exposure of deoxyguanine to hydroxyl radicals generates an intermediate radical (8-hydroxyguanine radical) which can either be oxidized to form 8-oxodG or reduced to create an open-ringed product (FAPyG; not shown; adapted from Breen *et al.* (1995) (50)). dR represents deoxyribose; (*) represent free electrons.

2.1.1.4.2. 8-oxo-7,8-dihydro-2'-deoxyguanosine

8-oxo-7,8-dihydro-2'-deoxyguanine (8-oxodG; Figure 2.1A) is formed by hydroxylating deoxyguanosine residues by direct oxidative stress (53-54), ionizing radiation (55), and through exposure to numerous agents that indirectly elevate ROS levels (56-57). This DNA base lesion is found at levels ranging from 10-250 molecules per 10^6 guanines in some mammalian tissues (58) and is largely regarded as the most abundant product of oxidative DNA damage (54, 59-60). *In vitro* studies suggest that 8-oxodG is pre-mutagenic; the lesion does not absolutely block polymerase progression and increased the likelihood of mutation during lesion bypass (18). 8-oxodG primarily exists as a 6,8-diketo tautomer (15) which can assume either a *syn* or *anti*-orientation when found in duplex DNA; this orientation dictates its base pairing partner (Figure 2.3; (59-62)). When paired with 2'-deoxycytosine, 8-oxodG takes on the *anti* configuration creating a normal Watson-Crick base pair (61-62); in the *syn* form, Hoogsteen pairing is permitted and 2'-deoxyadenosine is inserted opposite the lesion creating a guanine to thymine transversion event during the next round of DNA replication (59-60). The ratio of dAMP/dCMP insertion is dependent on which DNA polymerase is used; with replicative polymerases preferring dAMP while DNA repair polymerases favoring dCMP incorporation (17). In studies testing the extension of both 8-oxodG:dA and 8-oxodG:dC base pairs by *E. coli* Pol I and Pol II (both exonuclease deficient (*exo⁻*)), 8-oxodG:dA was preferentially extended by both polymerases while 8-oxodG:dC extension was impaired (63). The extension of this seemingly mismatched base pair is in part due to its geometric similarity in structure to the correct Watson-Crick A:T pair (60-62). The situation becomes more complex in a mammalian system; the addition of proliferating cell nuclear antigen (PCNA), a functional accessory protein in the replication complex acting to hold the polymerase to the DNA transcript, increases the amount of extended product beyond 8-oxodG 2.5-fold when compared with studies involving mammalian pol δ alone (64-65).

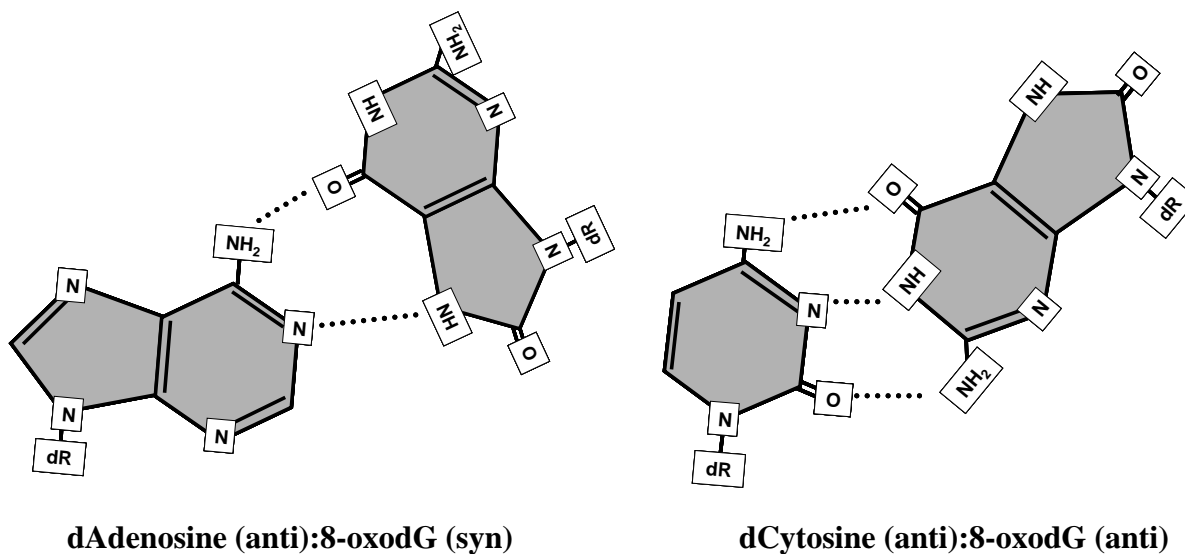


Figure 2.3 Base pairing of 8-oxodG. dR represents deoxyribose sugar. 2'-deoxyadenosine or 2'-deoxycytosine can pair with 8-oxodG. This differential base pairing is dictated by the orientation of the modified base relative to its deoxyribose sugar (adapted from Wang *et al.* (1998) (14)).

2.1.1.4.3. 8-oxo-7,8-dihydro-2'-adenosine

The adenine analog of 8-oxodG, 8-oxo-7,8-dihydro-2'-adenosine (8-oxodA), is formed by the exposure of adenine moieties to ionizing radiation resulting in the hydroxylation of the C-8 position through direct insult by hydroxyl radicals (Figure 2.1A; 66-67). Shibutani *et al.* (1993) used oligonucleotides, modified site-specifically with 8-oxodA, as templates in primer extension reactions to test the insertion and extension kinetics of DNA pol I (exo⁻), DNA pol α , and DNA pol β (68). While the authors do find that singular dGMPs could bind to 8-oxodA providing the potential for mutagenesis, in the presence of all four dNTPs at equimolar concentrations, the polymerases tested exclusively incorporate dTMP across from the lesion (68). *Taq* DNA polymerase also selectively incorporates dTMP opposite 8-oxodA (67).

More recent studies involving *E. coli* pol I (exo⁻), *Taq* DNA polymerase, rat DNA pol α and pol β conflict with the Shibutani findings. While the two bacterial polymerases still exclusively incorporated dTMP opposite 8-oxodA, mammalian polymerase α

misinserted dGMP and pol β misinserted both dAMP and dGMP (69). The reasons for these discrepancies in data are not known but the authors suggest that they may, in part, be due to differences in template sequences which have been shown to impact nucleotide insertion kinetics in studies involving other lesions (69, 70).

2.1.1.4.4. Abasic sites

Abasic sites consist of a 2'-deoxyribose moiety linked by 3' and 5' phosphodiester bonds to neighboring nucleotides (Figure 2.1B; (51)). These sites are formed by hydrolyzing the glycosidic bond connecting either purine or pyrimidine bases to the deoxyribose sugar (71). Abasic sites occur as a result of specific DNA glycosylase removal of damaged bases or the labilization of glycosidic bonds resulting from chemical modification of a DNA base (71). In addition, abasic sites can form as a result of spontaneous DNA base loss (72). Abasic sites severely hinder polymerase progression but do not completely block replication. The progression of both *E. coli pol I (exo⁻)* and calf thymus DNA pol α polymerases is stalled at the position immediately 3' to the abasic site; dNMPs are subsequently incorporated with dAMP being the nucleotide predominantly extended (51, 72). The mutational spectrum of abasic lesion bypass in eukaryotes is more complex. During replication of plasmid vectors inserted into simian kidney cells which contained an abasic site, dAMP, dCMP, and dTMP incorporate opposite the lesion site with similar frequencies (74-77). In studies concentrating on the mutational spectra of abasic lesion bypass by the recently identified Y family of DNA polymerases (reviewed below), n-1 deletions and n+1 insertions occur in addition to the base substitutions mentioned above (78).

Randall *et al.* (1987) report nearest-neighbor influences where base stacking interactions manipulate nucleotide insertion kinetics opposite an abasic site (71). Despite this early report, little is mentioned of these types of influences in later studies.

2.1.2. Ultraviolet radiation

The impacts of ultraviolet (UV) radiation on human health have been considered for more than 200 years. The first documented report of “melanoma” occurred in Europe

around the year 1800. The incidence of melanoma is on the rise; increasing approximately 3-7% yearly in Caucasian populations (79). Howe *et al.* (2001) report that, in the United States of America, the risk of developing malignant melanoma is 1 in 90 with a mortality rate of 1 in 400 (79). Melanomas arise from abnormal transformation of melanocytes as a result of both environmental (80-82) and genetic factors (83-84).

The most significant portion of sunlight contributing to an increase in the propensity for certain cancers is ultraviolet radiation (85). UV light lies in the wavelength range of 200-400 nm and can be divided into UVA (320-400 nm), UVB (280-320 nm), and UVC (200-280 nm) regions (85). UVC is blocked by the earth's ozone layer and, therefore, is assumed not to influence cancer prevalence (85). UVA is the largest component of ultraviolet radiation to which humans are exposed; the impact of UVA on skin cancer development is poorly documented and highly controversial (85). Exposure to UVB wavelengths, on the other hand, is largely associated with sunburn and an increased risk of skin cancer development. Damage associated with UVB results from the absorption of light by nucleic acids and proteins; both of which peak in the UVB range at 260 and 280 nm respectively (85).

2.1.2.1. Biological consequences of exposure to ultraviolet radiation

The majority of cellular responses to UV exposure stem from damage to DNA (reviewed below). UV damage events trigger a wide array of cellular processes; most are mediated by p53 (85). These include cell cycle arrest, DNA repair, and p53-dependent apoptotic pathways. Due to increased levels of the pro-survival protein Bcl-2, cells may proliferate despite excessive damage to DNA (85). If left unchecked, this aberrant proliferation can result in the formation of malignant melanoma.

2.1.2.2. Ultraviolet DNA damage

The two major populations of DNA lesions resulting from direct UVB exposure are cyclobutane (or pyrimidine) dimers and 6-4 photoproducts (85). 6-4 photoproducts are formed between the 5' sixth position and 3' fourth position of two adjacent pyrimidines; pyrimidine dimers are formed when bonding occurs between the number

four and five carbon atoms on any two adjacent pyrimidines (85). Dimers are considered to be more carcinogenic in part due to their abundance (86), an inefficiency of lesion removal mechanisms (86), and the observation that dimers permit translesion synthesis by certain replicative polymerases (87).

Transitions from doublet cytosines (CC) to doublet thymine (TT) bases represent the hallmark of UVB induced mutagenesis (88-91). Cytosine to adenine and guanine to thymine transversions, as well as DNA strand breaks, have also been documented resulting from UVB insult (88-91). Like UVB, UVA wavelengths can mutate DNA but in an indirect fashion. UVA radiation is absorbed by non-DNA molecules that generate ROS (56, 92). The resulting radicals can then lead to oxidative stress induced mutation as described above.

Cellular systems have adopted ways of combating UV induced DNA damage; these include the reversal of damage by photolyase, the removal of lesions through nucleotide excision repair (reviewed below), and the evolution of translesion polymerases such as eukaryotic DNA polymerase η (pol η) whose function appears to be the bypass of bulky lesions that stall high fidelity replicative polymerases (reviewed below; 93).

2.1.2.1.1. cis-syn Thymine-Thymine dimers

One of the major photoproducts produced when DNA is exposed to UV radiation, the *cis-syn* thymine-thymine dimer (Figure 2.1C; TT dimer), results from the cycloaddition of a 5,6-double bond between two adjacent thymine bases in DNA (52). Pyrimidine dimers alter DNA structure; bending DNA by 7-9° and unwinding it as much as 15° (94-96). This bending and unwinding inhibits transcription factor binding and may perturb gene regulation (97).

The mutagenicity of TT dimers, like other UV-induced photoproducts, is dependent upon which polymerase is responsible for replicating past the lesion. For example, Moloney murine leukemia virus reverse transcriptase (MMLV-RT) and *Vent* DNA polymerase (exo⁻) cannot bypass any UV DNA photoproducts, *Taq* DNA polymerase inefficiently passes *cis-syn* dimers, and Sequenase 2.0 (exo⁻; U.S.

Biochemical Corp., Cleveland, OH) is not stopped completely by any UV induced lesion (87).

2.1.3. DNA repair mechanisms

To combat mutagenesis, organisms have evolved complex mechanisms to remove damaged and mismatched bases. Repair mechanisms can be divided into several general categories: direct repair, excision repair, mismatch repair, tolerance systems, and retrieval systems (98). Direct repair involves the reversal/removal of damage; the best example of this is photoreactivation of pyrimidine dimers (98). Excision repair is more complex, involving the recognition of damaged bases, excision of the DNA sequence including the damage, and synthesis of the removed sequence effectively eliminating the altered base (98). Mismatch repair is responsible for removing mispaired bases resulting from incorrect base incorporation during replication, the creation of hybrid DNA during recombination, and base conversion (98). Tolerance repair occurs when replication is blocked at a damaged site and the system is forced to proceed by reducing polymerase fidelity (98). Retrieval systems are a specialized version of tolerance repair which recruit DNA recombination machinery to obtain an undamaged copy of the nucleotide sequence from another source (98).

2.1.3.1. Base excision repair and the removal of oxidative DNA damage

Excision repair can be further sub-divided into base excision repair (BER), where the damaged bases are the only bases to be removed, and nucleotide excision repair (NER), where the damage is eliminated along with a number of flanking nucleotides. NER is primarily responsible for removing bulk adducts like those resulting from UV exposure ((1, 99); discussed below). BER, on the other hand, plays an integral part in removing lesions resulting from oxidative stress (1, 100).

Base excision repair of oxidative DNA damage begins as damaged bases are recognized and removed by DNA glycosylases. In order to remove the damaged base, the N-glycoside bond between the base and sugar moiety is hydrolyzed. Next, the apurinic/aprimidinic site is recognized and a lyase either clips the 3' phosphodiester

linkage (β -elimination) or both the 3' and 5' phosphodiester bonds (β,δ -elimination). The resulting 3' phosphate is cleaved leaving an exposed hydroxyl residue. Then the gap is filled by DNA polymerase action and the remaining nick sealed by a DNA ligase (100).

8-oxodG is the most widely studied oxidative base lesion and therefore the most information is known about its removal by BER from DNA. First studied in *E. coli*, the removal of 8-oxodG requires three integral enzymes: MutM, MutY, and MutT. MutM functions as a glycosylase/lyase, removing the lesion from 8-oxodG/cytosine base pairs (101). MutY is a glycosylase responsible for removing adenine from adenine/8-oxodG mispairs (102). Base removal results in an abasic site and the cleavage of the phosphodiester bond (102-103). Strand synthesis is performed by DNA pol I completing repair of the damaged base (104). MutT is a triphosphatase enzyme that cleanses the nucleotide pool removing 8-oxodG as a substrate for DNA replication (105-107). Homologs for each protein exist in humans and are designated hOGG1/hMMH (108-109), hMYH (110), and MTH1 (111).

2.1.3.2. Nucleotide excision repair and the removal of ultraviolet DNA damage

A wide variety of bulky, DNA distorting lesions, such as those generated when DNA is exposed to UV radiation, are repaired through NER processes. Distortions in the double helix, brought about by the presence of these lesions, are recognized by a protein complex (XPC-hHR23B in humans (100); UVrABC in *E. coli* (112)) marking the initiation of NER. A series of proteins are recruited and an open complex formation is adopted (100). The DNA is unwound by inherent helicase activity and the damaged site verified in this open formation. Endonucleases cut 3' and 5' of the damaged site and the damaged section of DNA is excised. A DNA polymerase synthesizes the missing genetic information using the opposite DNA strand as a template; a DNA ligase then seals the nick completing the 'patch repair' (100).

2.1.4. Summary

The presence and removal of DNA base lesions in cellular DNA is well established. The accumulation of these DNA damage products increases in aging populations; this build up of damage has been implicated as a causative component in many cancerous phenotypes. Further rationale for these hypotheses is presented in the following sections as modified DNA impacts replication kinetics.

2.2. DNA Polymerases and Translesion Synthesis

Replicative DNA polymerases (replicases) are thought to maintain a high degree of fidelity due to strict intolerance toward distortions in DNA shape (113-114). Originally attributed solely to hydrogen bonding stringencies, observations that difluorotoluene, an analog of thymine incapable of forming hydrogen bonds, correctly incorporates opposite adenine during strand synthesis suggests other factors must impact nucleotide insertion (113, 115). Differences in the melting temperatures of copolymers (ATAT), in comparison with their respective homopolymer (AAAA or TTTT), implicates sequence specific base stacking interactions as one such factor (113).

The Klenow fragment of *E. coli* DNA polymerase I was the first polymerase structure to be determined (116). Analogous to a right hand, the polymerase has finger, palm, and thumb sub-domains (116).

2.2.1. Polymerase processivity

Replicases are capable of polymerizing thousands of nucleotides without dissociating from DNA (117). Two mechanisms by which different polymerase families ensure high processivity both require the aid of additional proteins to form complexes. Eukaryotic cellular replicases involve a sliding clamp complex (including PCNA) that encircles DNA and tethers it to the catalytic subunit of the polymerase (118). Bacteriophage T7 replicases have adopted a simpler method of maintaining close association to DNA. To become processive, T7 polymerase recruits host-encoded thioredoxin which increases the affinity of the polymerase for the primer terminus by 80-fold (117). Data suggest that thioredoxin forms a cap over the DNA groove locking the DNA strand inside the polymerase active site and increases the processivity of the enzyme (119).

Taq DNA polymerase and other members of the pol I family of polymerases usually work without auxiliary processivity factors. The X-ray structures of these polymerases, when complexed with DNA, show that the active site of the polymerase contains the 3' terminus of the primer. The polymerase thumb domain folds over and acts as a clamp, holding the DNA template strand in place. The clamping of the duplex can be

enhanced by the tip of the thumb; a mechanism thought to control the processivity of these enzymes (120).

2.2.2. Polymerase fidelity

Fidelity can be defined as a polymerase's ability to insert the correct nucleotide during DNA synthesis. As alluded to above, in addition to interstrand hydrogen bonding, the fidelity of a polymerase is influenced by intrastrand base-stacking and interstrand cross-stacking interactions (Figure 2.4; (113)). To incorporate these as factors, Goodman and colleagues propose the 'geometric selection' mechanism which contends that both geometric and electrostatic properties of the polymerase active site have profound impacts on nucleotide insertion specificity. The authors identify three possible checkpoints for proper geometric alignment during base insertion: initial nucleotide binding, post-binding selection by the correct geometric shape of proper base pairing (induced-fit mechanism), and the chemical step of phosphodiester bond formation (113, 121). Polymerases differ in the extent at which they use each checkpoint. Sequential application of each check point provides a high power of discrimination against the geometric abnormalities associated with mis-matched bases (121).

For the pol I family of polymerases, the junction between the palm and finger subdomains plays a crucial role in polymerase fidelity. It is in this junction that the terminal base pair of the primer-template association is held in a tightly constrained binding pocket. The geometric constraint of this pocket is unsuited for mis-matched base pairs which are detected by differences in hydrogen bonding, van der Waals' and base-stacking interactions (122).

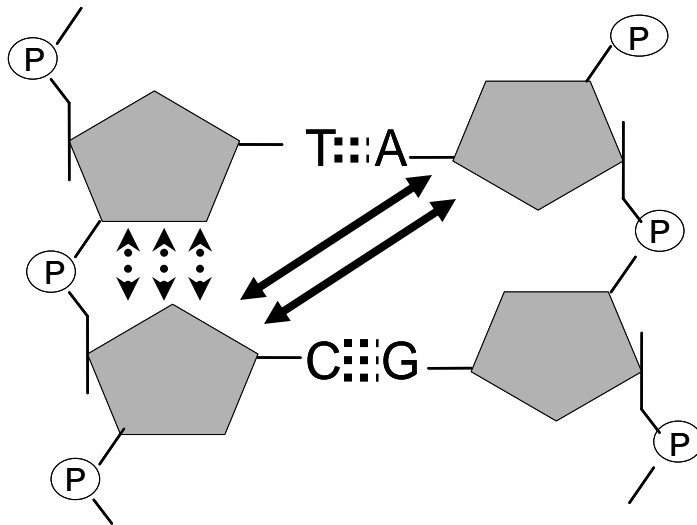


Figure 2.4 Multiple factors influence polymerase fidelity. Interstrand hydrogen bonding (•••), intrastrand base-stacking interactions (\uparrow \downarrow \uparrow), and interstrand cross-stacking interactions (\longleftrightarrow) all influence polymerase fidelity.

2.2.2.1. Nucleotide incorporation

Copying the genetic code requires the correct incorporation of the proper nucleotide into the growing DNA strand. DNA polymerases recruit incoming dNTPs and mediate the transfer of the phosphoryl group on these dNTPs to the exposed 3' hydroxyl on the synthesized DNA (114). The reaction is catalyzed by a two metal ion mechanism (normally Mg^{2+}) where one metal ion activates the 3' hydroxyl group on the primer, readying it for interaction with the incoming dNTP and the other stabilizes the interaction by negating the buildup of negative charges resulting from the departure of an oxygen molecule (Figure 2.5; (114, 123)).

Nucleotide incorporation can be broken down into six steps: polymerase binding to DNA, nucleotide binding, conformational change of the polymerase to a catalytically active state, phosphodiester bond formation, pyrophosphate release, and either translocation of the polymerase to the next residue or polymerase dissociation from DNA (93, 124-125). Using a low fidelity polymerase (yeast polymerase η (Pol η)), Washington *et al.* (2001) demonstrated that the nucleotide incorporation proceeds 150-fold faster when correct nucleotide incorporation occurred and this insertion is dependent on an induced-fit conformational change (126). The authors contend that the low fidelity of this polymerase likely results by an indiscriminant induced-fit mechanism (126).

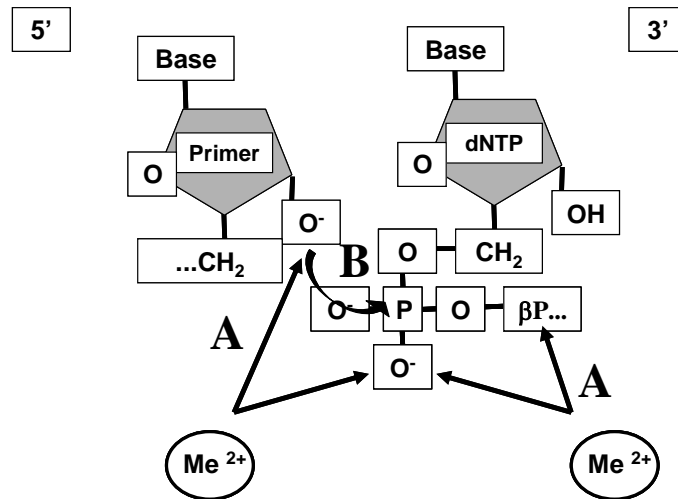


Figure 2.5 Mechanism of nucleotide insertion. Most DNA polymerases require the presence of two metal ions (designated Me^{2+}) to aid in polymerization. The ions are required for both A) stabilization of negative charges and B) the activation of 3'-OH groups, readying them to interact with incoming dNTPs (123).

2.2.2.2. Translesion DNA synthesis

Translesion synthesis by DNA polymerases can result in the misincorporation of nucleotides and the establishment of mutation. During normal replication, polymerization is stalled after the incorporation of mismatched bases. This occurs due to a mis-orientation of the 3'-hydroxyl group of the primer terminus onto which the next nucleotide is added (123). Various DNA lesions influence DNA structure and allow stable association between mismatched bases (18, 51, 68, 73, 94-96). To prevent mutagenesis resulting from polymerase replication of damaged DNA, highly specialized polymerases have evolved that function to synthesize DNA across replication-blocking lesions (127).

Found in prokaryotes, archaea, and eukaryotes, the Y family of DNA polymerases mediates translesion DNA synthesis (TLS). Due to a spacious active site that can accommodate various DNA lesions, these polymerases function to replicate damaged DNA. However, this loose active site decreases the fidelity of Y polymerases on undamaged template and prevents them from being useful as replicases (127). The Y family of translesion polymerases includes eukaryotic polymerases η , ι , κ , and Rev1, as well as prokaryotic polymerases IV and V (127).

2.2.2.2.1. Oxidative DNA damage mutagenesis

Most oxidative DNA adducts are not staunch replication road blocks. Bypass of these lesions by replicases occurs resulting in base substitutions, deletions, insertions, and frameshifting (15). The majority of oxidative damage derived mutations are substitutions; following a similar pattern with spontaneously generated mutation: GC→AT transitions followed by GC→TA transversions (15).

2.2.2.2.2. cis-syn Thymine-Thymine dimer bypass

A representative example demonstrating the need for TLS is the bypass of TT dimers by Pol η. Pol η exhibits low fidelity DNA synthesis (misincorporation frequency of 10^{-2} to 10^{-3}) on undamaged template (128-129). Using pre-kinetic steady state experiments, Washington *et al.* (2003) determined that the rate limiting step for bypass of TT dimers by Pol η, like that of undamaged template, occurs at the nucleotide incorporation steps. The maximum rate constants for nucleotide incorporation opposite TT dimers are nearly equivalent to those observed in experiments using undamaged template (93). This similarity in rate constant suggests that the geometric distortions in DNA brought on by the presence of dimers has no affect on the rate limiting step of nucleotide incorporation and furthers the author's contentions that Pol η bypasses thymine dimers by retaining the entire lesion in the active site and directly incorporating adenines opposite both thymine bases (93).

The need for TLS is further emphasized in xeroderma pigmentosum-variant (XP-V) individuals. XP is a genetic disorder which presents a high sensitivity to UV light resulting from deficiencies in UV lesion repair or bypass (130). XP-V is the only XP mutation not affecting DNA repair; individuals with mutations in XP-V lack functional Pol η activity (131). To overcome the deficiency in Pol η synthesis, Pol ζ is recruited to bypass TT dimers leading to an increase in mutation frequency and the resulting XP phenotype (131).

2.2.3. Summary

The premutagenic impacts of DNA base modifications have been studied in both *in vitro* and *in vivo* models using both prokaryotic and eukaryotic replication

components. Many DNA polymerases are not absolutely blocked by DNA lesions and, during the replication bypass of these lesions, the frequency of mutations is increased. Given that DNA damage increases mutagenesis during replication, the need for assays to monitor damage accumulation and repair should be clear.

2.3. Monitoring DNA Damage and Repair

Modifications to DNA bases alter base pairing kinetics which can lead to mutation. Genetic defects in DNA repair pathways confer susceptibility to certain cancers and developmental disorders. Taken together, these observations suggest that DNA damage is a preliminary step in carcinogenesis (3, 19-20). Assays for DNA damage are therefore needed for experimental monitoring of DNA repair pathways and clinical diagnosis of DNA repair abnormalities (5).

2.3.1. E-beam irradiation of DNA influences quality

DNA extracted from licked envelopes exposed to electron beam irradiation differ in both the quantity and quality of the DNA recovered when compared with non-irradiated controls (134). When typing DNA using the PCR for forensic purposes, differential amplification between short and long amplicons may be observed and is seen as an indicator of template quality (135-136). In complete agreement with previous reports, DNA quality is compromised in irradiated samples; loci fail to amplify in the order of increasing PCR target size as the extent of degradation increases (Figure 2.6; (134)). Non-irradiated samples exhibit balance between loci indicating less DNA degradation (134).

In these reactions, input template amounts are standardized; the observed decreases in amplification may be a result of damage to the target DNA in each reaction. The observation that amplification of larger loci in irradiated samples decreases in comparison to smaller targets from the same sample suggests that DNA damage by E-beam irradiation is random; the probability of encountering damage increases in reactions with larger sized PCR targets. These observations also suggest that the PCR can be used to determine DNA quality.

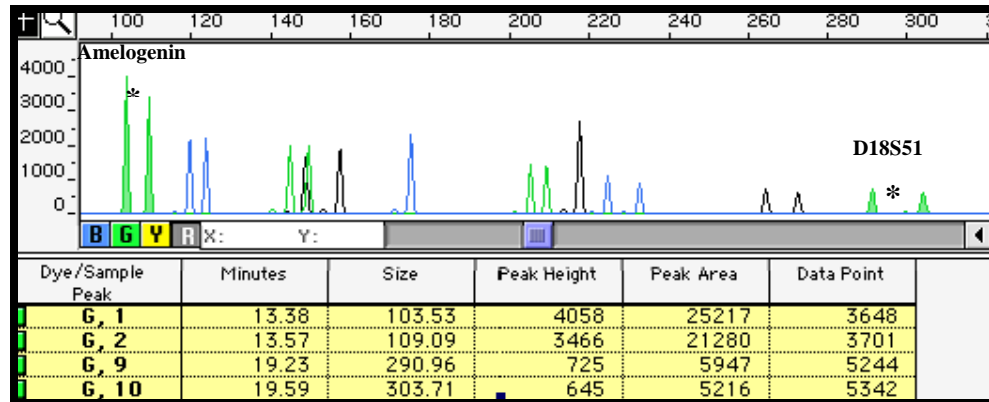


Figure 2.6. Forensic fragment analysis of DNA from electron beam irradiated envelopes. DNA from irradiated envelopes was isolated and then amplified using Perkin Elmer AmpF Φ STR Profiler Plus[®] kit. Analyzed data shows an apparent difference in the quality of DNA obtained from electron beam irradiated envelopes; a five-fold difference in peak heights exists between the smallest (Amelogenin; G1 and G2) and the largest (D18S51; G9 and G10) locus (adapted from 134). Numbers on the Y-axis and peak height values represent relative fluorescent units; size of loci is given in base pairs.

2.3.2. Southern blotting

Detection by Southern analysis involves treatment of damaged DNA with lesion-specific endonucleases followed by hybridization of filter-bound restriction fragments to a gene-specific probe (132-133). Lesion-specific digestion reduces the signal intensity of the target gene; the frequency of lesions is proportional to the decrease in probe hybridization (132-133). Using this method, the first observations suggesting differences in rates of repair between transcribed and non-transcribed sequences were made (132)

2.3.3. Quantitative polymerase chain reaction

The requirement for relatively large amounts of DNA in the Southern hybridization method led to the development of quantitative polymerase chain reaction (QPCR) assays (5-11). These methods, referred to as polymerase stop assays, are based on the blocking of thermostable DNA polymerase progression by lesions in DNA template which result in a decrease in the overall rate of PCR product formation (5, 8-11). Under the assumption that a single lesion is sufficient to block polymerase progression, the QPCR method effectively measures the fraction of undamaged templates. DNA damage results in a reduction in template amplification and can be expressed as lesions per kilobase (10). Using this method, differences in the rates of

DNA repair between mitochondrial (mtDNA) and nuclear DNA have been documented (8).

2.3.4. Summary

The advent of QPCR to detect and monitor DNA damage and repair dramatically reduced the amount of sample material needed for study and increased assay sensitivity compared with hybridization-based damage quantification methods. These assays are built on the assumption that thermostable DNA polymerases are blocked completely by DNA base lesions. Experimental validation of this assumption is not readily available in the current literature and seems improbable given the lesion bypass characteristics of most other DNA polymerase systems. The need to explore this fundamental assumption of QPCR resulted in the experiments presented in the following chapters.

2.4. Modeling the Polymerase Chain Reaction in Real-Time

The polymerase chain reaction measured in real-time is becoming the standard method for quantifying DNA and RNA (137). These assays utilize a variety of fluorescence based detection methods allowing high throughput, high sensitivity, and reliable specificity (137-139).

2.4.1. Real-time PCR mathematics

Several mathematical methods are available for determining input template copy number from real-time PCR data. Threshold cycle (C_T) methods determine input template amounts by comparing the C_T value from an unknown template to C_T values from templates of known copy number (Figure 2.7; (140-141)). In the standard curve method, C_T is plotted against the logarithm of copy number for a series of known input templates and the copy number of the unknown template is determined by linear regression (Figures 2.7B,C; (140)). When using a standard curve method, either relative or absolute quantification can be achieved (140). The comparative threshold method expresses relative changes in gene expression with normalization to a reference (housekeeping) gene using the $2^{-\Delta\Delta C_T}$ formula (141). The method rests on the assumptions that the amplification efficiencies of the target and reference genes are approximately equal and that the amplification efficiencies of both genes in exponential phase are close to one (141).

In an alternative method developed by Liu and Saint (2002), amplification efficiencies derived from kinetic curves are used to determine relative transcript abundance (Figure 2.7; (142)). This method does not require equivalent amplification efficiencies and obviates the need for standard curve construction. More recently, these workers observed that amplification efficiencies change dynamically during simulated PCRs and validated a mathematical method in which input template amounts are determined from amplification curve parameters (143).

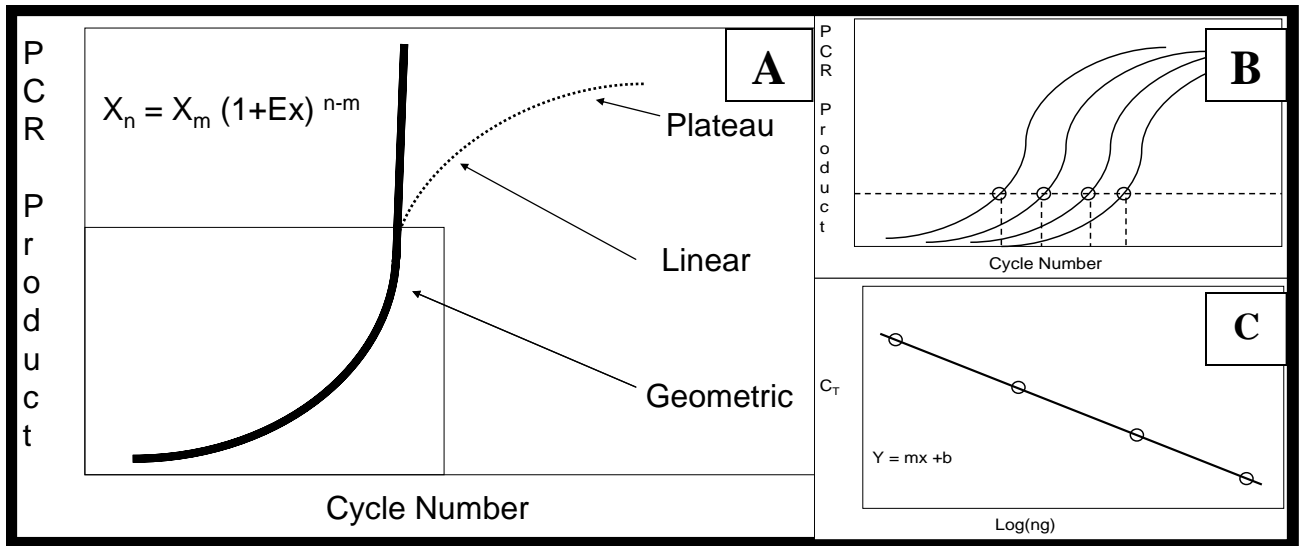


Figure 2.7 Exponential modeling of real-time PCR. A) Polymerase chain reaction curves can be separated into three distinct phases; geometric, linear, and plateau. Geometric phase is modeled mathematically using a formula for exponential growth (144); the efficiency of the reaction during this stage is constant due to all reagents being in excess quantities and the lack of reaction derived inhibitors (144). B) Using a series of diluted standards, threshold cycle values (C_T) are collected and C) plotted versus the log of the input DNA concentrations; copy number of unknown templates can then be determined using linear regression (140).

2.4.2. Real-time PCR calculations influenced by template secondary structure

Recent work by Nogva and Rudi (2004) call into question the assumption that amplification efficiency is equal for all cycles of real-time PCR (145). Two separate targets on the *Listeria monocytogenes* (LM) genome were amplified and result in an observed copy number ratio of approximately 2:1 (145). The true ratio of target copy numbers, previously identified through sequencing of the LM genome, is known to be 6 (145). Additional data imply that secondary structure in regions flanking PCR targets influenced the first few cycles of amplification. This impact was undetectable at the point in the reaction where fluorescent readings were measured (Figure 2.8; (145)). Work such as this emphasizes the need to account for inherent template influences on the PCR which may mask differences in subsequent mathematical comparisons.

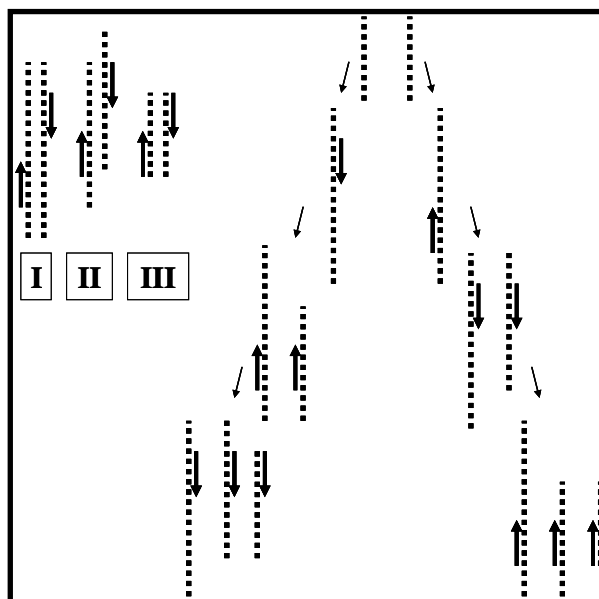


Figure 2.8 Early reaction cycles influence template quantification. Three types of DNA template exist in PCRs after the third cycle; (I) input DNA, (II) PCR derived large fragments with no defined ends, and (III) PCR derived amplicons with ends defined by the 5' termini of both primers. Inherent differences in template sequences, both in the target region and in the regions flanking the primer sites, alter the potential secondary structures of the duplexed DNA and result in a rightward shift in amplification curves. This rightward shift translates into an artificial decrease in reported copy number (adapted from Nogva and Rudi (2004) (145)).

2.4.3. *Thermus aquaticus* DNA polymerase

Taq DNA polymerase, a member of the pol I family of polymerases, is widely used as a replicative thermostable polymerase in PCRs. Under optimal conditions and with no apparent requirement for additional auxiliary factors, *Taq* polymerase exhibits moderate processivity (polymerization rate as high as 2800 nucleotides per min (146)) and fidelity (generating misincorporation events every 10^4 bases per cycle (147)).

Studies of *Taq* translesion synthesis during the PCR are limited. In the presence of all four dNTPs, *Taq* is not hindered when 8-oxodA is encountered nor is mis-pairing evident opposite the base lesion (67, 69). Slow bypass of TT dimers by *Taq* also occurs (87); greater than 53% of the polymerization reactions terminated opposite the 3'-T and between 7-15% terminated opposite the 5'-T (87).

2.4.4. Summary

Some QPCR assays require the use of radioisotope labeled dNTPs to detect PCR products as they are formed. By adapting real-time PCR protocols to estimate damage to DNA, the need for hazardous isotopes would be eliminated in polymerase stop assays for DNA damage detection. In addition, little attention has been given to the impact of lesion bypass on the mutational spectrum of *Taq* DNA polymerase. Work presented here describes the observed influences of specific DNA modifications on PCR mutagenesis.

2.5. Summary

Cellular DNA is damaged as a result of exogenous and endogenous stimuli (12). Repair systems are in place to prevent assault on nucleic acid (36-38) or eliminate altered DNA if damage occurs (1, 99-100). If damage to DNA is not repaired, the extent with which this damage influences replication of DNA is both lesion and polymerase dependent. Bulky adducts on DNA, such as *cis-syn* Thymine-Thymine dimers, greatly hinder replicative DNA polymerases. Translesion synthesis proceeds in these cases due to the recruitment of the highly specialized Y family of DNA polymerases whose function, to date, is lesion bypass (127). Other lesions, such as 8-oxodG, are considered pre-mutagenic as they don't substantially block replicative DNA polymerase progression and, during translesion synthesis, decrease the fidelity of template replication (2). The buildup of DNA damage increases in aging populations (21) and has been implicated as a causative component in many late-onset diseases and cancerous phenotypes (3, 148-150). These observations emphasize the need for assays to screen for damage in clinical settings.

Currently, real-time PCR is becoming the standard method for measuring DNA and RNA in a wide variety of disciplines (137). Differences in C_T values translate into differences in template abundance (141). The objective of the following body of research is to develop a real-time PCR method to screen for DNA damage based on the assumptions of the polymerase stop assays. The purpose of the following research is 1) to determine if different DNA base lesions influence the rate of the PCR to different degrees (LBR), 2) if lesion bypass occurs, characterize the influence of specific DNA base lesions on *Taq* polymerase fidelity (LIM), and 3) to redefine changes in C_T values as differences in amounts of DNA damage (both LBR and LF). By providing the experimental and mathematical basis for using real-time PCR as a screen for DNA damage, work toward the usage of polymerase stop assays in a clinical environment may become possible.

CHAPTER III

MATERIALS AND METHODS

3.1. Thermostable DNA Polymerase Lesion Bypass Rate

3.1.1. Synthesis of synthetic DNA templates

To study the lesion bypass rate (LBR) of DNA base modification by *Taq* DNA polymerase, the type and amount of base lesions must be controlled. In this study, ninety-base oligonucleotides were synthesized on an Applied Biosystems (ABI, Foster City, CA) Model 394 DNA Synthesizer in the Marshall University DNA Core Facility using low volume 200 nmole cycles with 30 s coupling time and standard phosphoramidite chemistry (152-153). The sequence of the unmodified 90 base oligonucleotide was equivalent to a portion of the human mitochondrial Hypervariable Region One (Anderson sequence #15989-16078 (154)). 7,8-dihydro-8-oxo-2'deoxyguanosine, 7,8-dihydro-8-oxo-2'deoxyadenosine, abasic site (tetrahydrofuran analogue), and *cis-syn* thymidine dimer were introduced at specific positions as indicated in Table 3.1 using DNA damage base cyanoethyl phosphoramidites (Glen Research, Sterling, VA). Oligonucleotides were synthesized in the trityl-on mode and cleaved from the polystyrene resin with ammonium hydroxide; 8-oxodG containing templates were cleaved with ammonium hydroxide containing 0.25 M β -mercaptoethanol (18, 155). Oligonucleotides were purified using ABI OPC cartridges (156). The OPC products were resolved using polyacrylamide gel electrophoresis (PAGE) (Figure 4.1), and with the RNA 6000 Nanochip assay and Agilent Bioanalyzer (Agilent Technologies, Palo Alto, CA) to ensure the removal of synthesis failure sequences during OPC purification (Figures 3.1, 3.2; protocol below). Oligonucleotide templates were quantified by measuring optical density at 260 nm, evaporated to dryness, and then stored at -80° C. A representative subset of 90-mers (Oxo CONTROL, 8-oxodG1, and Abasic) were analyzed by Matrix Assisted Laser Desorption Ionization coupled with a Time-Of-Flight (Maldi-TOF) mass spectrometry (HT Laboratories, San Diego, CA) to further confirm

oligonucleotide purity (Figure 3.3). Resulting profiles produced similar baselines and unique peaks approximately equal to the expected molecular weights of each 90-mer tested (Figure 3.3).

Oligonucleotide extinction coefficients were obtained using Oligo Primer Analysis Software v5.0 (Molecular Biology Insights, Cascade, CO). One hundred μM stock solutions of each 90-mer were prepared in low TE buffer (10 mM Tris pH 8.0; 0.1 mM EDTA) and maintained at -20°C with thawing only for analysis.

Table 3.1. 90-mer oligonucleotides used as templates for the PCR.

TEMPLATE ^a	OLIGONUCLEOTIDE SEQUENCE
Oxo CONTROL	<p>.....▶</p> <p>5'-CCCAAAGCTAAGATTCTAATTTAAACTATTCTCTGTTCTTTCATGGGGAAGCAGATTTGGGTACCACCCAAGTATTGACTCACCCATCAA-3'</p> <p>◀ — — — ▶</p>
OxodG1(48)	5'-CCCAAAGCTAAGATTCTAATTTAAACTATTCTCTGTTCTTTCATGGGXAAAGCAGATTTGGGTACCACCCAAGTATTGACTCACCCATCAA-3'
OxodG2A(48/61)	5'-CCCAAAGCTAAGATTCTAATTTAAACTATTCTCTGTTCTTTCATGGGXAAAGCAGATTTGGXtACCACCCAAGTATTGACTCACCCATCAA-3'
OxodG2T(47/48)	5'-CCCAAAGCTAAGATTCTAATTTAAACTATTCTCTGTTCTTTCATGGXXAAGCAGATTTGGGTACCACCCAAGTATTGACTCACCCATCAA-3'
OxodG3A(48/54/61)	5'-CCCAAAGCTAAGATTCTAATTTAAACTATTCTCTGTTCTTTCATGGGXAAAGCAxATTTGGXtACCACCCAAGTATTGACTCACCCATCAA-3'
OxodG3T(46-48)	5'-CCCAAAGCTAAGATTCTAATTTAAACTATTCTCTGTTCTTTCATGGXXAAGCAGATTTGGGTACCACCCAAGTATTGACTCACCCATCAA-3'
OxodG4T(45-48)	5'-CCCAAAGCTAAGATTCTAATTTAAACTATTCTCTGTTCTTTCATXXXXAAGCAGATTTGGGTACCACCCAAGTATTGACTCACCCATCAA-3'
OxodG6(45-48/59-60)	5'-CCCAAAGCTAAGATTCTAATTTAAACTATTCTCTGTTCTTTCATXXXXAAGCAGATTTXXGTACCACCCAAGTATTGACTCACCCATCAA-3'
OxodG9(35/45-48/54/59-61) ^b	5'-CCCAAAGCTAAGATTCTAATTTAAACTATTCTCTXtTCTTTCATXXXXAAGCAxATTTXXXtACCACCCAAGTATTGACTCACCCATCAA-3'
OxodA1(49)	5'-CCCAAAGCTAAGATTCTAATTTAAACTATTCTCTGTTCTTTCATGGGGYAGCAGATTTGGGTACCACCCAAGTATTGACTCACCCATCAA-3'
Abasic(49)	5'-CCCAAAGCTAAGATTCTAATTTAAACTATTCTCTGTTCTTTCATGGGGZAGCAGATTTGGGTACCACCCAAGTATTGACTCACCCATCAA-3'
Dimer CONTROL	5'-CCCAAAGCTAAGATTCTAATTTAAACTATTCTCTGTTCTTTCATGGGGTTCAGATTTTGGTACCACCCAAGTATTGACTCACCCATCAA-3'
TTDimer1(49/50)	5'-CCCAAAGCTAAGATTCTAATTTAAACTATTCTCTGTTCTTTCATGGGGDDGCAGATTTTGGTACCACCCAAGTATTGACTCACCCATCAA-3'

a- The position of modification relative to the 5' terminus of the oligonucleotide is indicated in parenthesis.

b- OxodG9 contains a base modification in the internal control region (at site 35) and was therefore only used to demonstrate decreased dye binding as it related to increased numbers of 8-oxodG modification (Figure 4.2).

X, Y, Z, and DD represent the insertion sites of 8-oxodG, 8-oxodA, abasic, and *cis-syn* TT dimer modifications, respectively, into the oligonucleotide. The dotted arrow, the solid arrow, and the dashed arrow indicate the binding sites of the forward, full-length amplicon reverse, and internal control region reverse primers respectively (adapted from Sikorsky *et al.* (2004) (159)).

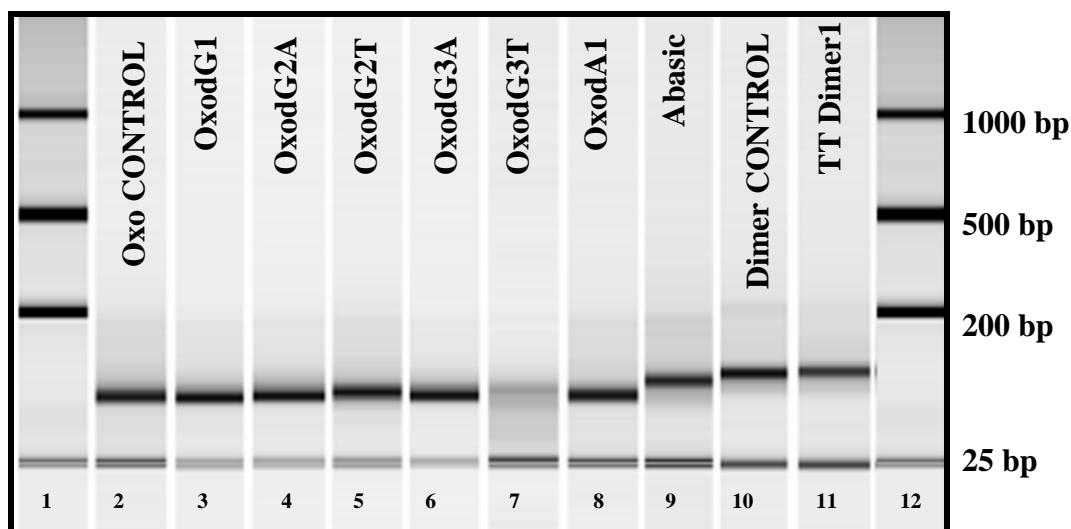


Figure 3.1 Purified 90-mer oligonucleotides. OPC purification of raw 90 base oligonucleotides removed failed coupling reactions that occurred during synthesis; lanes 1 and 12 are RNA mass ladders (suggested for ssDNA samples; Ambion, Inc., Austin, TX). As the number of 8-oxodG modifications increased, differences in the migration patterns of the single stranded oligonucleotides were observed (OxodG3T); these observations were also seen with PAGE (Figure 4.1) and high percentage agarose separations (data not shown) and can be explained by an increased perturbation of backbone structure (157).

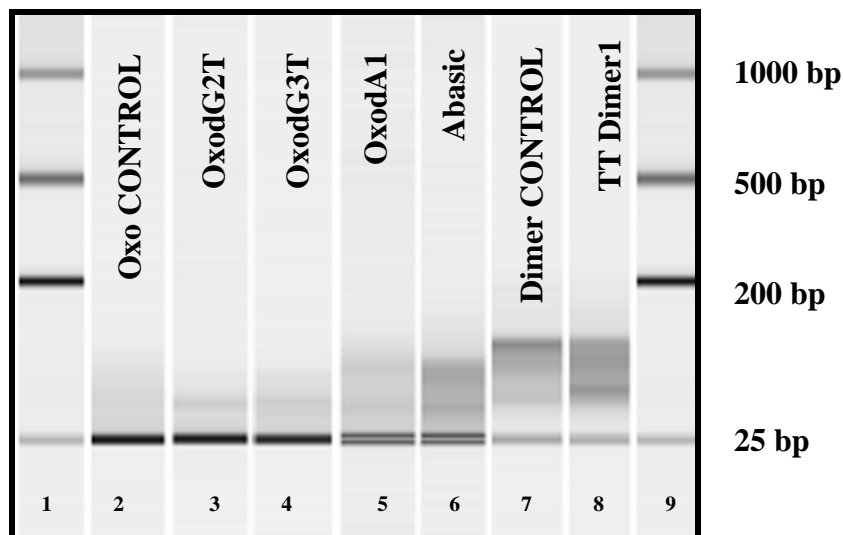


Figure 3.2 Failure products from 90-mer oligonucleotide synthesis. Crude material, obtained during purification of 90 base oligonucleotides, showed presence of truncated failure sequences; lanes 1 and 9 are RNA mass ladders (suggested for ssDNA samples; Ambion, Inc., Austin, TX). All samples contained a 25 bp size standard to normalize for interrunc variation.

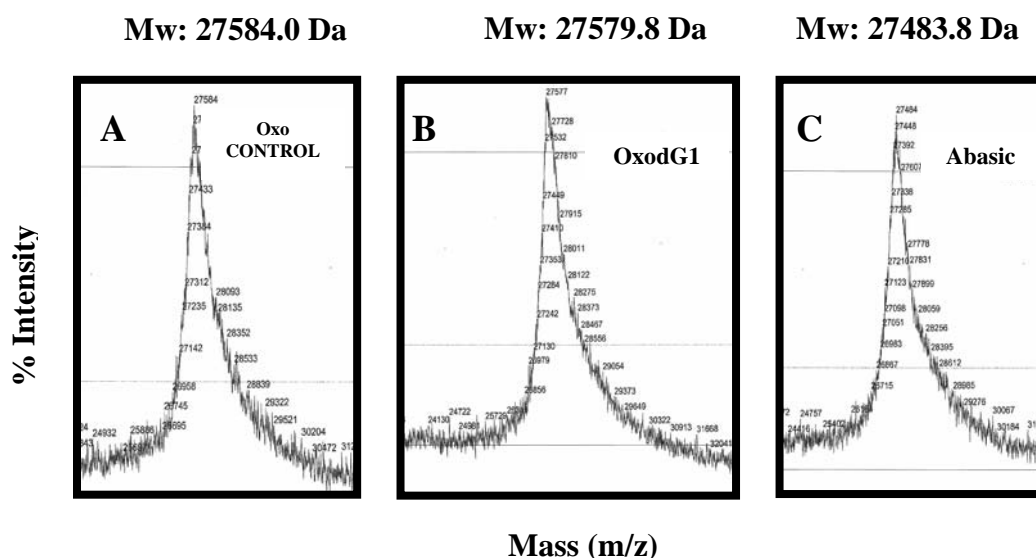


Figure 3.3 MALDI-TOF analyses of 90-mers. Purity of the A) Oxo CONTROL, B) OxodG1, and C) Abasic oligonucleotides were determined by mass spectrometry; expected molecular weights were 27579.0 Da, 27595.0 Da, and 27445.9 Da respectively. No secondary peaks were observed above baseline suggesting the presence of unique purification products; instrument resolution is approximately 1% (or equating to 270 Da).

3.1.1.1. Resolving oligonucleotide purity using a polyacrylamide gel electrophoresis assay

To confirm removal of synthesis failure sequences by OPC purification, the 90 base synthetic oligonucleotide templates were heat denatured at 95° C for 5 min followed by a rapid cool to 4° C and then resolved by electrophoresis in 1x TBE on 5% denaturing polyacrylamide at 60 watts for 1 hr. Post separation, gels were stained by immersion in GelStar (Cambrex, East Rutherford, NJ) for 30 min and viewed on an UV transilluminator (see Figure 4.2).

3.1.1.2. Resolving oligonucleotide purity using the Agilent 2100 Bioanalyzer and RNA 6000 Nanochip assay

To corroborate observations made from the PAGE analysis, the purified synthetic 90-mers and crude synthesis failure sequences were resolved using microchip separation technologies. The RNA 6000 Nanochip and Agilent 2100 Bioanalyzer were prepared according to manufacture recommended protocols. 1 µl of 100 µM crude and OPC purified sample material was added to respective sample wells on the nanochip and

separated using the Total Eukaryote RNA run module (suggested for ssDNA). Data was collected by the instrument and exported as .tiff picture files (see Figures 3.1, 3.2).

3.1.1.3. Amplification of 90 base oligonucleotides by Taq DNA polymerase using real-time PCR

PCR primers were designed to amplify either the full-length 90-mer oligonucleotide or a 45 base region with no base modifications [the internal control region (ICR); Table 3.1; Figure 4.1; (159)] with ABI Primer Express Software v2.0. Our standard 25 μ l PCR contained 12.5 μ l of ABI 2x SYBR® Green PCR Master Mix, 9.5 μ l of sterile deionized H₂O, 1 μ l of oligonucleotide template, 1 μ l of 10 μ M forward PCR primer (5'- CCC AAA GCT AAG ATT -3') and either 1 μ l of 10 μ M reverse PCR primer (5'- TTG ATG GGT GAG TCA -3') for full template amplification or 1 μ l of 10 μ M internal control primer (5'- CAT GAA AGA ACA GAG -3') for ICR amplification. A master mix without template was prepared based on the total number of reactions. Oligonucleotide templates ranging from 1 amole to 100 fmoles were then added to complete the reaction. Amplifications were performed in 96 well plates and capped with optical grade ABI PCR strip caps. Templates were amplified under the following conditions: 50° C for 2 min, 95° C for 10 min, then 40 cycles of 95° C for 20 s, 54° C for 30 s and 60° C for 1 min. PCR amplification and detection was carried out in an ABI Model 7000 Sequence Detection System (SDS) according to guidelines provided (140). C_T , dissociation curve data, and delta Rn values were exported from SDS data files in comma delimited (.csv) format.

3.1.1.4. Amplification of 90-base oligonucleotides by Restorase damage polymerase using real-time PCR

To test if alternative PCR components impacted experimental observations, the full-length 90-mer oligonucleotide or the ICR region were amplified using Restorase DNA polymerase (Sigma-Aldrich, St. Louis, MO). Big band modifications to the PCR primers were necessary to prevent degradation by Restorase's inherent exonuclease activity (Big Band Primers; Sigma-Genosys, Woodlands, TX). Modifications to the Restorase amplification protocol were made to allow data collection in real-time.

Reactions contained 1 μl of a 1:1000 dilution of SYBR Green Dye (Molecular Probes Inc., Eugene, OR), 0.5 μl of Rox internal standard dye (Epicenter Technologies, Madison, WI), 0.5 μl dNTP mix (Sigma-Aldrich), 2.5 μl of 10x Restorase reaction buffer (Sigma-Aldrich), 1 μl forward primer, and either 1 μl of ICR or full-length reverse primers; QS to 24 μl with dH_2O and add 1 μl of oligonucleotide template. Complete reactions were prepared on ice, transferred to 96 well plates, and capped with optical grade ABI PCR strip caps. Sample plates were incubated at 4° C for 5 min to limit exonuclease and repair activities. Plates were then transferred to an ABI 7000 sequence detection system and amplified according to guidelines provided (140). Templates were amplified under the following conditions: 95° C for 5 s, then 40 cycles of 95° C for 20 s, 54° C for 30 s and 60° C for 1 min and data exported as described above.

3.1.1.5. Calculation of lesion bypass rates from real-time PCR data from 90-mer synthetic templates

Measures of lesion bypass rate, Relative Threshold Cycle and Mean Modified Efficiency, were performed using Microsoft Excel software. Complete descriptions of each method are found in sections 3.4.1. and 3.4.2 respectively. Inherent Template Efficiency calculations required the fit of raw PCR data to sigmoid grow curves (section 3.4.3.); this was accomplished using SigmaPlot 2001 for Windows v7.0 (Systat Software Inc., Point Richmond, CA). Subsequent calculations were performed using Microsoft Excel.

3.2. Calculation of Lesion Abundance in Cellular DNA

In order to estimate cellular DNA damage by the calculation of lesion frequency (LF) from real-time PCR data, amplification of long targets is necessary to increase assay sensitivity to biologically appropriate damage levels (5). To transition into long template amplification for damage study, it was first necessary to test damage assays with long templates containing controlled modifications.

3.2.1. Synthesis of 593-base templates with controlled modifications

Using primers designed to flank the mammalian mtDNA sequence analogous to the Oxo CONTROL 90-mer (Anderson #15912-93 (154); Appendix A), 751 bp PCR products were generated from total cellular DNA. PCR master mixes were created as described in section 3.1.1.3. and amplified using the following conditions: 50° C for 2 min, 95° C for 10 min, then 40 cycles of 95° C for 30 s, 55° C for 20 s and 72° C for 1 min. These products were purified using QiaQuick PCR purification columns (Qiagen Inc., Valencia, CA). A nested PCR was performed under the sample amplification conditions using these purified 751 bp PCR products as templates and using the 90-mers described above (Table 3.1) as the reverse primer and a 5' biotin labeled primer (FWD#12; 5'-AAG CCT GTG ATC CAT CGT GAT-3'; Sigma-Genosys, Woodlands, TX) as the forward primer. Crude products from eight replicate reactions were combined, cleaned with the QiaQuick system, and concentrated in 50 µl of DNA elution buffer. 40 µl of purified PCR product was added to 13 µl of 20X SSC and 460 µl of dH₂O to enhance the formation of dsDNA. To remove the biotin labeled anti-sense strand, the PolyAtract® mRNA Isolation System (Promega, Madison, WI) was used. Para-magnetic particles coated with Streptavidin (SA-PMPs) were washed with 0.5X SSC buffer and then the contents of the sample/SSC/dH₂O mixture were added and incubated at room temperature for 10 min to allow maximum streptavidin-biotin association. The beads were then washed 4 times in 0.1X SSC; after each addition the SA-PMPs were collected at the side of the sample tube using a specialized magnet (Promega). One hundred µls of dH₂O were added and the samples incubated at 75° C to denature the dsPCR product and elute the anti-sense strand containing the PCR ligated synthetic 90-mer.

3.2.1.1. Separation of PCR products to determine homogeneity using agarose and gel electrophoresis

To estimate specificity of amplification, crude PCR products were separated using agarose gel electrophoresis. Unless otherwise noted, PCR products were separated in 1X TAE buffer through 2% SeaKem ME agarose (FMC Bioproducts, Rockland MA) containing 0.5 µg/ml of ethidium bromide at 50 to 100 V for 0.5 to 3 hrs to confirm product size. These parameters were sufficient to resolve products ranging from 50 bp to 3 kb in length. A 123 base pair nucleic acid mass ladder was included to confirm product size. Gels were viewed on an UV transilluminator and digital pictures taken using a Gel Doc 2000 (BioRad Inc., Hercules, CA).

3.2.1.2. Amplification of 593 base templates for damage study

PCR master mixes were created as described in section 3.1.1.3. and amplified using the following conditions: 50° C for 2 min, 95° C for 10 min, then 40 cycles of 95° C for 30 s, 55° C for 20 s and 72° C for 1 min. The FWD#12 primer was used in combination with either FWD#16138 and REV#16090 to create full-length and oligo-ligation internal control region (OL-ICR) amplicons (Appendix A).

3.2.1.3. Data analysis

Measures of lesion bypass rate were performed as described in section 3.1.1.5.

3.2.2. Ultraviolet irradiation of total cellular DNA

To determine if real-time PCR and changes in C_T values could be used to estimate damage in cellular DNA, the creation of samples with controlled amounts of damage to cellular DNA was necessary. Total cellular DNA was extracted from whole blood as described in section 3.2.2.1. Working DNA concentrations were 5 ng per µl (as determined by absorbance at 260 nm). One hundred µls of DNA stock solutions were spotted on parafilm and irradiated at short range UV (254 nm) for various times using a UVS-11 Mineralight lamp (Ultraviolet Products Inc., San Gabriel CA) fixed at a height

of 20 mm in a sterile hood. The amount of evaporation was determined and samples QS to 100 µl with dH₂O and stored at -20° C until analysis.

3.2.3. Validation of real-time PCR for detection of biologically relevant levels of UV damage

To validate real-time PCR as an assay for determining lesion frequency in total cellular DNA, UV damaged DNA was acquired from Drs. Bennett Van Houten and Joel Meyer at the National Institute of Environmental Health Sciences, Research Triangle, NC. DNA for QPCR and real-time PCR lesion frequency calculations was prepared as follows: MGH-U1 (bladder cancer) cells were grown as monolayers in 75 cm² tissue culture flasks in RPMI medium supplemented with 10% heat-inactivated fetal calf serum, 1% penicillin/streptomycin and 2 mM L-glutamine in a humidified atmosphere of 5% CO₂ in air. For the experiments, 10⁶ cells were seeded in 10 ml medium into 10 cm dishes and cultivated overnight at 37° C. After 24 h, the medium was aspirated, cells were washed with PBS, and then irradiated in 3 mL PBS with 0, 10 or 20 J/m² UV radiation, using a germicidal Spectroline X-Series lamp (Spectroline, Westbury, NY). Cells were harvested in 10 ml RPMI medium, centrifuged for 10 min at 1000 rpm, washed with 10 ml PBS and centrifuged again for 10 min at 1000 rpm. Cells were frozen immediately after the exposure and stored at -80° C to prevent DNA damage repair.

Frozen cell pellets were later thawed and immediately transferred to 2 ml lysis buffer (Genomic-tips kit; Qiagen Inc., Valencia, CA) supplemented with 4 µl RNase A (100 mg/ml; Qiagen) and 100 µl proteinase K (>600 mAU/ml; Qiagen). Samples were vortexed for 5 s and incubated at 50° C for 2 h. Samples were then vortexed again for 10 s and loaded immediately onto pre-equilibrated Genomic-tip 20/G (Qiagen) columns. Subsequent purification of genomic DNA was according to the Genomic-tips (Qiagen) protocol. The integrity of the extracted DNA was assessed by electrophoresis through 1% agarose gel at 30 V for 16 h.

Genomic DNA was quantitated using PicoGreen dye (Molecular Probes Inc., Eugene, OR) as described by Santos *et al.* (2002), and 15 ng of each sample was used as template for PCR reactions (11). PCR amplifications were performed as described by Santos *et al.* (2002), using primers 2372 (5'-CAT GTC ACC ACT GGA CTC TGC AC-

3') and 3927 (5'-CCT GGA GTA GGA ACA AAA ATT GCT G-3') for the polymerase beta gene, and primers 48510 (5'-CGA GTA AGA GAC CAT TGT GGC AG-3') and 62007 (5'-GCA CTG GCT TAG GAG TTG GAC T-3') to amplify a non-coding region 5' of the beta globin gene (11). PCR reaction mixtures and cycling conditions were as described in Santos *et al.* (2002) except that 25 cycles of amplification were used for both reactions (11). PCR products were quantified with PicoGreen dye and a fluorescence plate reader, and lesion frequency was calculated by application of the Poisson distribution (10).

3.2.2.1. Genomic DNA extraction

Total cellular DNA was extracted from whole blood using the Wizard Genomic DNA Purification kit (Promega, Madison, WI) and protocols for extracting DNA from blood (134). To lyse white cells, Cell Lysis Solution (Promega) was added to whole blood; nuclear membranes were disrupted by Nuclei Lysis Solution (Promega). RNAase was added to destroy any RNA present in the sample and Protein Precipitation Solution (Promega) added to precipitate out any protein material. The samples were centrifuged and the supernatant containing DNA transferred to a clean tube containing isopropanol. White strands, indicating the presence of DNA, were visible which were then pelleted by centrifugation. The DNA pellet was washed with 70% ethanol, the ethanol removed, and the pellet air dried. DNA was resuspended in DNA Rehydration Solution (Promega) and the concentrations determined by absorbance at 260 nm. Samples were aliquoted and stored at -20°C and thawed immediately prior to experimentation.

3.2.2.2. Long extension real-time PCR

A primer walking strategy was adopted to amplify various sized fragments from human mtDNA (Figure 3.4). Primers were adapted from Levin *et al.* (1999) (158), from Ayala-Torres *et al.* (2000) (10), or created using ABI Primer Express Software v2.0 to amplify sections of mtDNA; each amplicon contained the same reverse primer (REV#14841; 5'-TTT CAT CAT GCG GAG ATG TTG GAT GG-3'). Forward primers were designed to systematically increase amplicon size (Figure 3.4; Appendix A). A standard 25 μl long extension PCR contained 12.5 μl of ABI 2X SYBR® Green PCR

Master Mix, 9.5 μ l of sterile deionized H₂O, 1 μ l of template, 1 μ l of 10 μ M forward PCR primer, and 1 μ l of 10 μ M reverse PCR primer. Templates were amplified under the following conditions: 50° C for 2 min, 95° C for 10 min, then 40 cycles of 94° C for 30 s and 65° C for 4 min.

Template amounts were held constant in these reactions by prior amplification of an internal control region (LX-ICR; Figure 3.4; Appendix A) and application of a dilution factor determined by direct cycle threshold based comparison mathematics (141). Master mixes for the LX-ICR PCRs were constructed as described above, but reactions were performed under the following conditions: 50° C for 2 min, 95° C for 10 min, then 30 cycles of 94° C for 15 s and 60° C for 1 min. Data was exported and calculations performed using Microsoft Excel software.

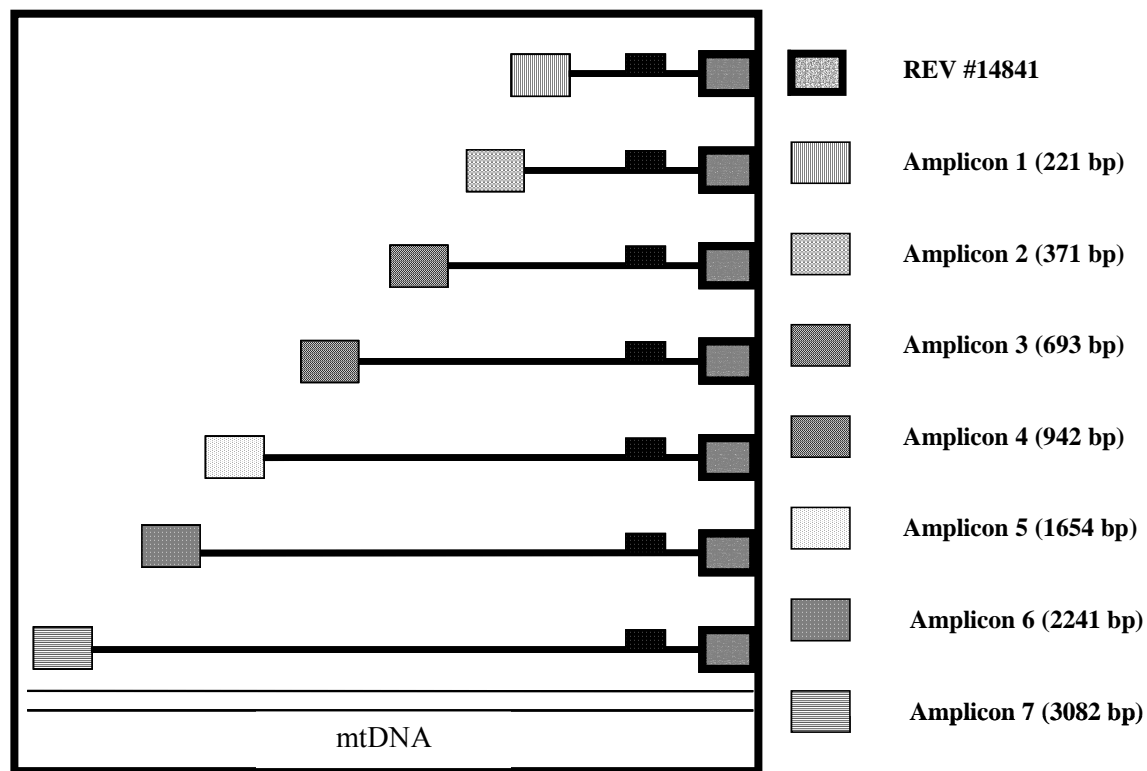


Figure 3.4. Amplification of mitochondrial DNA by primer walking. The schematic represents mammalian mtDNA; reverse primer (REV #14841) was held constant and forward primers moved to create amplicons ranging between 221 bp and 3082 bp. Actual fragment size is given in parenthesis. The LX-ICR (■■) is located within Amplicon 1 (from mtDNA #14642-#14693).

3.2.2.3. Data analysis

Measures of lesion bypass rate were performed as described in section 3.1.1.6. Lesion frequencies were calculated from real-time PCR data using Microsoft Excel software and equation 13 in section 3.4.4.

3.3. Characterization of Lesion Induced Mutagenesis

3.3.1. Synthesis and amplification of modified 90-mer oligonucleotides

To determine nucleotide incorporation opposite DNA base modification during the PCR (LIM), the amount and types of base lesions must be strictly controlled. The generation of modified oligonucleotides (section 3.1.1.) and their respective amplification (section 3.1.1.3.) are described above.

3.3.2. Purification of PCR product

Prior to sequencing, PCR products were electrophoresed through agarose to confirm the presence of the correct sized amplicon (section 3.2.1.1). PCR products were purified using the Qiagen[®] QiaQuick PCR amplification kit protocol (134). This protocol is designed to purify single or double stranded DNA from PCR and other enzymatic reactions; fragments ranging from approximately 100 bp to 10 kb are purified from primers, nucleotides, polymerases and salts. To prevent degradation post purification, PCR products were eluted in Buffer EB (Qiagen Inc.; 10mM Tris-Cl, pH 8.5) and stored at -20° C until needed for further analysis.

3.3.3. Dye terminator DNA sequencing

Purified DNA products were subjected to cycle sequencing using ABI Big Dye Terminator ready reaction kit with *Taq* FS polymerase (134). 2 µl of the purified PCR product were added to 8 µl of a master-mix; master mix contained 2 µl of the ready reaction mix (including *Taq*, ddNTPs, dNTPs, MgCl and buffer), 0.5 µl of a 10 µM unidirectional sequencing primer (either forward or reverse primer from PCR reaction) and 6.5 µl dH₂O. Note: for amplicons less than 100 bp, 1 µl of the purified PCR product was added to 9 µl of a master-mix containing 1 µl of the ready reaction mix, 0.5 µl of a 10 µM primer, and 7.5 ml dH₂O. The reaction mixes were cycle sequenced using optimized sequencing parameters (30 cycles: 95° C for 30 s, 50° C for 20 s, 60° C for 4 min; and then a terminal hold at 4° C).

3.3.3.1. Purification of cycle sequencing product

The cycle sequencing reaction products were cleaned using a Centri-sep 100 spin column (Princeton Separations, Princeton, NJ; (134)). Prior to use, spin columns were hydrated with dH₂O (either for 2 hrs at room temperature or overnight at 4° C) and spun at 750 x g twice, each for 2 min (discarding the flow through between spins). Note: if columns were soaked overnight, 30 min incubation at room temperature was necessary before proceeding further. The entire 10 µl cycle sequencing reaction mixture was then added to the center of the column and spun at 750 x g for 2 min. The flow through was collected and added to 25 µl of a template suppression reagent (ABI). The samples were denatured at 95° C for 4 min and loaded onto an Applied Biosystems 310 Genetic Analyzer for sequence analysis.

3.3.3.2. DNA sequence analysis

Samples were processed using standard analysis parameters provided in the Seq POP6 Rapid (1 ml) E module (Sequence Analysis software v3.3 (ABI)) and analyzed using the CE-1 base-calling algorithm. Computer analyzed base calls were manually edited for accuracy. Sequence comparisons were made ABI Sequence Navigator v1.0.1 software or the SeqLab Analysis platform (Accelrys, San Diego, CA).

3.4. Mathematical Modeling of the Polymerase Chain Reaction Involving Amplification of Multiple Templates with Differing Efficiencies¹.

To explain amplification of templates with different inherent efficiencies, four novel mathematical treatments were developed. Two of the mathematical methods, the relative threshold cycle and mean modified efficiency, are rate-based measures of DNA damage (measuring LBR) based on comparing data taken from the exponential phase of amplification in reactions containing a homogenous population of DNA template; e.g. types and amounts of damage do not vary intrasample. The inherent template efficiency model also uses homogenous input DNA and reports results in terms of modified template reaction efficiency (a measure of LBR) but fits raw PCR data to sigmoid growth curves and creates comparisons based on whole PCR curve kinetics. Damage quantification from cellular DNA involves samples with non-homologous damage and requires modeling proportions of damaged and undamaged template (CoLA); lesion frequency calculations take this into consideration. The rationale for and derivation of each is presented in the following sections.

3.4.1. Lesion bypass rate: the Relative Threshold Cycle method

The relative threshold cycle method was developed to estimate amplification efficiency of synthetic templates containing DNA base modifications thought to impede polymerase progression. Comparisons between data from full-length and internal control region (ICR) reactions were based on observed threshold cycle (C_T) values; the ICR contained no modifications and, therefore, provides a measure of intact template amount. Since the input template amounts in these two PCRs are equal, any increase in C_T must result from a decrease in amplification efficiency. For unmodified templates (e.g. the ICR), if amplification is 100% efficient, the exponential formation of PCR product is

$$x_n = 2^n x_0 \quad \mathbf{1}$$

¹ Novel mathematical formulae were developed in collaboration with Dr. James Denvir, Department of Microbiology, Immunology, and Molecular Genetics, Joan C. Edwards School of Medicine, Marshall University, Huntington, WV.

where (x_n) is the total fluorescence at cycle number (n) and (x_0) is the input template fluorescence at $n = 0$ (140, 144). During amplification of the full-length modified oligonucleotide, unmodified products were formed which then served as templates in subsequent cycles. During the exponential phase of these reactions, the amount of unmodified product (y_n) at cycle number n is

$$y_n = 2y_{(n-1)} + EM \quad \mathbf{2}$$

where (E) is the amplification efficiency of modified templates and (M) is the fluorescence of modified templates. Prior to any amplification, in reactions with modified input template, there was no unmodified template present. With $y_0 = 0$ equation **2** becomes

$$y_n = (2^n - 1)EM \quad \mathbf{3}$$

and the total PCR product (z_n) at cycle n is given by

$$z_n = ((2^n - 1)E + 1)M . \quad \mathbf{4}$$

In order to determine threshold cycle for the ICR and full-length PCRs, a threshold fluorescence (T) , fixed for all reactions was chosen, which was sufficiently larger than the background fluorescence but small enough that the reaction was still in the exponential phase. The cycles at which the ICR and full-length PCRs reach the threshold level are designated C_{TU} and C_{TM} respectively. By substitution into equations **1** and **4**, equations that relate threshold fluorescence to cycle number for the ICR were derived;

$$T = 2^{C_{TU}} x_o \quad \mathbf{5}$$

and for the full-length PCR

$$T = ((2^{C_{TM}} - 1)E + 1)M . \quad \mathbf{6}$$

If $M = x_0$ for a given template, equating equations **5** and **6** and solving for E produces:

$$E = (2^{C_{TU}} - 1)/(2^{C_{TM}} - 1) . \quad \mathbf{7}$$

This equation can be approximated to produce the simpler equation

$$E \cong 2^{C_{TU} - C_{TM}} \quad \mathbf{8}$$

which represents the Relative Threshold Cycle (RTC) amplification efficiency. If $C_{TM} \geq C_{TU}$ and $C_{TM} > 11$ the error of this last approximation is less than 0.1%.

3.4.2. Lesion bypass rate: the Mean Modified Efficiency method

The RTC calculations require two assumptions: 1) the efficiency of the PCRs of small DNA templates must be equal and close to 100% and 2) the input template amounts must be held constant between reactions. To eliminate these assumptions and provide a more precise means to quantify differences in PCRs containing damaged DNA template, the mean modified efficiency (MME) method was created.

In general, exponential amplification of DNA template is given by

$$x_n = (1 + E)x_{n-1}, \text{ or } x_n = (1 + E)^n x_0, \quad \mathbf{9}$$

where (x_n) is the total fluorescence at cycle (n) , and (E) is the amplification efficiency. Modified templates generate unmodified template at one efficiency and these PCR derived unmodified templates then amplify at a different efficiency (usually higher). In reactions containing templates with differing amplification efficiencies,

$$x_n = (1 + E_u)x_{n-1} + E_m M \quad 10$$

where x_n is the fluorescence of unmodified templates at cycle n , (E_u) is the efficiency of unmodified templates, (E_m) is the efficiency of modified templates, and (M) is the constant fluorescence due to the modified templates. E_u is solved for separately using equation **17** as shown in the *Numerical Bootstrapping* section of Materials and Methods. There is no unmodified template at the beginning of the PCR. When $x_0 = 0$, equation **10** has the following solution:

$$x_n = \frac{E_m M}{E_u} [(1 + E_u)^n - 1] \quad 11$$

Since x_n represents only the fluorescence due to unmodified templates, the total fluorescence, t_n , is given by

$$t_n = \frac{E_m M}{E_u} [(1 + E_u)^n - 1] + M . \quad 12$$

Equation **12** represents a model explaining the PCR containing competing templates with differing amplification efficiencies. In many treatments of similar analysis (for example, (138-139, 141)), the values of x_n are normalized to a control gene in order to determine relative fold increases in PCR product. Since the aim of this method is to arrive at an absolute measure of efficiency, M , x_n , and t_n here refer to background subtracted, raw fluorescence values. For this reason, a value for M , the initial fluorescence of modified template, must be derived (described in the *Numerical bootstrapping* section).

For any given set of data, the threshold cycle number C_T and a given threshold fluorescence T , equation **12** becomes

$$T = \frac{E_m M}{E_u} \left[(1 + E_u)^{C_T} - 1 \right] + M . \quad 13$$

Equation **13** can then be solved for the efficiency (E_m) of the modified templates

$$E_m = \frac{E_u (T - M)}{M [(1 + E_u)^{C_T} - 1]} \quad 14$$

3.4.2.1. Mean Modified Efficiency: numerical bootstrapping

In order to solve for modified efficiencies with equation **14**, it was necessary to generate values for the C_T , T , M , and E_u . The value of C_T is directly related to an arbitrary threshold value T and therefore determined experimentally. In order to derive the initial fluorescence of modified template M , internal control primers were used to amplify the unmodified ICR of the oligonucleotide templates. Using template concentrations that ranged over five orders of magnitude, C_T values (N=5) were collected, plotted against the base \log_{10} of the template concentration, and the slope (m) of the best fit line determined. The efficiency was then computed using a standard method for amplification efficiency calculation

$$E = 10^{-(1/m)} - 1 . \quad 15$$

The initial fluorescence value x_0 for each input template could be defined using the 45 base pair reaction data and the equation

$$x_0 = \frac{T}{(1 + E)^{C_T}} . \quad 16$$

Since the same template stocks are used for both the 45-mer and 90-mer experiments, it was appropriate to use the input fluorescent values x_0 from ICR data as input measures for 90-mer fluorescent values M .

The efficiency of the PCR derived unmodified templates E_u was computed in the same manner as the internal control reaction efficiencies using equation 15.² The efficiency of the modified templates E_m could then be determined using equation 14.

3.4.3. Lesion bypass rate: the Inherent Template Efficiency method

Despite eliminating assumptions necessary for the RTC estimation, the MME is limited to the portion of the PCR curve where amplification is exponential and also requires the amplification of a template at multiple input amounts. PCR kinetic data, derived from whole curve analysis, has been used to determine input template amounts and reaction efficiencies (141). In addition to looking at all the data points of a PCR curve, this method can determine these variables from a single PCR.

Sigmoid growth curves can be explained by

$$R_n = \frac{(R_{\max})}{(1 + e^{-(n-n_{1/2})/(k)})} \quad 17$$

where (R_n) is the quantity of template at cycle (n), (R_{\max}) is the maximum (plateau) value, ($n_{1/2}$) is the cycle at which R_n reaches $\frac{1}{2} R_{\max}$, and (k) is related to the efficiency of the reaction by

$$E = e^{1/k} - 1. \quad 18$$

Equation 18 satisfies the relationship

$$\Delta R_n = (1/(R_{\max})) (R_n / k) (R_{\max} - R_n), \quad 19$$

so that (ΔR_n) is proportional both to the amount of template already present, and to the amount of potential template left for the reaction to create.

² In theory, for the equation for our modified templates this data should no longer exactly fit a straight line. However the deviation from a straight line is of the order of $\frac{M}{K}$, which is negligible.

To derive a formula to incorporate the variable of having modified template present at the onset of the reaction, an analogy to ΔR_n above can be made, noting that the modified and unmodified templates will create new templates but with different efficiencies. To this end, let R_{nu} represent the amount of unmodified template in the reaction after n cycles and X_o represent the amount of modified template present (a constant). The rate of change of R_n is assumed proportional to $(x_o / a) + (R_n / b)$, and the amount of template the reaction is still able to create equates to $(R_{max} - R_n)$. That gives

$$\Delta R_n = (1/(R_{max}))((x_o / a) + (R_n / b))(R_{max} - R_n) \quad 20$$

where (a) and (b) are interpreted by

$$E_m = e^{1/a} - 1 \quad 21$$

and

$$E_u = e^{1/b} - 1; \quad 22$$

E_m is the efficiency of the modified template and E_u is the efficiency of the unmodified template. Equation 20 has the solution:

$$R_n + x_o = \frac{x_o + R_{max} (1 - e^{-n((1+bx_o)/(abR_{max}))})}{(1 + (aR_{max})/(bx_o))e^{-n((a+bx_o)/(abR_{max}))}} \quad 23$$

representing the Inherent Template Efficiency (ITE) where $(R_n + x_o)$ is the total template in the reaction.

3.4.4. Calculation of lesion abundance: determination of Lesion Frequency using C_T values

Equations **8**, **14**, and **23** (RTC, MME, and ITE respectively) represent measures of reaction rate for modified DNA template. These formulae assume that no unmodified templates are present at the beginning of each PCR. Therefore, strictly speaking, they do not represent meaningful measures of damage in cellular DNA due to the likelihood that cellular DNA would be a mixture of modified and unmodified template. For the successful adaptation of real-time PCR as a polymerase stop based assay for biologically significant DNA damage quantification, changes in C_T values must be redefined as lesion frequency, rather than reaction rate.

For polymerase chain reaction with efficiency (E), the number of target DNA molecules (x_n) after (n) cycles of the reaction is given by

$$x_n = (1 + E)^n x_0, \quad (144) \quad 24$$

where x_0 denotes the number of input DNA molecules.

In this assay, undamaged (control) DNA are amplified and compared to the amplification of damaged DNA. The aim is to estimate the proportion (p) of damaged bases in the DNA from the treated sample material. Previous work suggests the major DNA lesion created by UV radiation effectively blocks the PCR (151); the assumption that cellular DNA containing one or more damaged bases in the target region does not contribute to the reaction can therefore be made. Denoting the length of the target DNA molecule by N , the probability that an input molecule is undamaged over the whole length of the target is $(1-p)^N$. Thus the number of input molecules contributing to the reaction is $(1-p)^N x_0$. Thus, for damaged DNA with lesion frequency (p) the reaction is modeled by the equation

$$x_n = (1 + E)^n (1 - p)^N x_0. \quad 25$$

A threshold value (T) common to both the reaction for damaged and undamaged

templates was chosen, and input templates held constant as described above. The fractional cycle number at which the reaction reached the threshold was measured. For the reaction with undamaged DNA this threshold cycle is denoted as C_U ; for damaged DNA this threshold cycle is C_D . Applying equations (1) and (2) with $x_n=T$, produced

$$T = (1 + E)^{C_U} x_0, \text{ and}$$

$$T = (1 + E)^{C_D} (1 - p)^N x_0 .$$

Equating these two expressions for T gives

$$(1 + E)^{C_U} x_0 = (1 + E)^{C_D} (1 - p)^N x_0, \text{ and so}$$

$$(1 + E)^{C_U - C_D} = (1 - p)^N .$$

Denoting $C_U - C_D = \Delta C_T$, produced

$$(1 + E)^{\Delta C_T / N} = 1 - p, \text{ or}$$

$$p = 1 - (1 + E)^{\Delta C_T / N} .$$

26

It is important to note: theoretically, these two methods, the rate of lesion bypass (*RTC*, *MME*, and *ITE*) and the proportion of damaged bases at the beginning of the PCR (*lesion frequency*) can be used in combination to produce a more accurate measure of DNA damage. In addition, by amplifying two target lengths, both LBR and LF can be determined using more advanced formulae (Appendix E). Currently, limitations in instrument precision prevent this from being possible.

CHAPTER IV

Results

4.1. Quantification of DNA Damage

4.1.1. Modified oligonucleotides as templates for the PCR

To characterize the influence of defined lesions, both in terms of LBR and LIM, on the PCR, a series of 90-base oligonucleotides containing 8-oxodG, 8-oxodA, abasic site, or TT Dimer modifications were synthesized for amplification by the PCR (Table 3.1, Figure 4.1A). These modifications were selected because they are prevalent products of damage induced by oxidation and irradiation (15). To ensure oligonucleotide homogeneity, synthesis products were analyzed by nanochip electrophoresis (Figure 3.2), Maldi-TOF (Figure 3.3), PAGE (Figure 4.2), and high percentage agarose gel electrophoresis (data not shown) separation techniques. In all gel based separation methods, an apparent decrease in oligonucleotide fluorescence correlated with increased numbers of inserted 8-oxodG bases (Figures 3.2, 4.2).

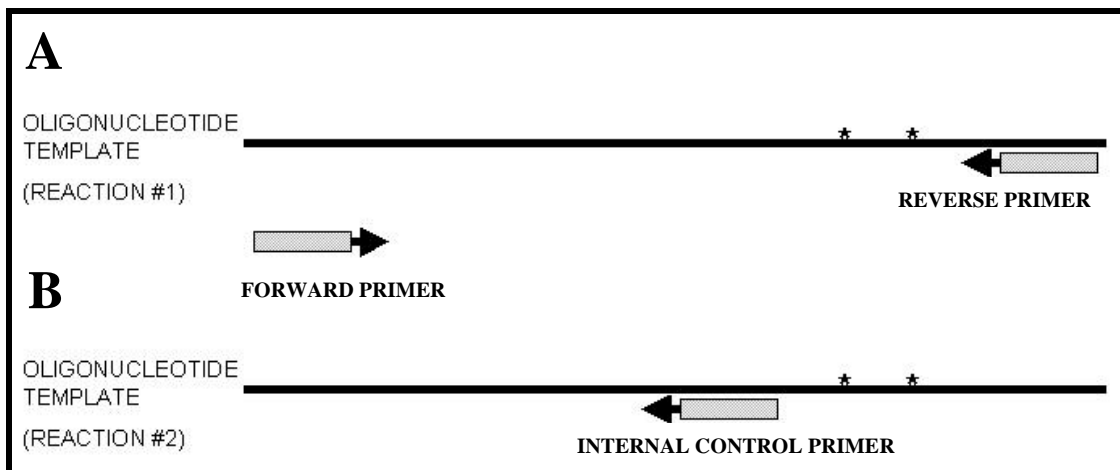


Figure 4.1. Model of oligonucleotide amplification. A) Amplification of the full-length oligonucleotides differing only in the type and number of modified bases. Any difference observed during amplification can be attributed to the incorporated modified bases and their influence on the PCR. B) Amplification of the internal control region (ICR); this ICR contains no modification and therefore amplifies with the same efficiency in each template providing the ability to quantify input template amounts and normalize concentrations in subsequent calculations. * represents sites of modified DNA bases.

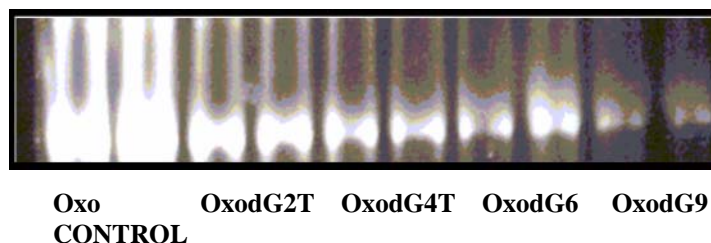


Figure 4.2. Polyacrylamide gel electrophoresis of 90-mer oligonucleotides. Oligonucleotides which contained increasing amounts of 8-oxodG modifications presented decreased staining intensities; each lane contained 20 pmol of oligonucleotide; each oligonucleotide was run in duplicate. Complete sequences of oligonucleotides are found in Table 3.1.

The decrease in dye binding as the number of tandem 8-oxodGs increases can be partially explained by a decrease in stable secondary structure. During cycle sequencing reactions containing no sequencing primer, Oxo CONTROL and OxodG2T oligonucleotides folded back upon themselves and auto-sequenced (Figures 4.3B and 4.3C respectively). This suggested that stable structures could form in the 90-mers at cycle sequencing extension temperatures. Auto-sequencing was perturbed as the number of tandem 8-oxodGs increased (OxodG4T and OxodG6; Figures 4.3D and 4.3E, respectively). This disruption of secondary structure would in turn result in decreased dye intercalation.

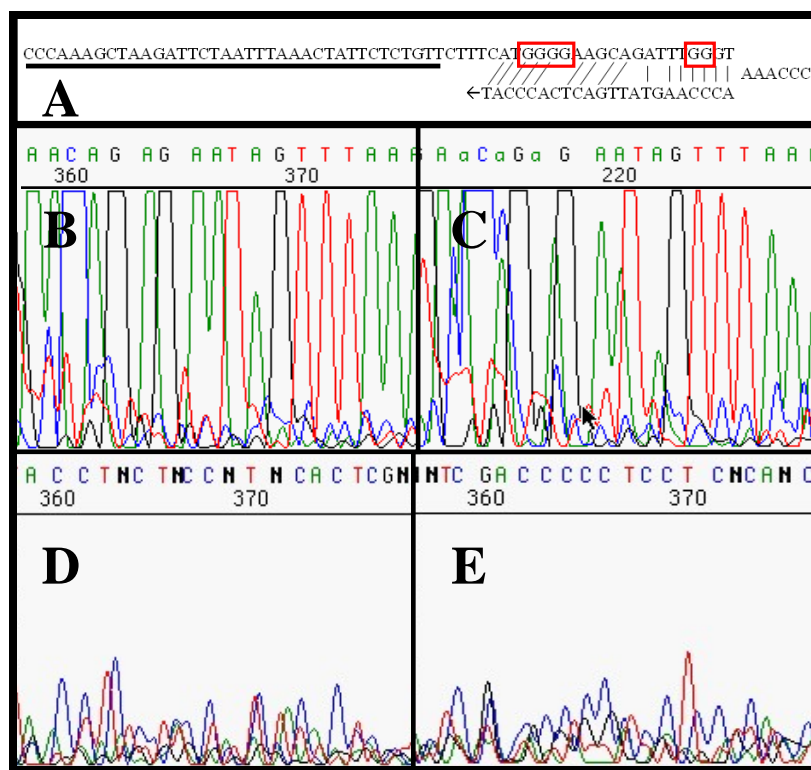


Figure 4.3. Auto-sequencing of 90-mer oligonucleotides. Black, green, red, and blue represent guanine, adenine, thymine, and cytosine bases respectively. A) The schematic represents a potential hairpin at the 3' end of the oligonucleotides. The potential sites of 8-oxodG modification are boxed in red; the underscored area represents total readable sequence in auto-sequencing reactions. 90-mer oligonucleotides, B) Oxo CONTROL, C) OxodG2T, D) OxodG4T, and E) OxodG6, were subjected to cycle sequencing as described in the materials and methods but without a sequencing primer. During these reactions, auto-sequencing occurred originating at the 3' end of the 90-mers (B,C) which was eliminated by the addition of multiple tandem 8-oxodG modifications (D,E).

Since oligonucleotides are synthesized in the 3' to 5' direction; an internal primer was developed to amplify a 45 base control region (ICR) on the 5' end of the oligonucleotides and confirm the synthesis of full-length template (Figure 4.1B). Positive amplification of this region indicated the presence of intact oligonucleotide. The benefits of this oligonucleotide model include the ability to control the amount, positioning, and specificity of DNA base modification during synthesis, as well as the elimination of any PCR inhibitors possibly present in cellular DNA. Oligonucleotide templates were amplified and PCR products compared after separation by agarose gel electrophoresis (Figure 4.4). After 40-cycles in the PCR, all oligonucleotides produced both full-length and ICR products; approximately 90 and 45 bps, respectively. This implied that the

templates were full-length and that the DNA modifications did not completely block polymerase progression as suggested previously (5).

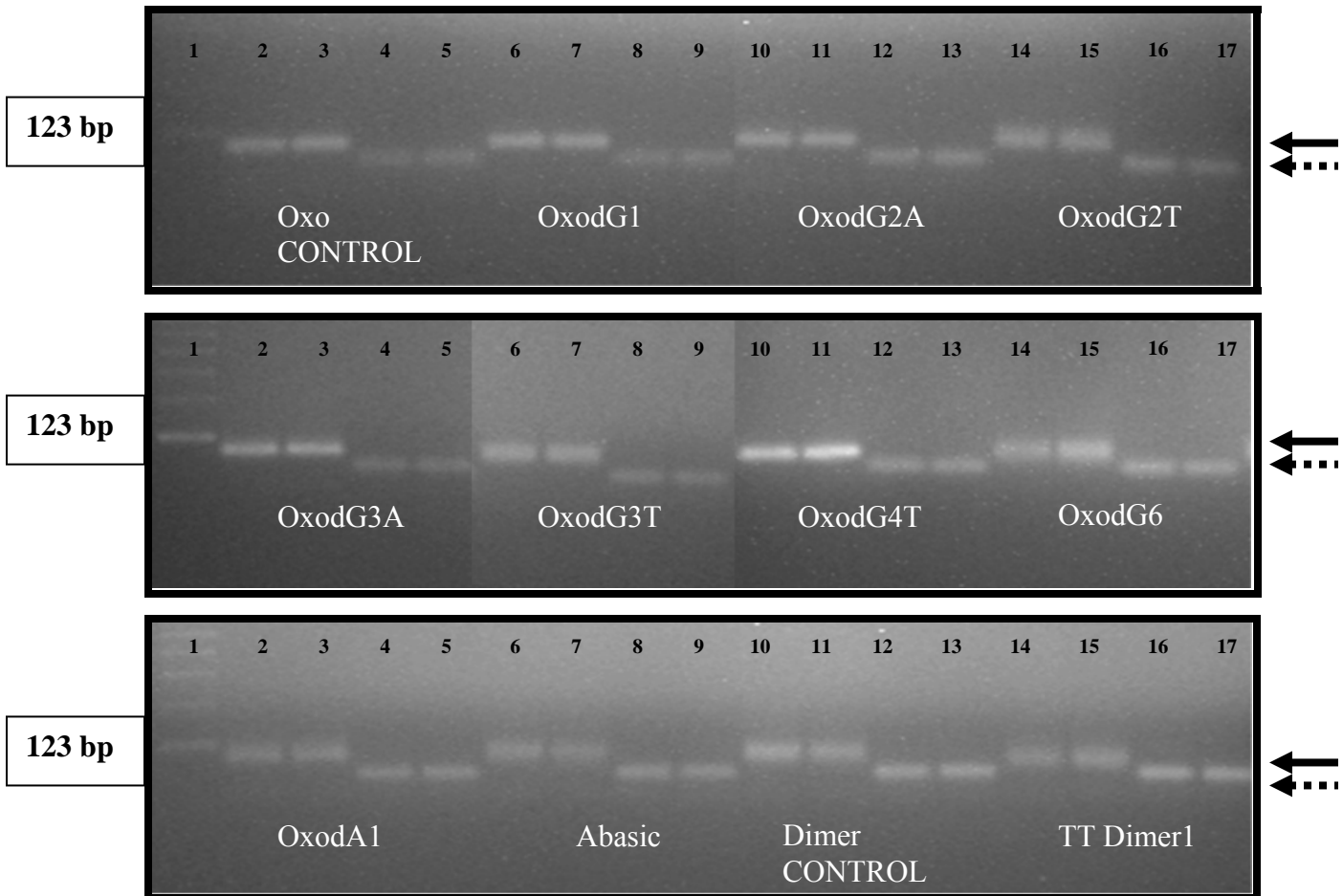


Figure 4.4. Product gels from PCRs with 90-mer oligonucleotides templates. Products obtained from full-length (←) and ICR (←···) reactions were electrophoresed through agarose in duplicate; sizes were approximately 90 and 45 base pairs respectively. Lane 1 is a 123 base DNA mass ladder; lanes 2-3, 6-7, 10-11, and 14-15 are full-length amplicons; lanes 4-5, 8-9, 12-13, and 16-17 are ICR amplicons.

4.1.1.1. Increasing the number of tandem 8-oxodG alters product formation.

To determine if tandem 8-oxodG modifications changed the amplification rate in the PCRs, a subset of oligonucleotides were amplified for 25 cycles (Figure 4.5). While the band intensities from the full-length Oxo CONTROL reactions mimicked those of the Oxo CONTROL ICR PCRs, bands from the full-length reaction products of OxodG2T decreased and those from the OxodG4T and OxodG6 were not detected. The presence of ICR PCR products from OxodG2T, OxodG4T, and OxodG6 indicated the apparent

decrease in full-length products was not due to lack of available oligonucleotide template. The observed differences in full-length product formation at cycle 25 versus cycle 40 from PCRs containing templates with tandem 8-oxodG modifications (e.g. OxodG4T; Figures 4.4, 4.5) signified that the plateau phase of the reaction was delayed as a result of tandem 8-oxodG base modifications.

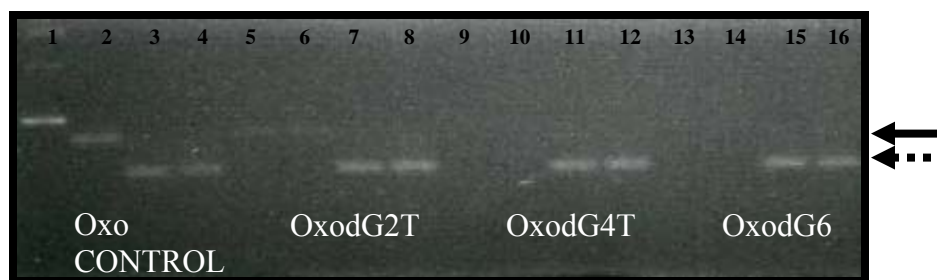


Figure 4.5. Product formation is delayed in PCRs with tandem 8-oxodGs. PCRs were stopped after 25 cycles; products were obtained from full-length (←) and ICR (← ···) reactions and electrophoresed through agarose in duplicate. Sizes were approximately 90 and 45 base pairs respectively. Lane 1 is a 123 base DNA mass ladder; lanes 2, 5-6, 9-10, and 13-14 are full-length products; Lanes 3-4, 7-8, 11-12, and 15-16 are ICR products. PCR products from full-length Oxo CONTROL reactions were unaffected by shortened cycling numbers, where as products from OxodG2T reactions decreased; full-length products from OxodG4 and OxodG6 were not detected. ICR reactions produced products from each template that mimicked 40 cycle results (Figure 4.4).

4.1.1.2. Base modifications perturb amplification efficiency to different degrees

To further investigate band differences between 25 and 40 cycle PCR data, the ABI 7000 Sequence Detection System was used to amplify both the full-length and ICRs from the 90-mer oligonucleotides (Figures 4.6-4.8). ICR amplification curves from reactions containing the Oxo and Dimer CONTROLS were equivalent to amplification curves from their respective full-length reactions (Figures 4.6, 4.8). This indicated that, devoid of any base modification, both amplification targets react similarly during the PCR. ICR curves from each template, when compared with one another, were superimposable demonstrating that template amounts were equal and that the ICR amplified with the same efficiency in each template (data not shown). While the full-length amplification curves from the controls mimicked the ICR curves, there were substantial right-shifts in the OxodA1, OxodG3A, OxodG2T, OxodG3T, OxodG4T, OxodG6, and Abasic amplification curves (Figure 4.7). A right-shift was also observed in the amplification of the full-length TT dimer template (Figure 4.8).

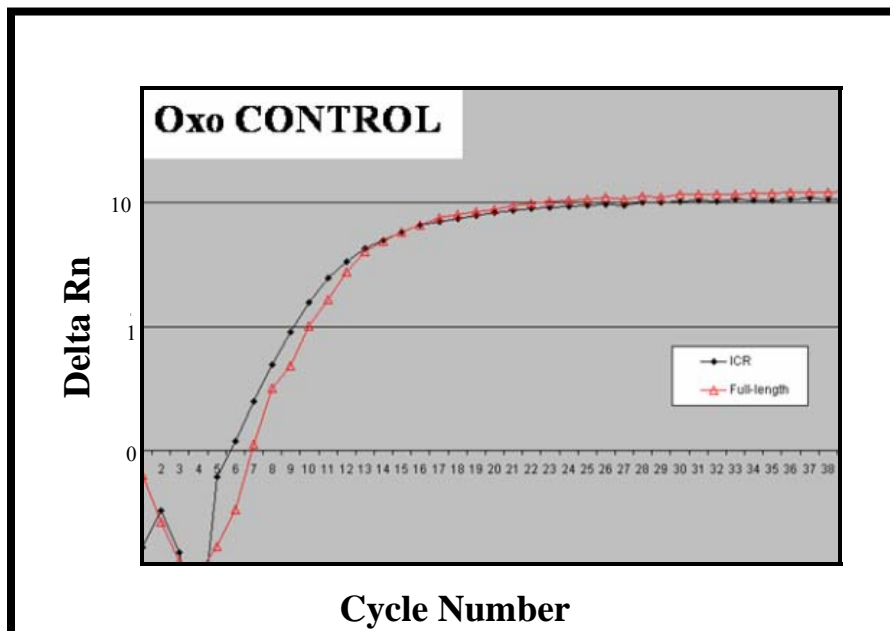


Figure 4.6. Amplification of unmodified Oxo CONTROL oligonucleotide in real-time. Oxo CONTROL templates containing no base modification were amplified (1fmole; N=5) using primers targeted for the 45 bp (—◆—) ICR and the (—△—) full-length oligonucleotide (85 bp PCR product). Delta Rn is the baseline subtracted PCR product fluorescence normalized to an internal dye (ROX).

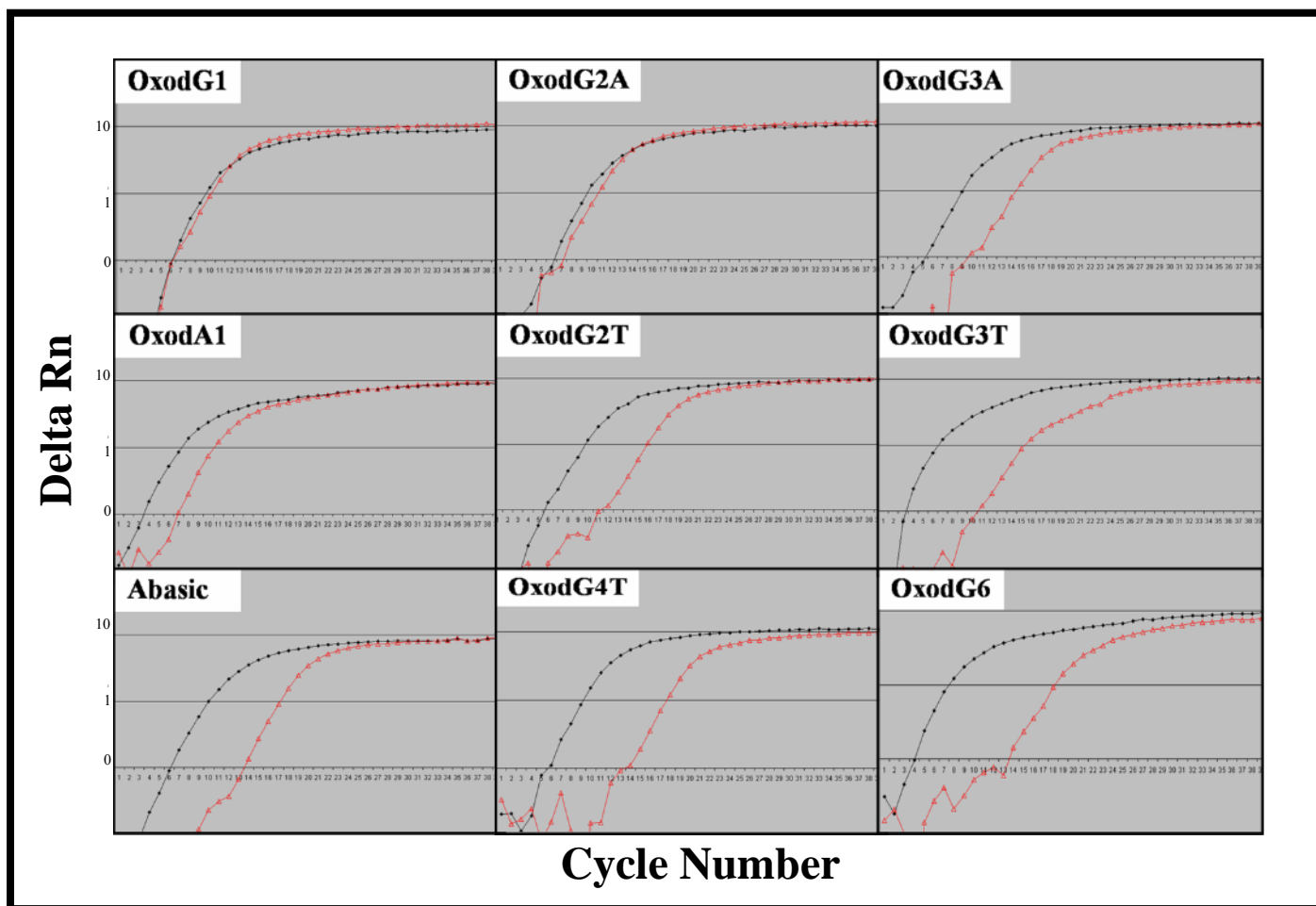


Figure 4.7. Amplification of oligonucleotides containing modified bases. Nine oligonucleotides containing varying types and amounts of base modification were amplified (1fmole; N=5) using primers targeted for the (\blacklozenge) ICR and the (\blacktriangle) full-length oligonucleotide (85 bp PCR product). Delta Rn is the baseline subtracted PCR product fluorescence normalized to an internal dye (ROX). A rightward shift in amplification profiles increased as the amount of modification to the oligonucleotide increased. In addition, shifts in amplification profiles varied depending on the specificity of base modification on the input template. Once *Taq* DNA polymerase bypassed the site of modification, a full-length PCR derived unmodified amplicon was created and resulted in curve shapes that mimicked the unmodified Oxo CONTROL (Figure 4.6). All data sets span cycles 1 through 40.

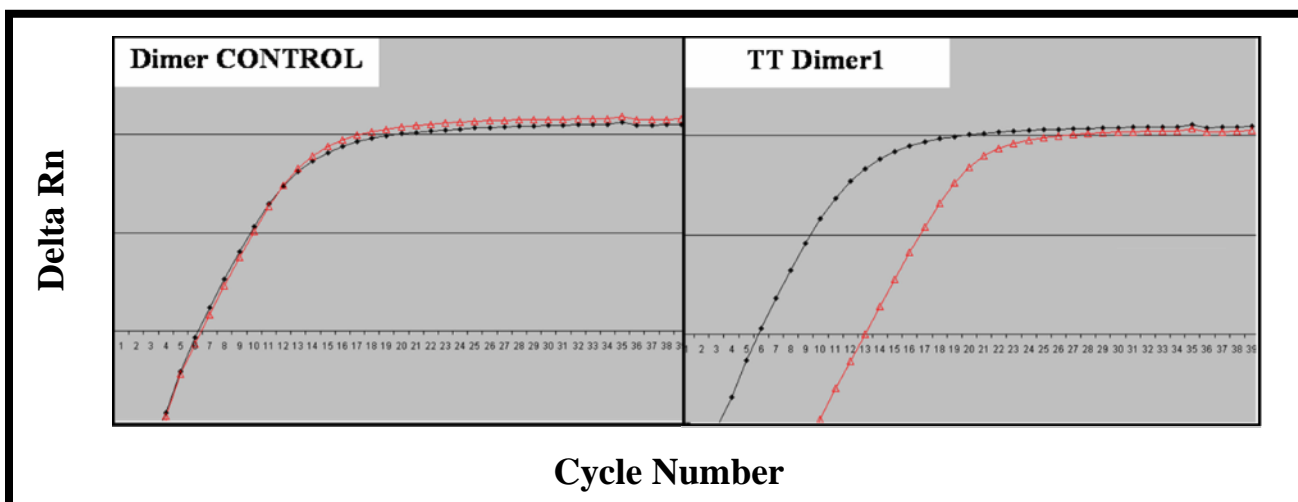


Figure 4.8. Amplification of oligonucleotides containing a *cis-syn* thymidine dimer modification. Oligonucleotides containing a *cis-syn* thymidine dimer were amplified (1fmole; N=5) using primers targeted for the (—◆—) ICR and the (—△—) full-length oligonucleotide (85 bp PCR product). Delta Rn is the baseline subtracted PCR product fluorescence normalized to an internal dye (ROX). A rightward shift in amplification profiles occurred in reactions with modified template that was not observed in the Dimer CONTROL.

Amplification of the ICRs (Figures 4.6-4.8) provides a measure of oligonucleotide quantity and quality. Relative input template amounts were calculated using an adaptation of the $2^{-\Delta\Delta CT}$ based method described by Livak *et al.* (2001) ($2^{-\Delta CT}$; Tables 4.1, 4.2; (141)).

Table 4.1. Relative input template amounts from ICR amplification data.

Sample	Mean C_T ^a	S. D. C_T ^b	$2^{-\Delta CT}$	Relative Change ^c
Oxo CONTROL	10.1	0.22	1.00	0.0%
OxodG1	9.57	0.31	1.47	46.6%
OxodG2A	9.47	0.37	1.57	56.9%
OxodG2T	10.0	0.11	1.05	4.5%
OxodG3A	9.91	0.17	1.15	15.4%
OxodG3T	13.0	0.34	0.14	-86.5%
OxodG4T	10.1	0.05	1.05	4.9%
OxodG6	10.2	0.06	0.94	-6.4%
OxodA1	10.5	0.06	0.76	-23.6%
Abasic	10.0	0.03	1.06	6.0%
Dimer CONTROL	10.3	0.35	0.88	-12.4%
TT Dimer1	10.1	0.09	1.04	4.4%

a- Mean C_T values were calculated by averaging five amplifications of the ICR target, each containing 1 fmole of input DNA, at a threshold (T) of 1.0.

b- S. D. C_T is the standard deviation of the threshold hold cycle values used to compute Mean C_T .

c- Relative change determined by comparison to Oxo CONTROL data.

In data taken from ICR reactions, relative changes in input template amounts ranged from an 86% decrease (OxodG3T) to a relative increase of 57% (OxodG2A), with the majority of input template amounts differing by less than 25%; when compared with Oxo CONTROL amplification results (Table 4.1). This indicated that most oligonucleotide concentrations were equivalent to that of the Oxo CONTROL. Data from full-length reactions provided a much wider range of variation; from a 99.9% decrease (OxodG6) to an 86% increase (Dimer CONTROL) in copy number with the majority of input template amounts differing by greater than 80% when compared with the Oxo CONTROL (Table 4.2).

Table 4.2. Relative input template amounts from 90-mer amplification data^a.

Sample	Mean C_T	S. D. C_T	$2^{-\Delta CT}$	Relative Change
Oxo CONTROL	11.0	0.26	1.00	0.0%
OxodG1	11.1	0.35	0.937	-6.3%
OxodG2A	11.1	0.05	0.916	-8.4%
OxodG2T	17.1	0.09	0.014	-98.6%
OxodG3A	15.8	0.09	0.036	-96.4%
OxodG3T	21.4	0.25	0.001	-99.9%
OxodG4T	18.4	0.04	0.006	-99.4%
OxodG6	21.5	0.08	0.001	-99.9%
OxodA1	13.6	0.07	0.162	-83.8%
Abasic	17.1	0.04	0.014	-98.6%
Dimer CONTROL	10.1	0.21	1.86	86.3%
TT Dimer1	17.3	0.12	0.013	-98.7%

a- Calculated as described in Table 4.1.

The formula used to calculate input template amounts in these tables assumes constant and equivalent reaction efficiency during exponential phase (141). Therefore, when using $2^{-\Delta CT}$ based mathematics, any difference in C_T values is reported as a difference in input template amount (141). Given the large discrepancies in apparent input template amount between the two sets of data (Tables 4.1, 4.2) and that reactions differed only by the presence of DNA base modification on the full-length target template, a conclusion that DNA modifications influenced the number of cycles needed to reach threshold fluorescence could be drawn.

Since the ICR in each oligonucleotide contains no DNA modification, template amounts calculated from ICR data are a correct representation of input template quantity. Therefore, the observed right-shifting of the amplification curves (Figures 4.6-4.8) in the full-length reactions (OxodA1, Abasic, TT Dimer1, and various templates with tandem OxodGs) must result from substantially reduced amplification efficiencies.

4.1.1.3. Lesion bypass rate: estimation of RTC efficiency for unmodified and modified templates

The relative threshold cycle (RTC) method was developed to quantify differences in the rates of amplification of modified templates (151). The RTC method compares C_T

data from the ICR (C_{TU}) and full-length (C_{TM}) reactions and reports results as changes in amplification efficiency. C_{TU} and C_{TM} were determined at six template amounts (1 amole to 100 fmole) for each oligonucleotide and the respective RTC efficiencies for each calculated using equation 8 (Tables 4.3-4.5). In early real-time PCR cycles, replication of the full-length modified oligonucleotide gave rise to unmodified PCR products which were exponentially amplified in subsequent cycles. Even though the amplification curves of unmodified and some modified templates had similar exponential phases, a rightward shift in the curves of templates with single 8-oxodA, abasic site, or TT dimer modifications and amplification curves of template with three non-adjacent or two-plus tandem 8-oxodGs were observed (Figures 4.6-4.8). These shifts stemmed from prolonged lag phases that could be described as a difference in C_T values and which then translated into RTC efficiencies.

The average RTC efficiency of the Oxo CONTROL was 0.544. The observation that Oxo CONTROL template RTC efficiency was less than 1.0 suggests that the inherent efficiency of the ICR was higher than that of the full-length template reaction. In order to prepare an appropriate control template for the TT dimer template, several thymidine substitutions in the Oxo CONTROL template were made (Table 3.1). It is interesting to note that the RTC efficiency from this Dimer CONTROL (1.03) was greater than that of Oxo CONTROL (0.544; Tables 4.3, 4.5). This difference could be explained by a reduction in the stability of secondary structure in the Dimer CONTROL template at PCR extension temperatures (Figures 4.9, 4.10), brought on by the aforementioned sequence change and resulted in improved *Taq* progression. These observations emphasize a need for matched template controls in the RTC and other direct C_T comparison methods.

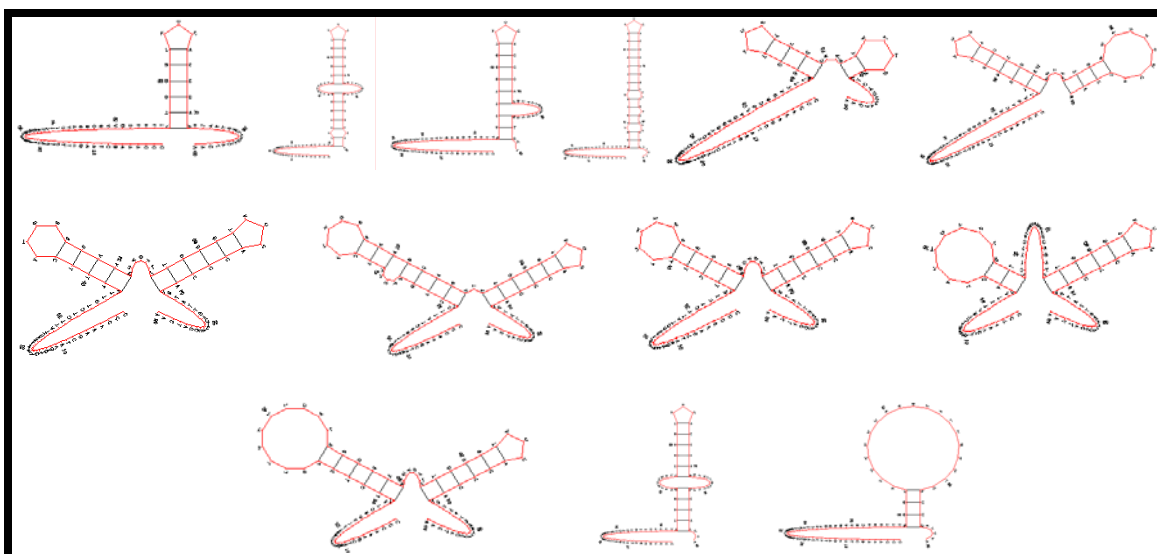


Figure 4.9. Predicted secondary structures of 90-mer Oxo CONTROL oligonucleotide sequence. The Oxo CONTROL oligonucleotide sequence was found to form 13 stable secondary structures at the PCR extension temperature (60° C). Structures are presented in order of decreasing stability; with the top-left being the most stable; energies ranged from -2.4 to -0.4 kcal/mole. Secondary structure predictions were computed using m-fold software (SeqLab Accelrys, San Diego, CA).

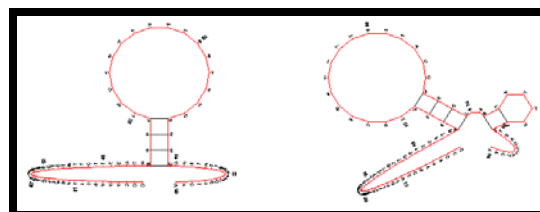


Figure 4.10. Predicted secondary structures of 90-mer Dimer CONTROL oligonucleotide sequence. The Dimer CONTROL oligonucleotide sequence was found to form 2 stable secondary structures at the PCR extension temperature (60° C). Structures are presented in order of decreasing stability; with the top-left being the most stable; energies were -0.7 and -0.1 kcal/mole respectively. Secondary structure predictions were computed using m-fold software (SeqLab Accelrys, San Diego, CA).

While the RTC efficiency of the Oxo CONTROL and OxodG1 templates showed no statistically significant difference ($p = 0.05$), the mean RTC efficiencies of the OxodA1 and Abasic were 0.114 and 0.009 which represented decreases of 81.2% and 98.5% respectively when compared to the Oxo CONTROL template (significantly

different at $p < 0.001$ in both cases; Table 4.3). The mean RTC efficiency from the TT Dimer1 template was 0.0079 which, when compared to the Dimer CONTROL template, represented a 99.2% decrease in RTC efficiency (significantly different at $p < 0.001$; Table 4.5). These observations, taken together, implied that different lesions on input DNA template altered amplification to differing degrees.

The amount and position of 8-oxodG modifications relative to one another influenced the PCR (Tables 4.3, 4.4). As the number of non-adjacent 8-oxodG modifications was increased (OxodG1, OxodG2A, and OxodG3A), the observed mean RTC efficiencies decreased (0.407, 0.313, and 0.018 respectively). When compared with the Oxo CONTROL, OxodG3A RTCs were reduced by 97% (statistically significant at $p < 0.001$). While the presence of two 8-oxodG modifications separated by 13 bases (OxodG2A) had no statistically significant impact on RTC efficiency, the mean RTC efficiency from reactions containing templates with two adjacent 8-oxodGs (OxodG2T) was 0.0214. This represented a 96% decrease in comparison to the Oxo CONTROL (significantly different at $p < 0.001$). The further addition of adjacent 8-oxodG modifications continued to impact RTC efficiency; decreasing RTC to 0.0035 for OxodG3T reactions (a 99% reduction; Table 4.4). Taken together, these data suggested that the progression of *Taq* polymerase was influenced by the number of and strongly impeded by the juxtaposition of 8-oxodG bases.

Table 4.3. RTC amplification efficiencies of templates with non-adjacent lesions.

	Input Template	Mean C_{TU}^a	Mean C_{TM}^a	ΔC_T (U-M)	RTC^b	Mean RTC	S.D.	C.V.^c
Oxo CONTROL	100fmole	3.93	4.16	-0.233	0.851	0.544	0.175	0.32
	10fmole	6.49	7.17	-0.679	0.625			
	1fmole	10.1	11.0	-0.874	0.546			
	100amole	13.4	14.5	-1.14	0.455			
	10amole	16.4	17.8	-1.34	0.396			
	1amole	19.9	21.2	-1.36	0.391			
OxodG1	100fmole	3.41	4.32	-0.910	0.532	0.407	0.123	0.30
	10fmole	5.97	6.81	-0.843	0.557			
	1fmole	9.57	11.1	-1.52	0.349			
	100amole	12.9	15.0	-2.05	0.241			
	10amole	16.1	17.3	-1.20	0.434			
	1amole	19.5	21.1	-1.60	0.330			
OxodG2A	100fmole	3.46	4.83	-1.37	0.388	0.281	0.150	0.53
	10fmole	6.22	7.26	-1.04	0.488			
	1fmole	9.47	11.1	-1.65	0.319			
	100amole	12.6	14.5	-1.90	0.267			
	10amole	15.9	19.2	-3.24	0.106			
	1amole	19.4	22.5	-3.08	0.119			
OxodG3A	100fmole	4.34	9.19	-4.86	0.0345	0.0185	0.00840	0.45
	10fmole	6.74	12.4	-5.62	0.0204			
	1fmole	9.91	15.8	-5.86	0.0172			
	100amole	13.2	19.3	-6.14	0.0142			
	10amole	16.4	22.8	-6.43	0.0116			
	1amole	19.5	25.7	-6.24	0.0133			
OxodA1	100fmole	4.80	7.65	-2.85	0.139	0.114	0.0222	0.20
	10fmole	7.30	10.2	-2.87	0.137			
	1fmole	10.5	13.6	-3.11	0.116			
	100amole	13.8	16.9	-3.11	0.116			
	10amole	17.2	20.7	-3.45	0.0914			
	1amole	20.4	24.0	-3.55	0.0852			
Abasic	100fmole	4.37	10.4	-6.06	0.015	0.0090	0.00310	0.35
	10fmole	6.90	13.6	-6.71	0.0096			
	1fmole	10.0	17.1	-7.11	0.0073			
	100amole	13.5	20.6	-7.11	0.0072			
	10amole	16.8	23.9	-7.12	0.0072			
	1amole	20.2	27.2	-7.07	0.0075			

a- Mean C_{TU} and C_{TM} values were calculated by averaging five amplifications of the ICR and full-length targets at a threshold (T) of 1.0.

b- RTC efficiencies were derived using equation 8 (151).

c- C.V. is the coefficient of variation calculated by dividing the standard deviation of the RTC by the mean RTC.

Table 4.4. RTC amplification efficiencies of templates with adjacent lesions^a.

	Input Template	Mean C_{TU}	Mean C_{TM}	ΔC_T (U-M)	RTC	Mean RTC	S.D.	C.V.
Oxo CONTROL^b	100fmole	3.93	4.16	-0.233	0.851	0.544	0.175	0.32
	10fmole	6.49	7.17	-0.679	0.625			
	1fmole	10.1	11.0	-0.874	0.546			
	100amole	13.4	14.5	-1.14	0.455			
	10amole	16.4	17.8	-1.34	0.396			
	1amole	19.9	21.2	-1.36	0.391			
OxodG2T	100fmole	4.07	10.1	-6.01	0.0156	0.0096	0.0032	0.34
	10fmole	6.83	13.6	-6.74	0.00940			
	1fmole	10.1	17.1	-7.08	0.00740			
	100amole	13.5	20.6	-6.95	0.00809			
	10amole	16.6	23.8	-7.21	0.00670			
	1amole	19.7	26.3	-6.62	0.0102			
OxodG3T	100fmole	6.50	14.4	-7.93	0.0041	0.0035	0.0009	0.26
	10fmole	9.34	17.7	-8.32	0.0031			
	1fmole	13.0	21.4	-8.38	0.0030			
	100amole	16.1	24.7	-8.57	0.0026			
	10amole	19.4	27.6	-8.28	0.0032			
	1amole	22.5	30.1	-7.60	0.0052			
OxodG4T	100fmole	4.01	11.8	-7.78	0.0046	0.0038	0.0010	0.25
	10fmole	7.08	15.2	-8.12	0.0036			
	1fmole	10.1	18.4	-8.37	0.0030			
	100amole	13.6	21.9	-8.26	0.0033			
	10amole	16.9	25.2	-8.33	0.0031			
	1amole	20.2	27.7	-7.53	0.0054			
OxodG6	100fmole	4.17	14.8	-10.7	0.0006	0.0005	0.0002	0.32
	10fmole	7.19	18.1	-10.9	0.0005			
	1fmole	10.2	21.5	-11.3	0.0004			
	100amole	13.8	24.8	-11.1	0.0005			
	10amole	17.0	28.2	-11.3	0.0004			
	1amole	20.1	30.3	-10.2	0.0009			

a- C_{TU} , C_{TM} , RTC, and C.V. were calculated as described in Table 4.3.

b- Data taken from Table 4.3.

Table 4.5. RTC amplification efficiencies of templates with *cis-syn* TT dimers^a.

	Input Template	Mean C_{TU}	Mean C_{TM}	ΔC_T (U-M)	RTC	Mean RTC	S.D.	C.V.
Dimer CONTROL								
	100fmole	4.21	4.11	0.096	1.07	1.03	0.195	0.19
	10fmole	6.94	6.62	0.319	1.25			
	1fmole	10.3	10.1	0.215	1.16			
	100amole	13.5	13.4	0.124	1.09			
	10amole	16.6	16.7	-0.071	0.952			
	1amole	19.6	20.1	-0.534	0.690			
TT Dimer1								
	100fmole	4.31	10.7	-6.42	0.0117	0.0079	0.0025	0.32
	10fmole	7.03	13.7	-6.71	0.0096			
	1fmole	10.1	17.3	-7.20	0.0068			
	100amole	13.4	20.4	-6.95	0.0081			
	10amole	16.6	23.8	-7.24	0.0066			
	1amole	19.3	27.0	-7.77	0.0046			

^a- C_{TU} , C_{TM} , RTC, and C.V. were calculated as described in Table 4.3.

The RTC method normalized the observed C_T value for each full-length PCR to the ICR PCR C_T value in calculating amplification efficiency. In deriving the RTC formula, the assumption was made that the ICR amplification efficiency was 100% because this region contained no base modifications. RTC efficiencies were calculated for unmodified templates based on simulated ICR efficiencies in the 80 to 100% range; no significant effect on RTC efficiencies was observed (data not shown). More refined mathematical models (140, 142, 160-165) may be needed to detect subtle differences between the amplification efficiencies of undamaged templates and templates containing modifications that have subtle influences on *Taq* polymerase progression.

4.1.1.4. Lesion bypass rate: calculation of MME for unmodified and modified templates

The mean modified efficiency method builds on the RTC method for quantifying aggregate damage to DNA template using real-time PCR. These mathematical formulae were designed to help explain differences observed in PCR curves from synthetic templates that contained DNA base lesions while holding input template quantity constant. It is evident, based on previous observations, that lesions perturb amplification to different degrees and that unmodified amplicons are created during cycling that

mimicked the reaction efficiencies of the control templates. The RTC method assumes that the reaction efficiencies from the ICR and full-length amplifications are identical and that these are interchangeable between templates (151). RTC efficiency can characterize large differences resulting from lesion bypass (Tables 4.3-4.5). When using this method to estimate DNA damage, no significant difference was measured between the Oxo CONTROL, OxodG1, and OxodG2A reactions. In order to further characterize slight differences between PCRs of modified templates not distinguishable using RTC, the reaction efficiencies for the ICR and full-length amplifications, as well as the amount of fluorescence generated by each input template (corresponding to input template amounts), were determined and incorporated into the equation for MME (equation 14).

Calculated ICR reaction efficiencies (E_{ICR}) from oligonucleotide templates ranged from 0.946 to 1.056 (Table 4.6). The reaction efficiencies for the full-length amplicons (E_u) ranged from 0.922 to 0.991 (Table 4.6). In both cases, there was no correlation between amount or type of modification and trends in unmodified template PCR efficiency. No statistically significant differences between PCR efficiencies were observed between synthetic templates.

Table 4.6. PCR efficiencies from oligonucleotide templates^a.

Sample	Efficiency ICR	Efficiency Full-length
Oxo CONTROL	1.01	0.936
OxodG1	0.990	0.943
OxodG2A	1.01	0.922
OxodG2T	1.04	0.954
OxodG3A	1.06	0.963
OxodG3T	1.02	0.991
OxodG4T	1.01	0.986
OxodG6	1.03	0.989
OxodA1	0.946	0.968
Abasic	0.997	0.946
Dimer CONTROL	1.01	0.962
TT Dimer1	0.996	0.975

a- PCR efficiencies were calculated using equation 15.

To account for slight differences in input template amount, equation 16 was used to generate x_0 values representing input template fluorescence (Table 4.7). With the

exception of the OxodG3T template (decreased by 87%), all calculated fluorescence values for oligonucleotide templates differed less than 2-fold when compared to the Oxo CONTROL. Most template x_0 values were within 30% of one another. These values are representative of input template fluorescence and accounted for any changes in E_{ICR} or input template amount between templates. Given the equivalent efficiencies (close to 1.0) for the ICR (Table 4.6), it is not surprising to see the same trends in calculated x_0 as were seen with relative input template amounts (Table 4.1). This observation implied that the calculated input fluorescence corresponded to input template amount.

Table 4.7. Input template fluorescence.

Sample	Mean C_T^a	Efficiency Unmodified (E_{ICR}^b)	Template Fluorescence (X_0^c)	Relative Change ^d
Oxo CONTROL	10.1	1.01	8.64E-04	0.00%
OxodG1	9.57	0.990	1.38E-03	60.15%
OxodG2A	9.47	1.01	1.36E-03	57.32%
OxodG2T	10.1	1.04	7.71E-04	-10.80%
OxodG3A	9.91	1.06	7.91E-04	-8.52%
OxodG3T	13.0	1.02	1.08E-04	-87.53%
OxodG4T	10.1	1.01	9.12E-04	5.53%
OxodG6	10.2	1.03	7.35E-04	-14.99%
OxodA1	10.5	0.946	9.17E-04	6.08%
Abasic	10.0	0.997	9.68E-04	12.04%
Dimer CONTROL	10.3	1.01	7.64E-04	-11.56%
TT Dimer1	10.1	0.996	9.58E-04	10.90%

a- Mean C_T values were calculated by averaging five amplifications of the ICR targets at a threshold (T) of 1.0.

b- E_{ICR} values were derived as described in Table 4.6.

c- x_0 values were calculated using equation 16.

d- Relative change determined by comparison to Oxo CONTROL data

Using the same data set from which the RTC efficiencies were derived (Tables 4.3-4.5), MMEs were calculated using equation 14 (Tables 4.8-4.10). The mean MME efficiencies of the Oxo CONTROL and Dimer CONTROL templates were 0.776 and 1.28 respectively. These values represented 42.6% and 24.3% differences when compared to the previously reported RTC efficiency values. It is important to note that the confidence intervals for these data sets were much smaller demonstrating a more

precise measurement (data not shown). Theoretically, the MMEs of the unmodified controls should equal 1.0. The observed differences in MME from this theoretical mark suggested that the inherent efficiencies of the ICR sequence differed from that of the full-length template reaction and therefore an over- or underestimation of the MME occurred. The decrease in MME below 1.0 in the Oxo CONTROL can be attributed to the numerous stable secondary structures presented in Figure 4.9; the increase in MME above 1.0 in the Dimer CONTROL could be due to increased SYBR Green Dye incorporation as the target template in the full-length reactions is double that of the ICR (discussed in Appendix B). Regardless of the reason, these differences point to the need for sequence matched controls for any real-time analysis.

The OxodG1 and OxodG2A templates showed no significant difference in RTC efficiency (Table 4.3). Calculated MMEs for both templates were 0.509 and 0.414, equating to reductions of 34.4% and 46.6% respectively (Table 4.8; both significantly different at $p < 0.05$). For all other templates, calculated MMEs followed similar patterns to those seen in with the RTC estimations. Given this, plus the significant MME results from the OxodG1 and OxodG2A templates, the simplified RTC formula was appropriate to compare large differences in amplification rates, brought upon by DNA damage, whereas the more complex MME formula provided increased precision, which allowed small damage influences on reaction rate to be detected.

Table 4.8. Mean modified efficiencies of templates with non-adjacent lesions.

	Input Template	Mean C_{TM}	X_o^a	Threshold (T)	Efficiency Unmodified (E_u)^b	Efficiency Modified (E_m)^c	Mean E_m	S.D. E_m
Oxo CONTROL	100fmole	4.16	6.48E-02	1	0.936	0.925	0.776	0.0792
	10fmole	7.17	1.09E-02	1	0.936	0.760		
	1fmole	11.0	8.65E-04	1	0.936	0.760		
	100amole	14.5	9.10E-05	1	0.936	0.720		
	10amole	17.8	1.07E-05	1	0.936	0.704		
	1amole	21.2	9.68E-07	1	0.936	0.789		
OxodG1	100fmole	4.32	9.57E-02	1	0.943	0.536	0.509	0.113
	10fmole	6.81	1.65E-02	1	0.943	0.618		
	1fmole	11.1	1.38E-03	1	0.943	0.432		
	100amole	15.0	1.40E-04	1	0.943	0.328		
	10amole	17.3	1.60E-05	1	0.943	0.622		
	1amole	21.1	1.54E-06	1	0.943	0.518		
OxodG2A	100fmole	4.83	8.97E-02	1	0.922	0.418	0.414	0.140
	10fmole	7.26	1.31E-02	1	0.922	0.613		
	1fmole	11.1	1.36E-03	1	0.922	0.475		
	100amole	14.5	1.49E-04	1	0.922	0.463		
	10amole	19.2	1.49E-05	1	0.922	0.223		
	1amole	22.5	1.31E-06	1	0.922	0.290		
OxodG3A	100fmole	9.19	4.40E-02	1	0.963	0.043	0.0319	0.00600
	10fmole	12.4	7.80E-03	1	0.963	0.030		
	1fmole	15.8	7.91E-04	1	0.963	0.029		
	100amole	19.3	7.60E-05	1	0.963	0.028		
	10amole	22.8	7.58E-06	1	0.963	0.027		
	1amole	25.7	7.97E-07	1	0.963	0.035		
OxodA1	100fmole	7.65	4.10E-02	1	0.968	0.128	0.1009	0.0245
	10fmole	10.2	7.75E-03	1	0.968	0.127		
	1fmole	13.6	9.18E-04	1	0.968	0.104		
	100amole	16.9	1.01E-04	1	0.968	0.101		
	10amole	20.7	1.07E-05	1	0.968	0.0768		
	1amole	24.0	1.27E-06	1	0.968	0.0692		
Abasic	100fmole	10.4	4.86E-02	1	0.946	0.0179	0.0134	0.00250
	10fmole	13.6	8.49E-03	1	0.946	0.0129		
	1fmole	17.1	9.71E-04	1	0.946	0.0108		
	100amole	20.6	8.71E-05	1	0.946	0.0117		
	10amole	23.9	9.02E-06	1	0.946	0.0127		
	1amole	27.2	8.81E-07	1	0.946	0.0143		

a- X_o values were calculated as described in Table 4.7

b- E_u values were derived as described in Table 4.6

c- MMEs were derived using equation 14.

Table 4.9. Mean modified efficiencies of templates with adjacent lesions ^a.

	Input Template	Mean C_{TM}	X_o	Threshold (k)	Efficiency Unmodified (Eu)	Efficiency Modified (Em)	Mean Em	S.D. Em
Oxo CONTROL^b	100fmole	4.16	6.48E-02	1	0.936	0.925	0.776	0.0792
	10fmole	7.17	1.09E-02	1	0.936	0.760		
	1fmole	11.0	8.65E-04	1	0.936	0.760		
	100amole	14.5	9.10E-05	1	0.936	0.720		
	10amole	17.8	1.07E-05	1	0.936	0.704		
	1amole	21.2	9.68E-07	1	0.936	0.789		
OxodG2T	100fmole	10.1	5.47E-02	1	0.954	0.0192	0.0171	0.0051
	10fmole	13.6	7.65E-03	1	0.954	0.0140		
	1fmole	17.1	7.70E-04	1	0.954	0.0129		
	100amole	20.6	6.72E-05	1	0.954	0.0142		
	10amole	23.8	7.18E-06	1	0.954	0.0156		
	1amole	26.3	7.93E-07	1	0.954	0.0265		
OxodG3T	100fmole	14.4	1.04E-02	1	0.991	0.0046	0.0045	0.0014
	10fmole	17.7	1.41E-03	1	0.991	0.0037		
	1fmole	21.4	1.08E-04	1	0.991	0.0037		
	100amole	24.7	1.20E-05	1	0.991	0.0034		
	10amole	27.6	1.24E-06	1	0.991	0.0043		
	1amole	30.1	1.32E-07	1	0.991	0.0073		
OxodG4T	100fmole	11.8	6.14E-02	1	0.986	0.0046	0.0045	0.0012
	10fmole	15.2	7.23E-03	1	0.986	0.0040		
	1fmole	18.4	9.14E-04	1	0.986	0.0035		
	100amole	21.9	7.66E-05	1	0.986	0.0039		
	10amole	25.2	7.70E-06	1	0.986	0.0038		
	1amole	27.7	7.88E-07	1	0.986	0.0069		
OxodG6	100fmole	14.8	5.25E-02	1	0.989	0.0007	0.0007	0.0002
	10fmole	18.1	6.23E-03	1	0.989	0.0006		
	1fmole	21.5	7.35E-04	1	0.989	0.0005		
	100amole	24.8	5.99E-05	1	0.989	0.0006		
	10amole	28.2	6.32E-06	1	0.989	0.0006		
	1amole	30.3	6.72E-07	1	0.989	0.0013		

a- Calculations were performed as described in Table 4.8.

b- Data from Table 4.8.

Table 4.10. Mean modified efficiencies of templates with *cis-syn* TT dimers^a.

	Input Template	Mean C_{TM}	X₀	Threshold (k)	Efficiency Unmodified (Eu)	Efficiency Modified (Em)	Mean Em	S.D. Em
Dimer CONTROL	100fmole	4.11	5.35E-02	1	0.962	1.14	1.28	0.159
	10fmole	6.62	7.98E-03	1	0.962	1.40		
	1fmole	10.1	7.64E-04	1	0.962	1.40		
	100amole	13.4	8.26E-05	1	0.962	1.41		
	10amole	16.7	9.34E-06	1	0.962	1.33		
	1amole	20.1	1.19E-06	1	0.962	1.04		
TT Dimer1	100fmole	10.7	5.09E-02	1	0.975	0.012	0.0091	0.0022
	10fmole	13.7	7.76E-03	1	0.975	0.011		
	1fmole	17.3	9.58E-04	1	0.975	0.0080		
	100amole	20.4	9.22E-05	1	0.975	0.0099		
	10amole	23.8	1.05E-05	1	0.975	0.0084		
	1amole	27.0	1.65E-06	1	0.975	0.0060		

a- Calculations were performed as described in Table 4.8.

4.1.1.5. Lesion bypass rate: the Inherent Template Efficiency method

The use of standard curves to generate unmodified efficiency values was necessary in obtaining precise estimates of DNA damage (MME and equation 6). The generation of and subsequent amplification of standards is costly from both a time and reagent perspective. In an effort to eliminate the standard curve requirement, an alternative mathematical treatment for real-time PCR data was adopted which calculates input template amounts and efficiency values based on whole reaction curve kinetics (142-143). Mathematical formulae were developed to adapt this methodology to compare amounts of DNA damage.

Raw PCR data was collected from a subset of the damaged oligonucleotides (presented in Table 3.1) and then fit to a logistic/sigmoid curve from which variables representing efficiency and input template amounts were derived. Using equation 23, inherent template efficiencies (ITE) were calculated from these data (Table 4.11).

Values representing both ITE and PCR derived unmodified template efficiencies (E_{PCR}) were determined. ITEs followed similar patterns seen in the RTC and MME data; OxodG2T, OxodG4T, and OxodG6 dropped 98.0%, 99.6%, and 99.9% respectively when compared with the Oxo CONTROL values (Table 4.11; all significant at $p < 0.001$).

E_{PCR} increased as the number of 8-oxodG modifications on the input template increased (Table 4.11). These values were expected to remain constant between templates as the value being measured, PCR derived unmodified template reaction efficiency, is thought to be consistent between reactions.

Table 4.11. Inherent template efficiencies^a.

	Mean Unmodified Efficiency (E_{PCR})	Mean Inherent Template Efficiency (ITE)
Oxo CONTROL	0.482	0.201
OxodG2T	0.579	0.0040
OxodG4T	0.641	0.0007
OxodG6	0.711	0.0001

a- Means were calculated by averaging five amplifications of the ICR and full-length targets with input amounts equal to 1 fmole at a threshold (T) of 1.0.

To determine the reason for the differences in observed E_{PCR} , a serial dilution of Oxo CONTROL templates was prepared and amplified. Variables necessary for input into equation 23 to produce ITE and E_{PCR} values were generated. The R_{max} value (finite plateau) is defined by the point at which no growth occurs in a reaction (Figure 4.11). Recognizing that amplification curves for the oligonucleotide templates were not achieving true plateau after 40 cycles, reaction data was collected out to the instrument limit of 99 cycles. By increasing the amount of data used in the fit, the observation that the raw PCR data did not produce a true fit to a logistic model became clear (Figure 4.11). The linear phases of the reactions (point at which the reaction curves exited exponential growth and began to plateau) were not symmetric with the detectable exponential growth phases in the data (point at which the curve data rises above background; Figure 4.11). Notice the difference between the curve fit and raw data increased as the amount of data points included increased; e.g. the variation between raw and fit data during the initial ramping phase increases when 75 cycles of data are used versus a fit from the same raw data cropped at 35 cycles (Figure 4.11). The result of this

improper fit was variation in kinetic data (R_{\max} , $N_{1/2}$ and K), which ultimately produced differences between derived input template and efficiency values from the same data set (Table 4.12). For calculation of input template, the values obtained using the $2^{-\Delta CT}$ comparison method closely paralleled those of the expected values with the greatest discrepancy existing in the 10 fmole samples which differed by 35.9% (Table 4.12; (141)). Measures of input template R_o , derived from curve-fit data, differed greatly from the expected values; an apparent difference that was influenced by the number of data points used in the fit (Table 4.12). For example, in the samples containing 10 fmole of input Oxo CONTROL, $R_{o_{35cyc}}$, representing derived input template amounts using 35 cycle data, was 0.0101 fmoles and $R_{o_{75cyc}}$ was 0.0028 fmoles (representing 89.9% and 99.7% deviations from the expected value; Table 4.12). These data emphasize the need for a proper curve-fit to PCR raw data and suggest the rate at which PCRs plateau must be equivalent to the rate at which reactions proceed into detectable exponential phase to authorize the use of curve-fitting methods of real-time PCR comparative analysis.

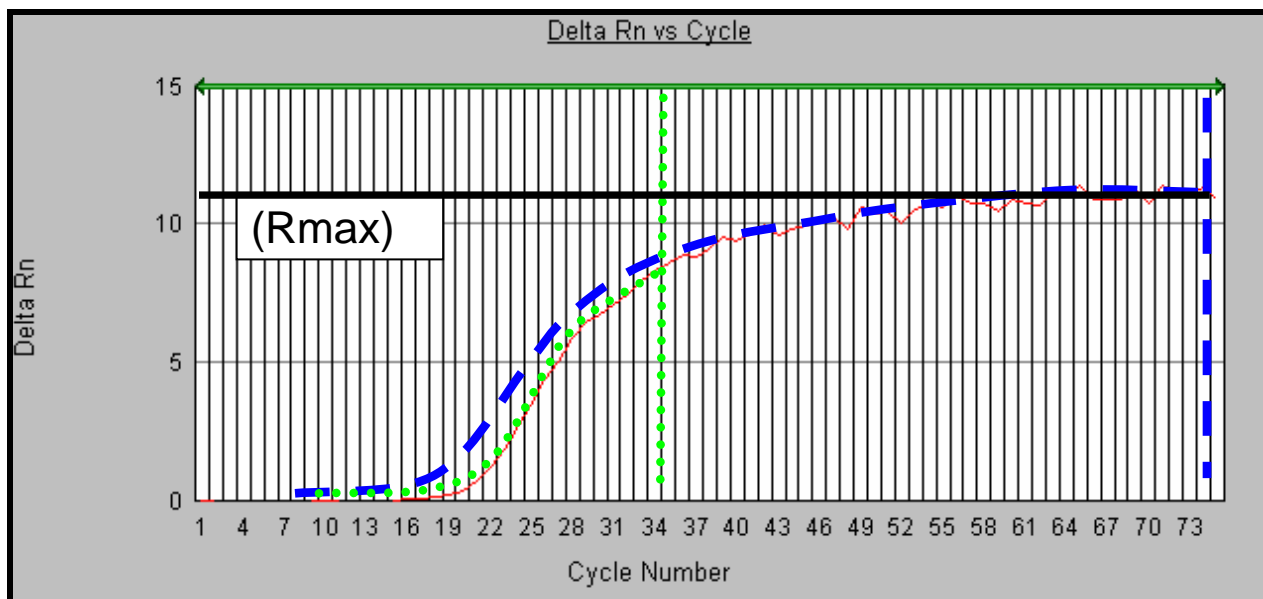


Figure 4.11. Kinetic analysis of raw PCR data. Variables derived from the logistic fit of raw PCR data were influenced by the number of reaction cycles used in the curve fit; raw PCR data (—), fit curve representing data cropped at 35 cycles (* *), and fit curve representing data cropped at 75 cycles (- -). The gradual plateauing toward a finite R_{\max} value in the raw data influenced the overall shape of the fit curve as the number of cycles used in curve fitting increased.

Table 4.12. Comparison between $2^{-\Delta CT}$ and curve-fit calculations.

Input Template	Efficiency Unmodified (Eu)^a	Efficiency (E_{35cyc})^b	Efficiency (E_{75cyc})^b	Input Template (2^{-ΔCT})	Input Template (Ro_{35cyc})^c	Input Template (Ro_{75cyc})^c	Expected
10fmole	0.936	0.42	0.32	13600	1020	27.8	10000
1fmole	0.936	0.43	0.32	1230	243	9.40	1000
100amole	0.936	0.47	0.30	120	45.4	4.97	100
10amole	0.936	0.44	0.29	11.1	7.97	1.83	10.0
8amole	0.936	0.45	0.28	9.08	6.52	1.75	8.00
6amole	0.936	0.44	0.27	5.82	5.41	1.57	6.00
4amole	0.936	0.46	0.28	4.63	3.85	1.51	4.00
2amole	0.936	0.46	0.26	1.91	2.23	1.35	2.00
1amole	0.936	0.49	0.27	1.00	1.00	1.00	1.00

a- E_U values were derived as described in Table 4.6

b- E_{35cyc} and E_{75cyc} were derived from curve-fit data cropped at 35 and 75 cycles respectively.

c- Ro_{35cyc} and Ro_{75cyc} represent input template amounts derived from 35 and 75 cycle curve-fit data and normalized to 1 amole.

To correct for this lack of curve symmetry, experimental design was created to limit a single reaction component, thereby creating a unique rate-limiting step in the PCR, and forcing amplification curves to plateau at a much greater rate. As stated in the materials and methods section, PCRs contain 1 μ l of 10 μ M forward and reverse primers which was estimated to be approximately 300 nmoles of each per reaction (data not shown). Reactions with primer amounts ranging from 30 to 300 nmoles were amplified; the rates of plateau and corresponding curve-fits were observed (Figure 4.12; data not shown). Decreasing both primer amounts to 37.5 nmoles provided a better fit to raw PCR data using both 40 and 50 cycles of data when compared with that of the 300 nmole primer reactions (Figure 4.12).

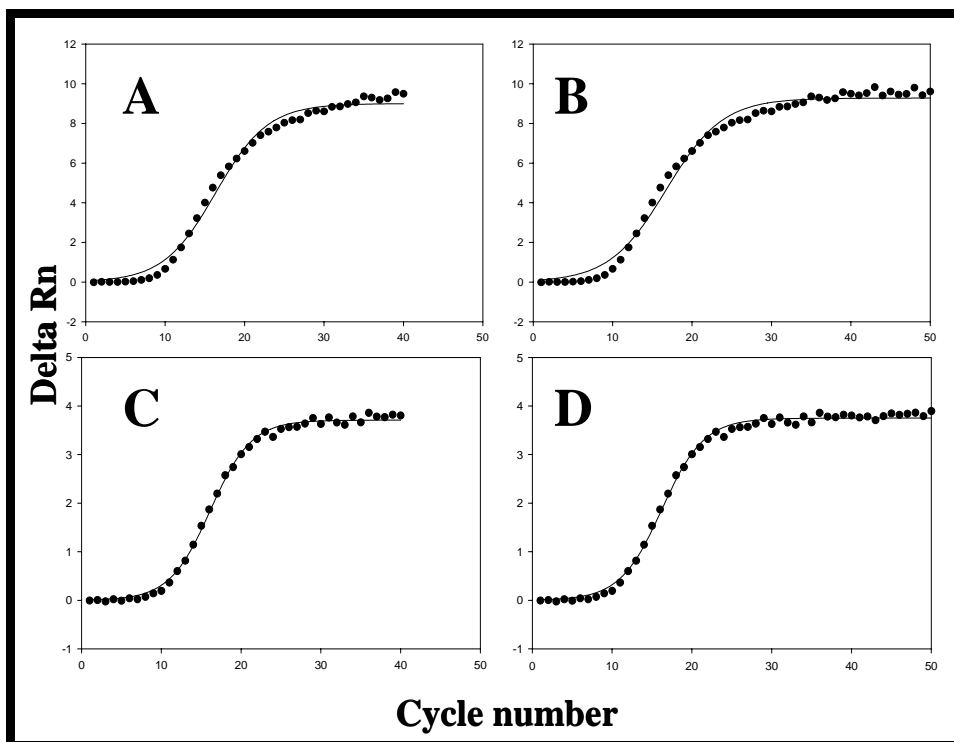


Figure 4.12. Real-time PCR raw data fit to a logistic curve. (**) represent raw data points, (-) are the data post logistic fit. Reactions containing 300 nmoles of total primer present a divergence between the fit and raw data; this divergence increased as the amount of raw data used in the fit is increased from A) 40 to B) 50 cycles. Decreasing the amount of primer to 37.5 nmoles lessened the degree of difference between raw and curve-fit data using both C) 40 and D) 50 cycles of data.

Values for efficiency and input template were derived from curve-fit data from reactions containing 300 and 37.5 nmoles of forward and reverse primers (Table 4.13). The difference between the normalized Ro and expected values was not as dramatic in the reactions where primer amounts were the rate-limiting step; for example, in reactions with 10 fmoles of input oligonucleotide, 300 nmoles of primer produced normalized Ro_{40cyc} and Ro_{50cyc} of 3.23 and 2.97 fmoles where normalized values for 37.5 nmoles were 5.512 and 5.141 fmoles (Table 4.13). Values for unmodified efficiency increased from approximately 0.32 to 0.46 when primer amounts were limited (Table 4.13).

While decreasing primer amounts provided results closer to expected values, accuracy and precision are critical for the evaluation of damaged template. Curve-fit methods, in their current format, could not be adapted for reliable measurement of DNA damage in synthetic template. Derivation of new formulae characterizing the

discrepancies between raw and curve-fit data is necessary before the utilization of these methods for DNA damage detection is achieved.

Table 4.13. Curve-fit calculations from reactions with differing primer amounts^a.

Primer Concentration	Template Amount	Efficiency (E_{40cyc})	Efficiency (E_{50cyc})	Input Template (Ro_{40cyc}) ^b	Input Template (Ro_{50cyc}) ^b	Expected
300nmole	10fmole	0.34	0.31	3.23	2.97	10.0
300nmole	8fmole	0.34	0.31	2.59	2.28	8.00
300nmole	6fmole	0.32	0.29	2.81	2.64	6.00
300nmole	4fmole	0.34	0.30	1.94	1.98	4.00
300nmole	2fmole	0.35	0.32	1.37	1.36	2.00
300nmole	1fmole	0.36	0.32	1.00	1.00	1.00
300nmole	100amole	0.35	0.31	0.340	0.440	0.100
300nmole	10amole	0.36	0.30	0.100	0.170	0.010
300nmole	1amole	0.32	0.27	0.040	0.090	0.001
Primer Concentration	Template Amount	Efficiency (E_{40cyc})	Efficiency (E_{50cyc})	Input Template (Ro_{40cyc}) ^b	Input Template (Ro_{50cyc}) ^b	Expected
37.5nmole	10fmole	0.46	0.45	5.52	5.14	10.0
37.5nmole	8fmole	0.46	0.45	4.49	4.05	8.00
37.5nmole	6fmole	0.45	0.44	4.13	3.88	6.00
37.5nmole	4fmole	0.51	0.49	1.97	1.95	4.00
37.5nmole	2fmole	0.48	0.46	1.57	1.64	2.00
37.5nmole	1fmole	0.48	0.46	1.00	1.00	1.00
37.5nmole	100amole	0.45	0.43	0.270	0.290	0.100
37.5nmole	10amole	0.42	0.39	0.080	0.110	0.010
37.5nmole	1amole	0.34	0.30	0.050	0.100	0.001

a- E_{cyc} and Ro_{cyc} values were derived as described in Table 4.12.

b- Ro_{cyc} values were normalized to 1 fmole data.

4.1.1.6. Alternative PCR components increase lesion bypass rate

A subset of 90-mer oligonucleotides were amplified using the Restorase DNA polymerase system (Sigma) to determine if changes in the PCR reagents impacted observed RTC efficiencies. Restorase DNA polymerase is a mixture of Sigma AccuTaq LA and a proprietary DNA damage repair enzyme that is thought to be specific for the repair of abasic lesions (165). RTC efficiencies were calculated from real-time data. OxO CONTROL, OxodG2A, OxodA1, and Abasic mean RTC efficiencies were 0.614,

0.460, 0.611, and 0.0298 respectively (Table 4.14). While neither the OxodG2A nor OxodA1 RTC efficiencies differed significantly from those of the Oxo CONTROL, the Abasic RTC efficiency dropped 95.1% (significantly different at $p < 0.001$).

When compared with amplifications using AmpliTaq Gold (Table 4.3; Applied Biosystems), no significant differences were seen between RTC efficiencies from Oxo CONTROL or OxodG2A amplifications (Figure 4.13). However, when using Restorase, OxodA1 RTC efficiencies increased from 0.114 to 0.611 (levels mimicking the control reactions; Figure 4.13; significantly different at $p < 0.001$). Abasic RTC efficiencies were also increased; from 0.009 to 0.029 (Figure 4.13; significantly different at $p < 0.05$). These data suggested that the PCRs with Restorase and matching reagents were more efficient than AmpliTaq Gold protocols at processing templates with 8-oxodA and abasic lesions.

Table 4.14. RTC efficiencies from PCRs with Restorase DNA polymerase^a.

	Input Template	Mean C_{TU}	Mean C_{TM}	ΔC_T (U-M)	RTC	Mean RTC	S.D.	C.V.
Oxo CONTROL	1fmole	11.6	12.6	-0.949	0.518	0.614	0.0862	0.14
	1fmole	11.8	12.3	-0.536	0.690			
	1fmole	12.1	12.6	-0.547	0.685			
	1fmole	11.8	12.6	-0.824	0.565			
OxodG2A	1fmole	11.1	12.0	-0.898	0.537	0.460	0.134	0.29
	1fmole	11.1	11.9	-0.792	0.578			
	1fmole	11.1	12.3	-1.16	0.449			
	1fmole	10.4	12.3	-1.86	0.276			
OxodA1	1fmole	11.7	12.4	-0.688	0.621	0.611	0.0959	0.16
	1fmole	11.6	12.0	-0.477	0.719			
	1fmole	11.3	12.4	-1.04	0.485			
	1fmole	11.7	12.4	-0.692	0.619			
Abasic	1fmole	11.0	15.7	-4.70	0.0384	0.0298	0.0074	0.25
	1fmole	10.5	16.1	-5.62	0.0203			
	1fmole	11.4	16.5	-5.02	0.0308			
	1fmole	11.4	16.5	-5.08	0.0296			

^a- C_{TU} , C_{TM} , RTC, and C.V. were calculated as described in Table 4.3.

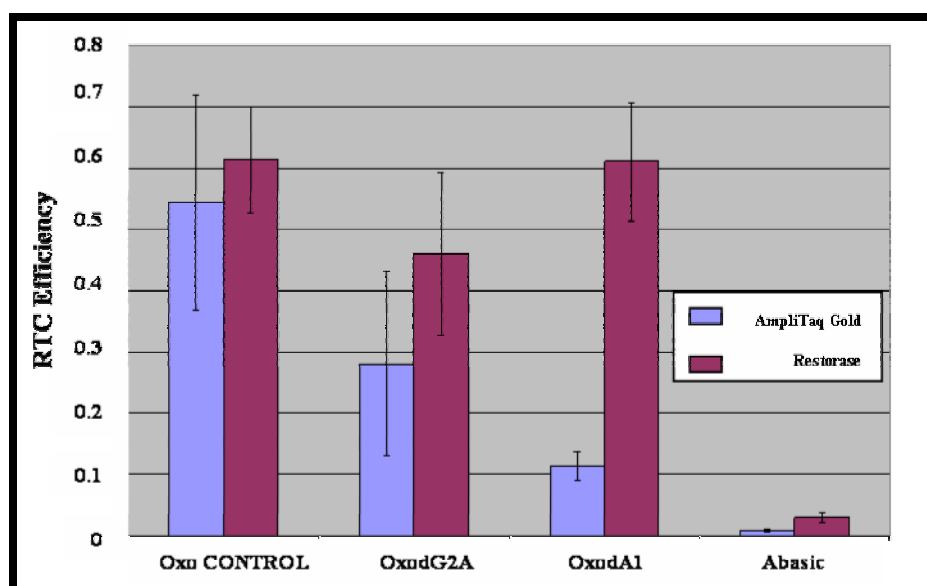


Figure 4.13. RTC efficiencies from PCRs using AmpliTaq Gold and Restorase. RTC efficiencies from Oxo CONTROL, OxodG2A, OxodA1 and Abasic templates were calculated from PCRs using either AmpliTaq Gold (average of 6 DNA template amounts, each with N=5) or Restorase DNA polymerase (1 template amount; N=4) master mixes.

4.1.1.7. Lesion bypass rate: long template amplification

To transition from real-time damage quantification from short synthetic templates to quantification of damage in cellular DNA, amplicon target size must be increased and assay sensitivity must be determined. Instrument limitations do not permit the usage of PCR extension times comparable to *Taq* DNA polymerase processivity (reported to be as high as 2.8 kb per minute or less than 5 s to traverse 90 bases; (146)). Therefore, to estimate the sensitivity of real-time polymerase stop assays for damage detection, longer templates with controlled modification were necessary. To study the influence of base modifications under native polymerase conditions, a subset of the synthetic 90 base oligonucleotides were used as primers and ligated into PCR products (Figure 4.14). To remove the original template and anti-sense strand, PCR products were separated using biotin:streptavidin association (Figure 4.14B). Primers were designed and used to amplify a full-length 593 base template (Figure 4.14C) and a ligated oligo internal control region (LO-ICR) containing no base modification (Figure 4.14D). Extension times in these PCRs were 1 min; still in excess of the time necessary to replicate the templates but not to the degree seen with the 90-mer oligonucleotides. MMEs for the control templates were 0.559 (Oxo CONTROL) and 0.819 (Dimer CONTROL) (Table 4.15). MMEs from reactions with 8-oxodG modifications showed a steady trend lower as the number of base modifications increased; OxodG1, OxodG2A, and OxodG3A had MMEs of 1.03, 0.739, and 0.514 respectively (Table 4.15). The OxodA1 template generated a MME of 0.614; which mimics trends in the 90-mer data when compared with the OxodG2A and OxodG3A templates but not when compared with the Oxo CONTROL (Table 4.15). Abasic and TT Dimer1 containing templates substantially altered their respective reactions; generating MMEs of 0.062 and 0.014, similar to those observed in the short template data (Table 4.15).

While these modified templates present decreasing trends similar to those observed with the 90-mer data, the differences with respect to the Oxo CONTROL are not easily explained. The data suggests that multiple factors influenced the kinetics of these PCRs. The decrease in the Oxo CONTROL MME can be partially explained by the previously mentioned secondary structures (Figure 4.9) which may play a role in limiting

primer annealing. In the 8-oxodG reactions, it is possible that the insertion of the base modifications altered the backbone dynamics in the single stranded template (159), which decreased stable secondary structures, and therefore increased observed MMEs. Then, as the number of 8-oxodGs was increased, the influence of 8-oxodG base modification on *Taq* DNA polymerase progression became evident.

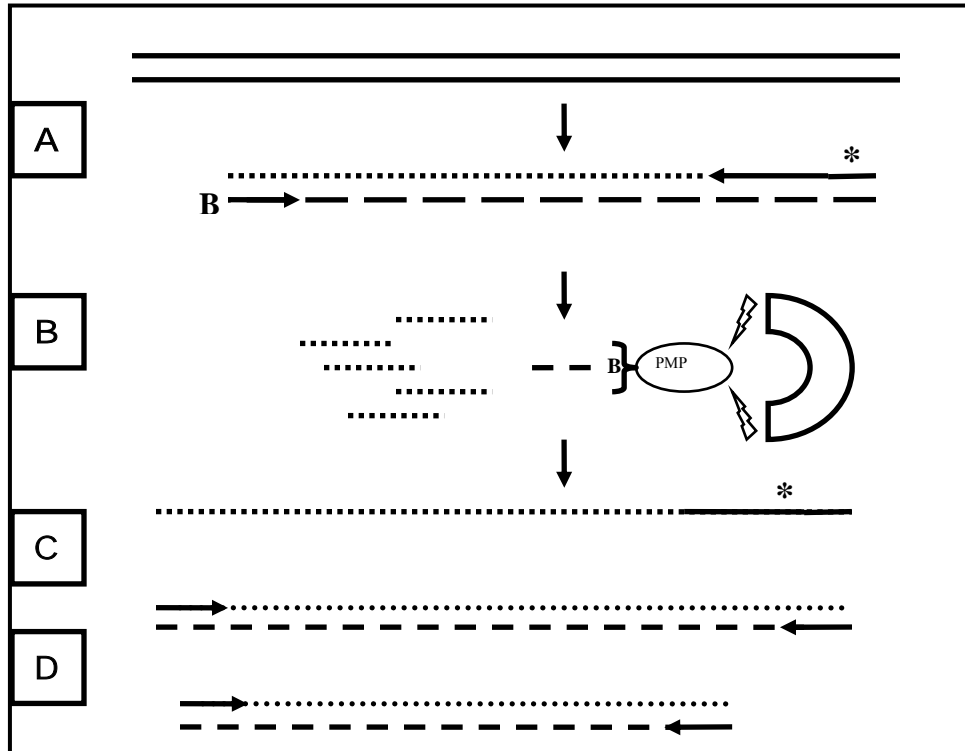


Figure 4.14. Creation of long templates containing controlled DNA base modification. A) To increase the availability of template for modified oligonucleotide ligation, 751 bp PCR products were created from human mtDNA. Modified and unmodified 90-mers were then used as primers to amplify a 593 bp nested PCR target; the forward primer in these reactions was labeled with biotin. B) 593 bp PCR products, containing the 90-mers, were associated with streptavidin coated magnisphere beads (Promega), collected, and denatured; the sense strands containing the 90-mers were collected and used as templates in C) full-length PCRs (593 bp) or D) LO-ICR reactions (545 bp). (*) represents modified nucleotides; (.....) represents synthetic oligonucleotide containing sense strand; (— — —) represents biotin containing anti-sense strand; (.....) represents PCR sense strand; (— — —) equals PCR anti-sense strand.

Table 4.15. Mean modified efficiencies from long templates^a.

	Mean MME	S.D. MME
Oxo CONTROL	0.559	0.0849
OxodG1	1.04	0.0718
OxodG2A	0.739	0.0309
OxodG3A	0.514	0.0382
OxodA1	0.614	0.0428
Abasic	0.062	0.0354
Dimer CONTROL	0.819	0.0585
TT Dimer1	0.0144	0.0002

a- MMEs were derived using equation 14 as described in Table 4.8.

4.1.2. Quantification of cellular DNA damage

To this point, quantification of DNA damage has involved 90-mer oligonucleotides with set amounts and types of base damage. In order to be useful as a general research tool to study DNA damage and repair, characterization of damage in cellular DNA sample material must be achieved. Given that the majority of damage events to DNA are random, the sensitivity of polymerase stop assays in detecting damage increases with the size of the PCR amplicon (5, 11). To validate real-time PCR as a method to estimate damage in cellular DNA, primers were designed to amplify a segment of human mtDNA; by holding the reverse primer constant and moving the forward primer, amplicon sizes were increased and observed differences in the PCRs attributed to differences in amounts of DNA damage (Figure 4.15).

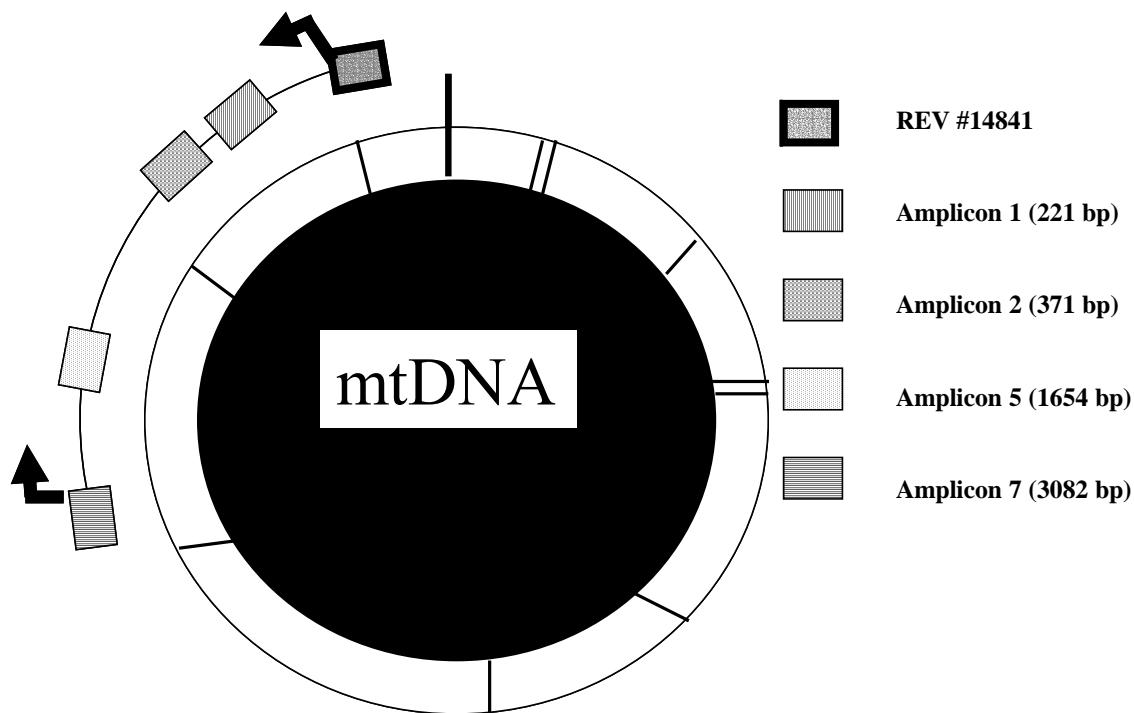


Figure 4.15. Amplification of mitochondrial DNA by primer walking. The schematic represents a model of mammalian mtDNA; reverse primer (REV #14841) was held constant and forward primers moved to create amplicons ranging between 221 bp and 3082 bp. Actual fragment size is given in parenthesis.

Prior to damage estimation, it was first necessary to validate the use of long cellular DNA targets in PCRs on the ABI 7000 sequence detection system. To do so, three amounts of total cellular DNA (4.5 ng, 9.0 ng, and 13.5 ng) were amplified with different primer sets ranging from 200 bp to 8.0 kb (Figure 4.15; data not shown). Input template fluorescence was calculated using equation **16** and normalized to the 4.5 ng DNA sample data (Table 4.16). For amplicons up to 3.0 kb, normalized template fluorescent amounts mirrored the expected values (Table 4.16). For amplicons greater than 4.0 kb, the reliability of X_o calculations were found to be inconsistent and therefore not sufficient for further experimentation (data not shown). These data suggested that the real-time PCR protocols presented here were adequate for amplification of DNA targets up to 3.0 kb.

Table 4.16. Input template fluorescence at different amplicon sizes.

	Input Template^a	X₀^b	Normalized X₀	Expected
Amplicon 1				
	4.5 ng	1.57E-08	1.00	1.00
	9.0 ng	3.12E-08	1.99	2.00
	13.5 ng	4.71E-08	3.00	3.00
Amplicon 2				
	4.5 ng	4.60E-08	1.00	1.00
	9.0 ng	9.08E-08	1.97	2.00
	13.5 ng	1.38E-07	3.01	3.00
Amplicon 5				
	4.5 ng	2.16E-08	1.00	1.00
	9.0 ng	4.31E-08	2.00	2.00
	13.5 ng	6.47E-08	3.00	3.00
Amplicon 7				
	4.5 ng	1.82E-09	1.00	1.00
	9.0 ng	3.79E-09	2.09	2.00
	13.5 ng	5.41E-09	2.98	3.00

a- Estimated using optical density at 260nm.

b- X₀s were derived using equation 16 as described in Table 4.7.

Extracted total cellular DNA was irradiated at 254 nm for various times and then amplified using real-time PCR. Rightward shifts in amplification curves were observed (data not shown). Input template amounts were held constant and input fluorescent values calculated for each amplicon size using non-irradiated controls; therefore, any differences in amplification (observed changes in C_T values) can be defined as differences in amounts of DNA damage (151). Using the mean modified efficiency calculation method, a decrease in amplification was observed that correlated to increased PCR product size and increased time of exposure to UV radiation (Table 4.17). To account for inherent differences in amplification between different sized templates (including differences in the efficiencies of PCR derived unmodified templates and different amounts of fluorescent dye incorporation (Appendix B)), MMEs were normalized to untreated controls at each amplicon size. While the normalized MME from the amplification of Amplicon 1 (221 bp) was 0.786 after 0.5 min of exposure, Amplicons 2 (371 bp), 5 (1654 bp), and 7 (3082 bp) had normalized MMEs of 0.793, 0.175, and 0.128, respectively (Table 4.17). Doubling the exposure time decreased normalized MMEs to 0.716, 0.413, 0.068, and 0.028 for Amplicons 1, 2, 5, and 7

respectively (Table 4.17). Further decreases in normalized MMEs were observed as exposure times were increased (Table 4.17). Amplification in the no template controls, as a result of stable primer dimer formation, provided an experimental baseline value for MMEs which was specific for each primer set (data not shown). These results are consistent with reports that the sensitivity of polymerase stop based assays increases with the size of the PCR target (5, 11) and also suggest that real-time PCR can be used to estimate damage in cellular DNA.

Cellular DNA does not contain templates with homogenous damage in a particular target region; more appropriately, cellular DNA is a mixture of damaged and undamaged template. Both the MME and RTC are rate based methods of estimating DNA damage and assume no unmodified templates exist at the beginning of the PCR (151). Therefore, the observed changes in C_T values from damaged sample PCRs, it was necessary to redefine damage in terms of probability rather than reaction rate (10); equation **26** was developed which defined differences in C_T values as *lesion frequency* (proportion of damaged bases in treated sample material). Using equation **26**, lesion frequencies were calculated from data used to generate MMEs for UV irradiated cellular DNA (Table 4.18). Lesion frequencies increased as the time of UV exposure increased in all amplicon sizes tested (Table 4.18). Lesion frequencies seemingly decreased as amplicon size increased; this was not expected as UV damage to DNA is assumed to be random and should, therefore, increase with fragment size. This apparent decrease could be explained by increased precision in lesion frequency estimation at longer template lengths; increased precision was a result of an observed decrease in unmodified reaction efficiencies (E_u values), which resulted in an increase (spread out) in C_T values. This finding suggested that damage studies involving short fragments were unreliable; even at excessive UV exposure dosages.

While these studies were encouraging and suggested that damage to DNA could be measured using real-time polymerase stop assays, further refinement of amplicon targets and the use of samples enduring biologically relevant amounts of UV exposure were necessary to determine the applicability of these methods in clinical and research settings.

Table 4.17. Mean modified efficiencies from UV irradiated DNA.

Sample	Exposure^a	MME	Normalized MME^b
Amplicon 1	0	0.943	1
Amplicon 2	0	1.04	1
Amplicon 5	0	0.967	1
Amplicon 7	0	0.869	1
Amplicon 1	0.5	0.741	0.786
Amplicon 2	0.5	0.822	0.793
Amplicon 5	0.5	0.169	0.175
Amplicon 7	0.5	0.112	0.128
Amplicon 1	1	0.675	0.716
Amplicon 2	1	0.428	0.413
Amplicon 5	1	0.0658	0.0680
Amplicon 7	1	0.0241	0.0278
Amplicon 1	3	0.499	0.530
Amplicon 2	3	0.253	0.244
Amplicon 5	3	0.0109	0.0113
Amplicon 7	3	0.00240	0.0028
Amplicon 1	7	0.309	0.328
Amplicon 2	7	0.170	0.164
Amplicon 5	7	0.0020	0.0021
Amplicon 7	7	0.0004	0.0004
Amplicon 1	15	0.178	0.189
Amplicon 2	15	0.0439	0.0424
Amplicon 5^c	15	0.0002	0.0002
Amplicon 7^c	15	0.0002	0.0002

a- Listed in minutes of exposure to 254 nm UV radiation.

b- Normalized to the control sample to account for inherent differences between template sizes.

c- Samples approached background MME values as exposure times increased; background MMEs were derived from no template controls and were a result of primer-dimer amplification (data not shown).

Table 4.18. Lesion frequencies from UV irradiated DNA.

	Exposure ^a	C_T Mean ^b	C_T S.D.	ΔC_T	Unmodified Efficiency (Eu) ^c	Lesion Frequency ^d	L.F./10 kb
Amplicon 1	0	17.5	0.137	0.000	0.950		
(N=221)	0.5	18.0	0.0730	-0.516	0.950	0.0016	16
	1	18.1	0.251	-0.626	0.950	0.0019	19
	3	18.8	0.403	-1.36	0.950	0.0041	41
	7	19.2	0.0350	-1.77	0.950	0.0053	53
	15	20.3	0.159	-2.85	0.950	0.0086	86
Amplicon 2	0	17.7	0.0880	0.000	0.900		
(N=371)	0.5	18.1	0.0950	-0.326	0.900	0.00056	5.6
	1	18.2	0.133	-0.492	0.900	0.00085	8.5
	3	19.7	0.919	-1.98	0.900	0.0034	34
	7	20.3	0.0310	-2.54	0.900	0.0044	44
	15	22.2	0.316	-4.44	0.900	0.0077	77
Amplicon 5	0	18.3	0.119	0.000	0.751		
(N=1654)	0.5	19.5	0.0650	-1.28	0.751	0.00043	4.3
	1	20.9	0.262	-2.67	0.751	0.00090	9.0
	3	23.6	0.0330	-5.33	0.751	0.0018	18
	7	26.1	0.301	-7.81	0.751	0.0026	26
	15	31.7	0.298	-13.4	0.751	0.0045	45
Amplicon 7	0	21.1	0.143	0.000	0.650		
(N=3082)	0.5	23.3	0.160	-2.25	0.650	0.00036	3.6
	1	25.8	0.232	-4.70	0.650	0.00076	7.6
	3	29.5	0.181	-8.38	0.650	0.0014	14
	7	32.4	1.04	-11.4	0.650	0.0018	18
	15	33.6	0.770	-12.5	0.650	0.0020	20

a- As described in Table 4.17.

b- Mean C_T s were calculated from an N=3 at threshold of 1.0.

c- Calculated using equation 15.

d- Calculated using equation 26 (listed per base).

4.1.2.1. Validation of real-time PCR to estimate biologically relevant UV DNA damage

In order to establish if changes in C_T values could be detected from biologically relevant amounts of UV DNA damage and translated into lesion frequencies, damaged cellular DNA was acquired from Drs. Bennett Van Houten and Joel Meyer; lesion

frequencies were estimated using conventional QPCR (11). Three template samples were generated by exposing MGH-U1 bladder carcinoma cells to 0, 10 or 20 J/m² UV radiation and extracting total cellular DNA. Using the QPCR method, lesion frequencies of these samples (designated 0 L, 0.5 L and 1.0 L respectively) were estimated to be 0, 0.5 and 1 lesion per 10,000 bp. To determine if polymerase stop assays for DNA damage quantification could be adapted for use on a real-time PCR platform, the primer walking strategy was adapted as described in sections 3.2.2.2. and 4.1.2. (Figure 3.4, 4.15). By holding the reverse primer constant and moving the position of the forward primer, four fragment lengths were amplified ranging from 700 bp to 2.25 kb (Table 4.19).

This method relies on the assumption that templates containing one or more damaged bases do not contribute to the PCR, and so for reactions with equal input template quantities, samples with damage will show higher C_T values than samples with no damage. For a given lesion frequency, the probability that any input template contains a damaged base increases as the template length increases. Thus the difference in C_T values (ΔC_T) between undamaged and damaged samples will be higher for longer templates.

For each sample at each template length, ΔC_{Ts} were computed, along with 95% confidence intervals for these ΔC_T values (Table 4.19). Where the confidence interval does not contain the value zero, a significant difference between the C_T value for the damaged sample and that for the undamaged sample was inferred. Significant differences could also be predicated based on a relatively low standard deviation within samples (data not shown). ΔC_{Ts} were determined from two independent real-time PCR data sets. For the first data set, significant differences between 0 L and 1.0 L samples were inferred at all template lengths (Table 4.19). Significant differences between 0 L and 0.5 L samples were inferred at template lengths of 1654 bp and 2241 bp, but not at template lengths of 693 bp or 942 bp (Table 4.19). For the second data set, significant differences were inferred between both damaged samples and the undamaged sample at all template lengths (Table 4.19). The standard deviations of C_T values were generally lower in the second data set, particularly for the shorter template lengths and may have provided a degree of precision necessary to calculate significance (Table 4.19).

Lesion frequencies were computed for both damaged samples (0.5 L and 1.0 L) at each template length and for each data set, using equation **26** (Table 4.19). The variation between data sets was smaller at templates lengths of 1654 and 2241 bp than at the shorter template lengths of 693 bp and 942 bp, consistent with the confidence interval analysis. Lesion frequency estimates using this method were generally 2-fold to 3-fold higher than the estimates of 0.5 lesions and 1.0 lesions per 10,000 bases provided by QPCR.

4.1.2.2. Lesion bypass does not affect estimation of lesion frequencies in simulated data

Data presented by Sikorsky *et al.* (2004) suggest the assumption that damaged templates are completely blocked in the PCR is not technically correct, and that damaged templates contribute to the PCR with reduced efficiency E_D (151). For templates containing single *cis-syn* thymine-thymine dimers, E_D is on the order of 1% (151). In order to test the significance of this effect on lesion abundance calculations, a range of simulated lesion bypass efficiencies from damaged templates were created and, using equation **27** with each estimate, lesion frequencies were computed (Table 4.20; for full derivation of equation **14**, see Appendix E). With simulated efficiencies in the range 0%-5%, differences in the computed lesion frequency were less than 10% (Table 4.20). Therefore, assuming that templates with UV lesions in the target region did not contribute to the reaction was valid in these lesion abundance calculation experiments.

Other types of DNA base modifications, such as 8-oxodG and 8-oxodA, allow lesion bypass at a much higher rate (151). Without an independent, and accurate, measurement of lesion bypass rate, the method presented here is unsuitable for the measurement of such damage. In theory, it is possible to compare ΔC_T values from reactions at two different amplicon lengths and simultaneously calculate both lesion frequency and lesion bypass rate (Appendix F). However, at this time, current limitations in instrumentation and fluorescent detection do not provide the precision necessary to perform these assays.

Table 4.19. Lesion frequencies calculated using real-time QPCR.

	Sample Name	C_T Mean ^a	C_T S.D.	ΔC_T	Significant ^b	Unmodified Efficiency (Eu)	Lesion Frequency ^c	Mean L.F.	S.D. L.F. ^d
Amplicon 3	CNTL#1	18.1	0.157	0.000		0.891			
(N= 693)	0.5L #1	18.1	0.149	-0.0460	No	0.891	0.42	1.1	0.90
	1.0L #1	18.5	0.153	-0.394	Yes	0.891	3.6	3.2	0.54
	CNTL#2	17.8	0.100	0.000		0.891			
	0.5L #2	18.0	0.087	-0.184	Yes	0.891	1.7		
	1.0L #2	18.1	0.032	-0.310	Yes	0.891	2.8		
Amplicon 4	CNTL#1	18.2	0.139	0.000		0.849			
(N=942)	0.5L #1	18.4	0.223	-0.202	No	0.849	1.3	1.7	0.60
	1.0L #1	18.7	0.243	-0.486	Yes	0.849	3.2	4.0	1.1
	CNTL#2	18.5	0.134	0.000		0.849			
	0.5L #2	18.8	0.151	-0.332	Yes	0.849	2.2		
	1.0L #2	19.2	0.351	-0.736	Yes	0.849	4.8		
Amplicon 5	CNTL#1	19.4	0.229	0.000		0.751			
(N=1654)	0.5L #1	19.7	0.162	-0.344	Yes	0.751	1.2	1.4	0.35
	1.0L #1	20.1	0.200	-0.755	Yes	0.751	2.6	2.7	0.27
	CNTL#2	19.5	0.111	0.000		0.751			
	0.5L #2	20.0	0.134	-0.489	Yes	0.751	1.7		
	1.0L #2	20.4	0.208	-0.866	Yes	0.751	2.9		
Amplicon 6	CNTL#1	20.6	0.177	0.000		0.692			
(N=2241)	0.5L #1	21.3	0.471	-0.703	Yes	0.692	1.7	1.3	0.49
	1.0L #1	21.6	0.0980	-0.938	Yes	0.692	2.2	2.2	0.059
	CNTL#2	21.0	0.0590	0.000		0.692			
	0.5L #2	21.5	0.0950	-0.411	Yes	0.692	0.97		
	1.0L #2	21.9	0.0540	-0.903	Yes	0.692	2.1		

a- Mean C_T s were calculated from an N=4 at threshold of 1.0.

b- Significance of mean C_T , using a 95% confidence interval, as established by comparing treated versus control samples (see materials and methods).

c- Calculated using Equation 26 and listed as lesion per 10000 bases.

d- S.D. is the standard deviation of the LF calculations.

e- Amplicons 1 and 2 are not shown.

Table 4.20. Influence of lesion bypass (E_D) on lesion frequency (p) estimation^a.

0.5 L Sample				
	Target Base Length			
Simulated E_D	693	942	1654	2241
0%	1.7	2.2	1.7	0.97
0.1%	1.7	2.2	1.7	0.97
0.2%	1.7	2.2	1.7	0.97
0.5%	1.7	2.2	1.7	0.97
1%	1.7	2.2	1.7	0.98
2%	1.7	2.2	1.7	1.0
5%	1.8	2.3	1.8	1.1
10%	1.9	2.5	2.0	1.2

1.0 L Sample				
	Target Base Length			
Simulated E_D	693	942	1654	2241
0%	2.8	4.8	2.9	2.1
0.1%	2.9	4.8	2.9	2.1
0.2%	2.9	4.8	2.9	2.1
0.5%	2.9	4.8	3.0	2.1
1%	2.9	4.9	3.0	2.2
2%	2.9	4.9	3.0	2.2
5%	3.0	5.2	3.2	2.3
10%	3.3	5.6	3.5	2.6

a- Lesion frequencies are computed using equation 27, using the E_U , C_U , and C_D values from Table 4.19 and presented as lesions per 10000 bases.

4.2. Characterization of Lesion Induced PCR Mutation

When present in synthetic templates, 8-oxodG, 8-oxodA, and abasic sites are known to retard but not absolutely block extension by the Klenow fragment of *E. coli* DNA polymerase I (2, 18, 51, 68) and *Taq* DNA polymerase is able to slowly bypass *cis-syn* thymidine dimers (87). These properties are consistent with observations presented above that replication of some damaged templates is impeded, but not absolutely blocked, during early rounds of the PCR (151).

4.2.1. Melt curves of PCR products from damaged template suggest multiple products

One benefit of amplifying DNA in real-time using SYBR green dye detection is the ability to generate dissociation curves of PCR products to determine melting temperature and the presence of spurious product formation. Annealing kinetics of duplex DNA are mainly influenced by interstrand hydrogen bonding (113); differences in nucleotide sequences can result in changes in duplex melting temperatures. To determine the melting temperatures of PCR products generated from amplification of 90-mer oligonucleotide templates, dissociation curve profiles were generated (Figure 4.15). Oxo CONTROL templates generated PCR products with a unique peak suggesting the formation of a single product; the melting temperature for this 90 bp sequence was approximately 75° C (Figure 4.16). As the amount of 8-oxodG modifications increased in the input oligonucleotide, the ability to resolve definitive peaks in the dissociation curves decreased (OxodG2T, OxodG4T, and OxodG6; Figure 4.16). Dissociation curves from OxodG1, OxodG2A, and OxodG3A templates mimicked those of the Oxo CONTROL (data not shown). These observations implied that multiple products were formed in the PCRs of templates with increased 8-oxodG lesions.

PCR products from OxodA1 templates generated a unique peak with decreased amplitude when compared with that of the Oxo CONTROL (Figure 4.16). This suggested the majority of PCR product formed in these reactions had similar melting temperatures to those from the controls. The Abasic template profiles were less definitive; at least three peaks were observed, one of which occurred at a point similar to

the Oxo CONTROL (Figure 4.16). These data indicated that multiple products were formed as a result of abasic site bypass.

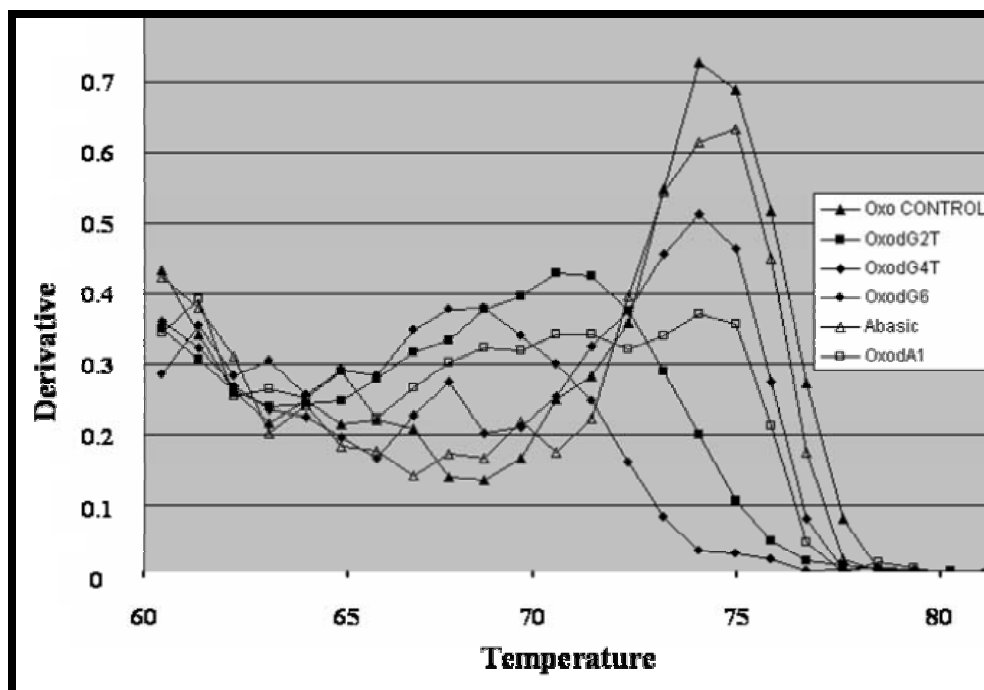


Figure 4.16. Dissociation curves of PCR products from modified oligonucleotides. Melting temperatures of PCR products from the amplification of 90-mer Oxo CONTROL oligonucleotides were approximately 75° C. The amount and type of modification influenced the ability to resolve definitive peaks in the dissociation profiles; all graphs represent N=5.

4.2.2. The fidelity of Taq polymerase is influenced by lesions on the input DNA template.

To determine if lesions on the oligonucleotide templates influenced nucleotide incorporation, the real-time PCR products from modified oligonucleotide amplifications were purified and the sequences determined (Figures 4.17-4.20; summarized in Table 4.21; data not shown). The forward amplification primer was used to sequence the PCR products. This primer binds to the complement of the input oligonucleotide used and therefore any sequence obtained is suggestive of lesion bypass and full-length product formation. Sequence data from all oligonucleotides tested is summarized below (Table 4.21).

The Oxo CONTROL and Dimer CONTROL matched their expected sequences (Figure 4.17; 4.20A). In all templates with 8-oxodG lesions, a mixture of reaction products was obtained (Figure 4.18). The majority of amplicons contained the normal Watson-Crick insertion of dCMP opposite the lesion site; the minority amplicon sequence from most 8-oxodG containing templates included dAMP pairing opposite the base lesion, creating a stable transversion [guanine to thymine] (Figure 4.18). When two 8-oxodGs were adjacent on the input template, in addition to the incorporation of dCMP and dAMP opposite the lesion sites, a pronounced n-1 deletion event occurred (Figure 4.18). The addition of subsequent adjacent 8-oxodGs resulted in indistinct product sequences (Table 4.21; data not shown).

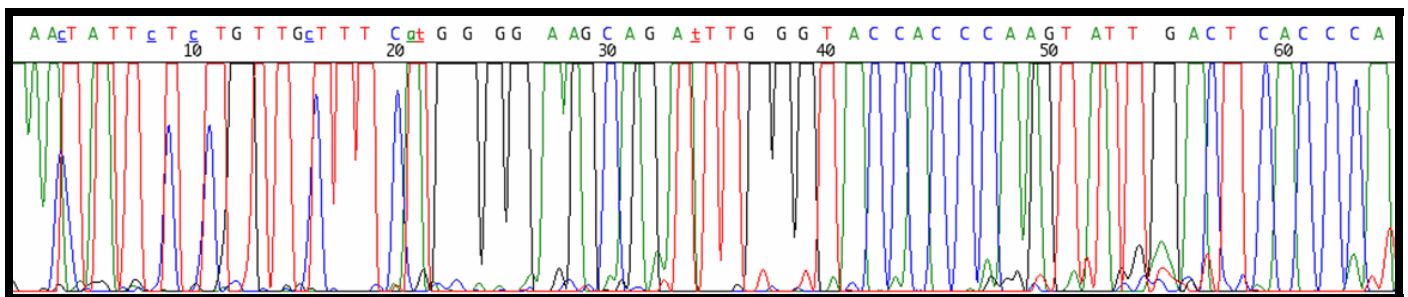


Figure 4.17. Sequence analysis of PCR product from Oxo CONTROL oligonucleotide. Black, green, red, and blue represent guanine, adenine, thymine, and cytosine bases respectively. PCR product sequences from the amplification of 90-mer Oxo CONTROL oligonucleotides were equivalent to the expected input synthesis sequence; neither failed synthesis products nor PCR derived mutations were detected. Background fluorescence was observed and could be attributed to increased peak amplitude resulting from excess fluorescent dye incorporation.

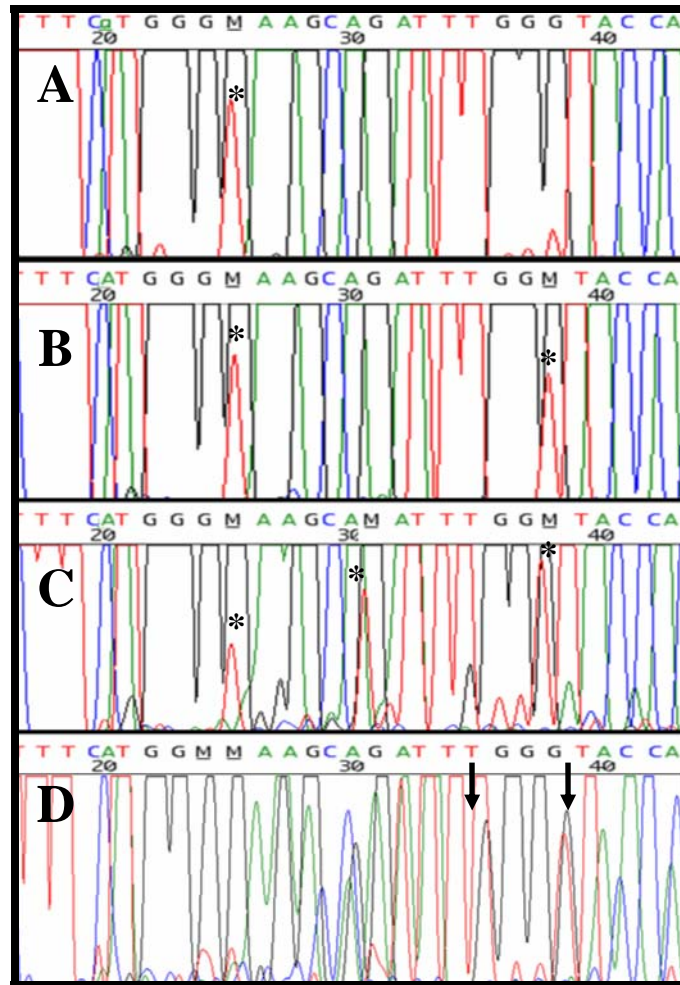


Figure 4.18. Sequence analysis of PCR product from oligonucleotides containing 8-oxodG base modifications. Black, green, red, and blue represent guanine, adenine, thymine, and cytosine bases respectively. Amplification of 90-mer oligonucleotides, A) OxodG1, B) OxodG2A, C) OxodG3A, and D) OxodG2T, resulted in multiple PCR products; sites of DNA modification are designated (**M**) in the sequence header. In all products examined, G→T transversions at the site of modification were observed (*). In addition, two adjacent 8-oxodGs (OxodG2T) resulted in n-1 deletion products (solid down arrows).

Amplicons created by replication through 8-oxodA were also mixed. The predominant sequence generated contained the incorporation of dTMP opposite the lesion site (Figure 4.19A). In addition, a pronounced n-1 deletion occurred during amplicon synthesis, originating opposite the 8-oxodA (Figure 4.19A). Nucleotide incorporation opposite single abasic sites also resulted in mixtures of amplicons (Figure 4.19B); n-1 deletions, n+1 insertions, and a mixture of dNMP incorporations were observed. Base association across from single thymine dimer modifications and subsequent strand extension were not clear (Figure 4.20B). While the predominate base incorporated

opposite the TT Dimer modification appeared to be dCMP, an unambiguous characterization of extension products could not be determined (Figure 4.20B). Like that seen in products from multiple adjacent 8-oxodGs (greater than 3), this ambiguity can be attributed to the presence of multiple extension products (deletions and insertions), none of which could be considered a majority sequence, which disrupt the dye terminator sequencing reactions.

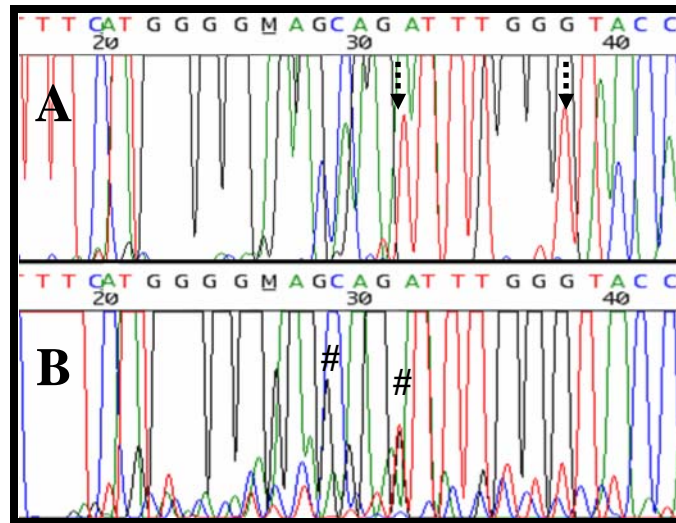


Figure 4.19. Sequence analysis of PCR product from oligonucleotides containing 8-oxodA and abasic base modifications. Black, green, red, and blue represent guanine, adenine, thymine, and cytosine bases respectively. Amplification of 90-mer oligonucleotides, A) OxodA1, and B) Abasic templates resulted in multiple PCR products; sites of DNA modification are designated (M) in the sequence header. In addition to the majority sequence (dTMP incorporation opposite modification), a pronounced n-1 deletion originated at the 8-oxodA site (dashed down arrows). Guanine is present at the site of modification in PCR products from Abasic template (suggesting dCMP incorporation); in addition, minority peaks were observed (#).

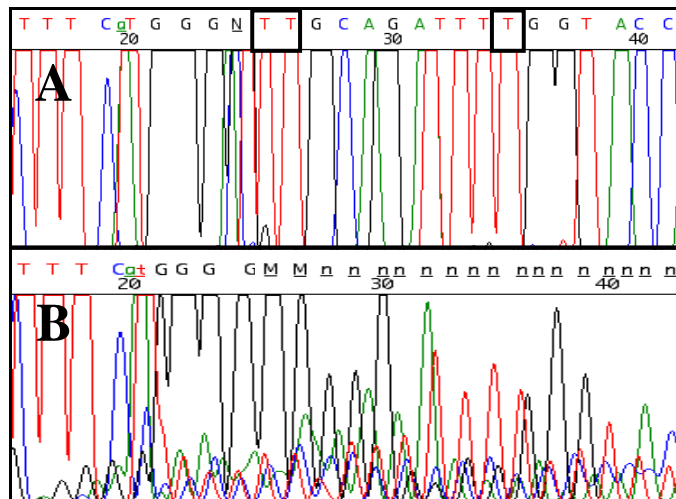


Figure 4.20. Sequence analysis of PCR product from oligonucleotides containing a *cis-syn* Thymine-Thymine dimer. Black, green, red, and blue represent guanine, adenine, thymine, and cytosine bases respectively. Amplification of the A) Dimer CONTROL oligonucleotide resulted in PCR products containing the appropriate thymine substitutions (boxed). PCR products from amplification of the B) TT Dimer1 template resulted in multiple sequences; guanine is present in the sense strand at the site of modification suggesting dCMP was predominately incorporated across from the dimer; multiple minority peaks were observed but could not be distinguished. Sites of DNA modification are designated (**M**) in the sequence header.

Table 4.21. Summary of PCR derived mutation as a result of lesion bypass.

Sample	Majority Nucleotide ^a	Minority Nucleotide ^b
Oxo CONTROL	no modification	no modification
OxodG1 (48)	dCMP	dAMP
OxodG2A (48/61)	dCMP	dAMP
OxodG3A (48/53/61)	dCMP	dAMP; possible n-1 ^c
OxodG2T (47/48)	dCMP	n-1 ^c ; dAMP
OxodG3T (46-48)	NA	NA
OxodG4T (45-48)	NA	NA
OxodG6 (45-48/59/60)	NA	NA
OxodA1 (49)	dTMP	n-1 ^c
Abasic (49)	possible dCMP	possible n-1 ^c , possible n+1
Dimer CONTROL ^d	no modification	no modification
TT Dimer1	dCMP	possible n-1 ^c , possible n+1

a- Predominant nucleotide incorporated opposite site of DNA base modification.

b- Secondary sequences created, in addition to the majority sequence, during the PCR; listed by order of observed fluorescent intensity.

c- Observed frame-shifting originated at site of modification.

d- To create Dimer CONTROL, with respect to the Oxo CONTROL sequence and the 3' terminus, thymine base substitutions were made at positions 49, 50, and 59 (Table 3.1).

4.2.3. Restorase DNA polymerase misincorporates nucleotides opposite base lesions

Four 90-mer oligonucleotides were amplified using the Restorase DNA polymerase system (Sigma). To determine base incorporation opposite the modifications, PCR products were sequenced as described above (section 3.3.3.). PCR products from all templates tested contained the sequencing primer binding site which suggested lesion bypass and full-template amplification (summarized in Table 4.22). Sequences of products from the Oxo CONTROL oligonucleotide template were as expected (Figure 4.21A; Table 3.1). Restorase bypass of 8-oxodG modifications (OxodG2A) produced multiple sequences, the majority of which mimicked the control; however, some products contained guanine to thymine transversions suggesting dAMP incorporation opposite the

site of modification (Figure 4.21B). Templates containing 8-oxodA resulted both in expected and PCR products with n-1 deletions originating at the site of modification (Figure 4.21C). The majority of products produced from abasic site bypass by Restorase followed the “A-rule”, with dAMP being the predominate nucleotide incorporated opposite the empty abasic site (Figure 4.21D; (73)). In addition to dAMP incorporation, n-1 deletions were present, originating at the abasic site, in some PCR products (Figure 4.21D).

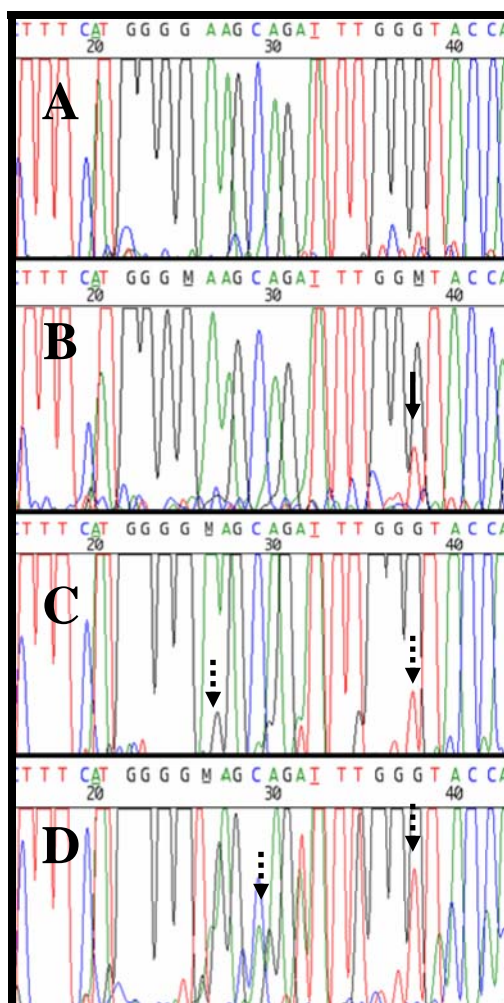


Figure 4.21. Sequence analysis of PCR product from modified oligonucleotides amplified by Restorase DNA polymerase. Black, green, red, and blue represent guanine, adenine, thymine, and cytosine bases respectively. Amplification of 90-mer A) Oxo CONTROL oligonucleotides using Restorase DNA polymerase resulted in the expected Anderson sequence (156). B) The majority of nucleotide insertions opposite 8-oxodG modifications (OxodG2A) were dCMPs; some dAMP insertion was observed at one of the modified sites (solid down arrow). C) OxodA1 oligonucleotide template produced products with dTMP incorporations (majority) and n-1 deletions (minority; designated with dashed down arrows). D) Abasic templates resulted in multiple PCR products; dAMP incorporation (majority) and n-1 deletions (minority; designated with dashed down arrows) were observed. Sites of DNA modification are designated (**M**) in the sequence header

Table 4.22. Restorase lesion bypass products^a.

Sample	Majority Nucleotide	Minority Nucleotide
Oxo CONTROL	no modification	no modification
OxodG2A (48/61)	dCMP	dAMP ^b
OxodA1 (49)	dTMP	n-l
Abasic (49)	dAMP	n-l

a- Sequence descriptions were as described in Table 4.18.

b- dAMP incorporation was only detected above background fluorescence opposite the 8-oxodG modification at position 61 and not the modification at position 48.

CHAPTER V

Summary and Conclusions

5.1. Quantification of DNA Damage

Implicating DNA damage as a preliminary step in carcinogenesis and aging emphasizes a need for clinical assays to screen for aberrant amounts of damage to cellular DNA. Current QPCR methods are the most sensitive of the polymerase stop based assays but require long template amplification (greater than 10 kb; (5)) and, in some cases, the use of hazardous radioisotopes. To alleviate these requirements, real-time PCR mathematics and protocols were adapted to quantify damage to DNA. In addition to redefining changes in C_T values as degrees of damage rather than differences in input template, data indicated that different types and amounts of DNA base modification impact the rate of the PCR to different degrees. The observation that lesions did not terminally block *Taq* polymerase progression lead to the discovery of lesion induced PCR mutagenesis.

5.1.1. Lesion bypass

When present in synthetic templates, 8-oxodG, 8-oxodA, and abasic sites are known to retard but not absolutely block extension by the Klenow fragment of *E. coli* DNA polymerase I (2, 18, 51, 68, 73) and *Taq* DNA polymerase is able to slowly bypass cis-syn thymidine dimers (87). These properties are consistent with the observation that replication of some damaged templates is impeded, but not absolutely blocked, during early rounds of the PCR (Figures 4.6-4.8).

Lesion bypass during the PCR results in the creation of unmodified amplicons that mimic the reaction kinetics of the control templates masking any influence of modifications on reaction efficiency at detectable fluorescent levels (Figure 5.1). Creation of novel mathematical treatments to define differences between PCRs with

equal template amounts as differences in the rate of reaction efficiencies from templates with DNA modification were necessary to characterize this apparent lag in early exponential amplification (Figure 5.2).

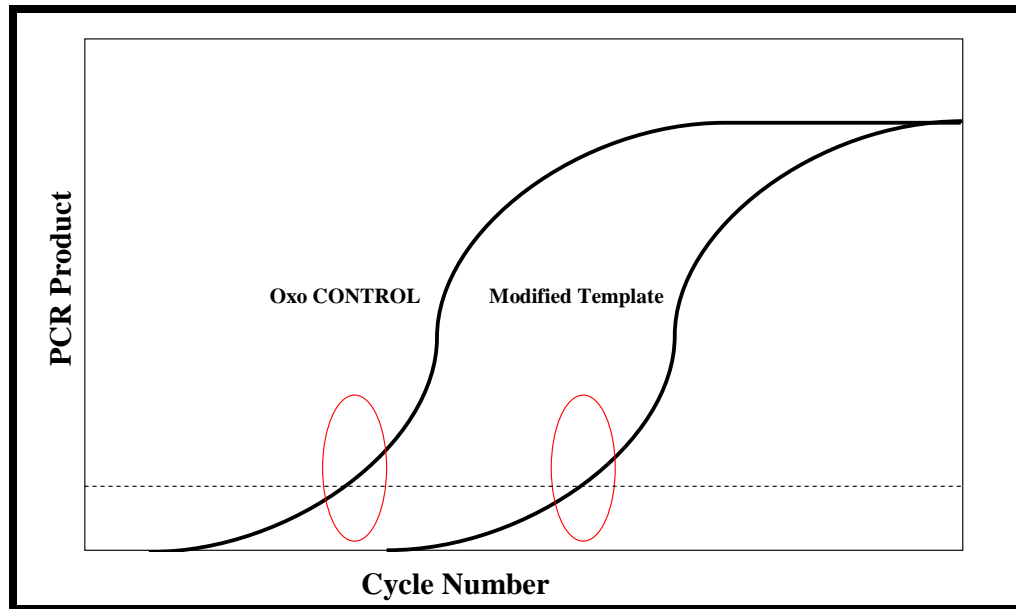


Figure 5.1. Observed PCR curves of modified and unmodified templates. Templates containing DNA base modifications hinder but do not halt the PCR. PCR derived unmodified amplicons are present in each subsequent cycle and produce reaction curves, at detectable fluorescence levels, that mimicked those of unmodified control templates.

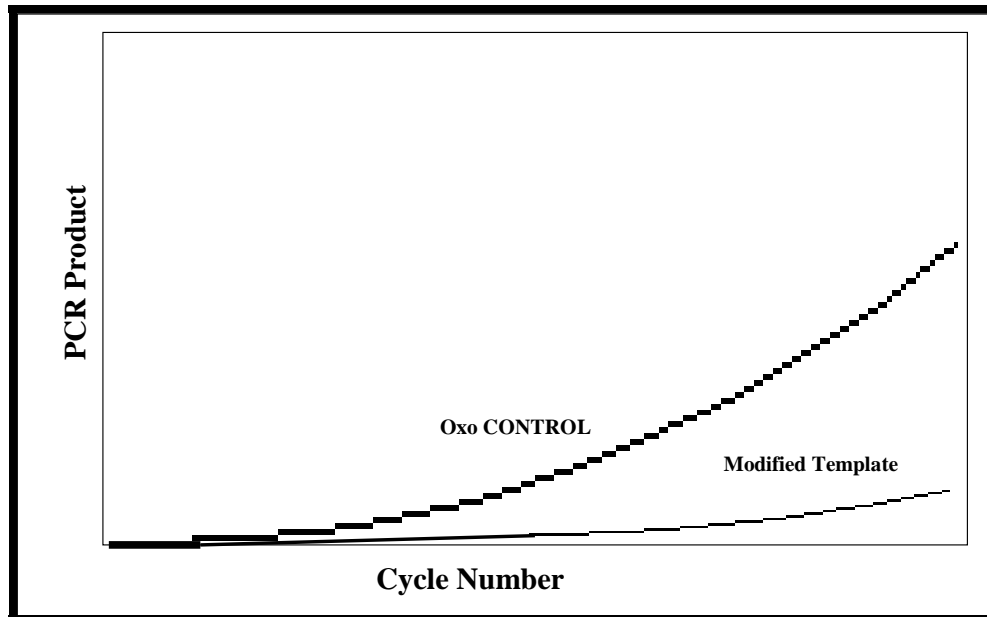


Figure 5.2. DNA base lesions create a delay in early exponential phase. Templates containing DNA base modifications decrease the rate of the PCR. This decreased rate is observed as a rightward shift in amplification curves prior to detectable amplification.

5.1.1.1. Rate of lesion bypass: the RTC efficiency method

The RTC method was designed to explain differences in PCR curves resulting from inherent input template quality while holding input template quantity constant (151). In early real-time PCR cycles, replication of full-length modified oligonucleotides gave rise to unmodified PCR products which were exponentially amplified in subsequent cycles. Even though the amplification curves of unmodified and some modified templates had similar exponential phases (Figure 5.1), rightward shifts in the amplification curves of templates with single 8-oxodA, abasic site, TT dimer, with three separated 8-oxodG, or with any number of tandem 8-oxodG modifications were observed (Figures 4.6-4.8). This shift stemmed from a prolonged lag in early exponential phase (Figure 5.2) that could be described as a difference in C_T values and translated into RTC efficiencies (Tables 4.3-4.5). Although a single 8-oxodG base had no detectable effect on RTC efficiency, the presence of a single 8-oxodA, abasic site, and TT dimer modifications dramatically reduced RTC efficiencies by 81.2%, 98.5%, and 99.2%

respectively. Two tandem 8-oxodG bases reduced RTC efficiency by 98.5%. Assuming that the reaction efficiencies from the ICR and full-length amplifications are identical and assuming that these are interchangeable between templates, RTC efficiency is an appropriate method to characterize large differences in the rate of the PCR resulting from lesion bypass (Tables 4.3-4.5).

5.1.1.2. Rate of lesion bypass: the MME method

The mean modified efficiency method builds on the RTC method for quantifying aggregate damage to DNA template using real-time PCR. By calculating the reaction efficiencies for the ICR and full-length amplifications, as well as the amount of fluorescence generated by each input template, and incorporating these into the equation **14**, significant differences in MMEs were observed between the Oxo CONTROL and both the OxodG1 and OxodG2A templates (statistically significant at $p < 0.05$; Table 4.9). These observations suggest the MME calculations are appropriate to characterize small differences in the rate of lesion bypass during the PCR, not detectable using the RTC method.

5.1.1.3. Different lesions influence PCRs to different degrees

DNA base lesions cause extended lags in exponential amplification during the PCR. These lags result in rightward shift in real-time PCR curves and translated into differences in RTC (Tables 4.3-4.5) and MME (Tables 4.8-4.10). Contrary to current QPCR assumptions that thermostable polymerase progression is blocked by single lesions, observations presented here indicated different lesions impact the PCR to different degrees (Figure 5.3).

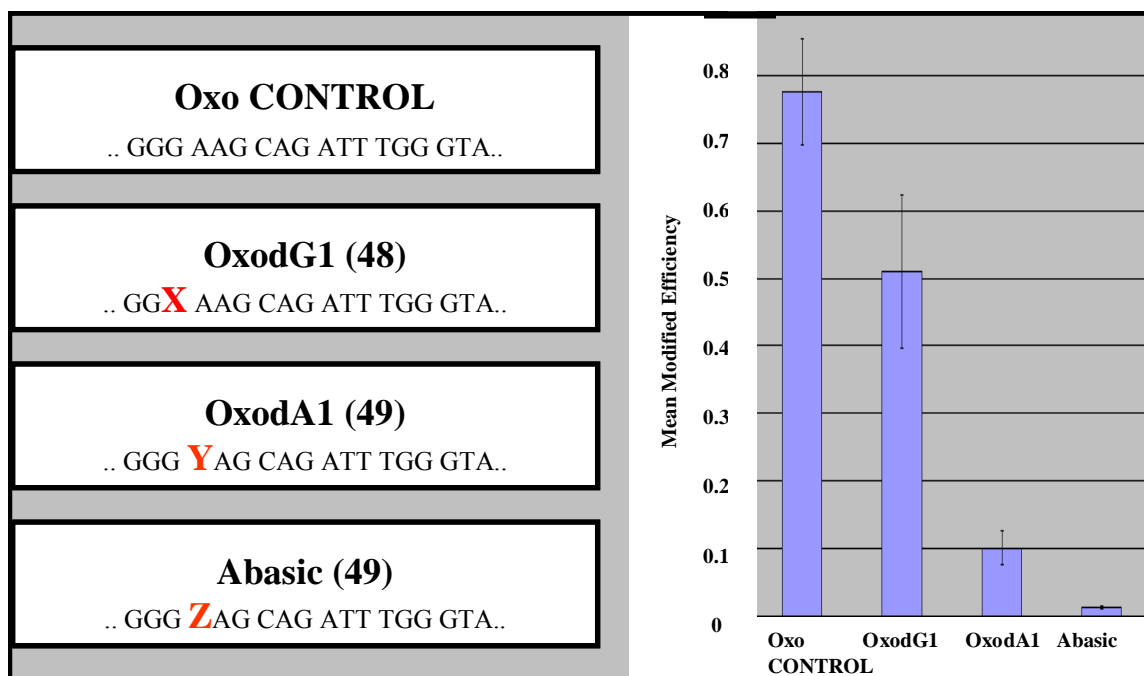


Figure 5.3. Different base modifications influence the PCR to different degrees. When compared to sequence matched controls, mean modified efficiencies of templates containing single 8-oxodG (X), 8-oxodA (Y), and abasic site (Z) modifications were reduced. These reductions in MME were base lesion specific.

The observation that single 8-oxodA lesions decreased amplification efficiency by 82% when compared with 8-oxodG was unexpected and not easily explained. These base modifications both contain additional hydroxyl groups at the 8th position on their respective purine rings (8-oxodG formation reviewed in above; Figure 2.2). Both modifications impact backbone dynamics of short oligonucleotides (157) but neither severely impedes the progression of Klenow (18, 68). Initial reports diagramming 8-oxodA bypass by Klenow indicate very low chain termination opposite 8-oxodA (67). Studies also show that, in the presence of excess polymerase, the insertion and extension of dTMP opposite the 8-oxodA lesion far exceed that of any other dNTP (68). Given that dTMP is exclusively incorporated opposite the 8-oxodA modification, one possible explanation of the observed drop in RTC and MMEs from 8-oxodA containing templates is the presence of dUTP (rather than dTTP) in the experimental dNTP mixture; a measure used to decrease PCR carryover contamination. The insertion kinetics of an incoming dUMP opposite 8-oxodA has not been characterized and it is certainly possible that this

could impact the PCR. The increase in observed RTC efficiencies from 8-oxodA templates in the Restorase reactions strengthens this hypothesis. These reactions contained dTTP and corroborated earlier reports of 8-oxodA bypass by *Taq* (Figures 4.4, 4.13; (67)). Results must be viewed with caution because the possibility of lesion repair exists in reactions with Restorase; however, the likelihood of this impacting reactions with 8-oxodA is decreased due to repair selectively (165), the use of ssDNA (Restorase repair works on duplex DNA (167)), and the short incubation times (less than 5 min) at low temperatures (4° C; (165)).

A tetrahydrofuran analog (synthetic abasic site) creates a more formidable block to Klenow progression but full-length extension products are eventually generated (73). Smith *et al.* (1998) report that both Klenow and *Taq* are able to bypass *cis-syn* dimers slowly; with both polymerases stopped one nucleotide prior to and directly opposite the 3'-T and with *Taq* synthesis also stopped opposite the 5'-T (87). Observations presented here are in full agreement with these results; PCRs from templates with abasic sites and TT dimers are slowed dramatically but not stopped completely, which resulted in significantly lower RTC and MMEs (Tables 4.3, 4.5 and 4.8, 4.10 respectively).

5.1.1.4. The position of 8-oxodG lesions relative to each other impacts the PCR

The presence of the 8-oxo group can cause pronounced changes in base interactions and changes in phospho-deoxyribose backbone (157). These alterations in template secondary structure could prevent *Taq* DNA polymerase advancement resulting in the observed reduction in RTC and MMEs. Increased numbers of 8-oxodGs systematically reduced RTC and MMEs; coupled with observations that placing 8-oxodGs adjacent to one another (OxodG2T; OxodG3T; OxodG4T; OxodG6) enhanced the reduction (Figure 5.4), an argument that the position of base modifications on a DNA template has a much greater influence in reducing template amplification than does the number of 8-oxodG modifications can be made and that these reductions may, in part, be attributed to altered oligonucleotide backbone structure.

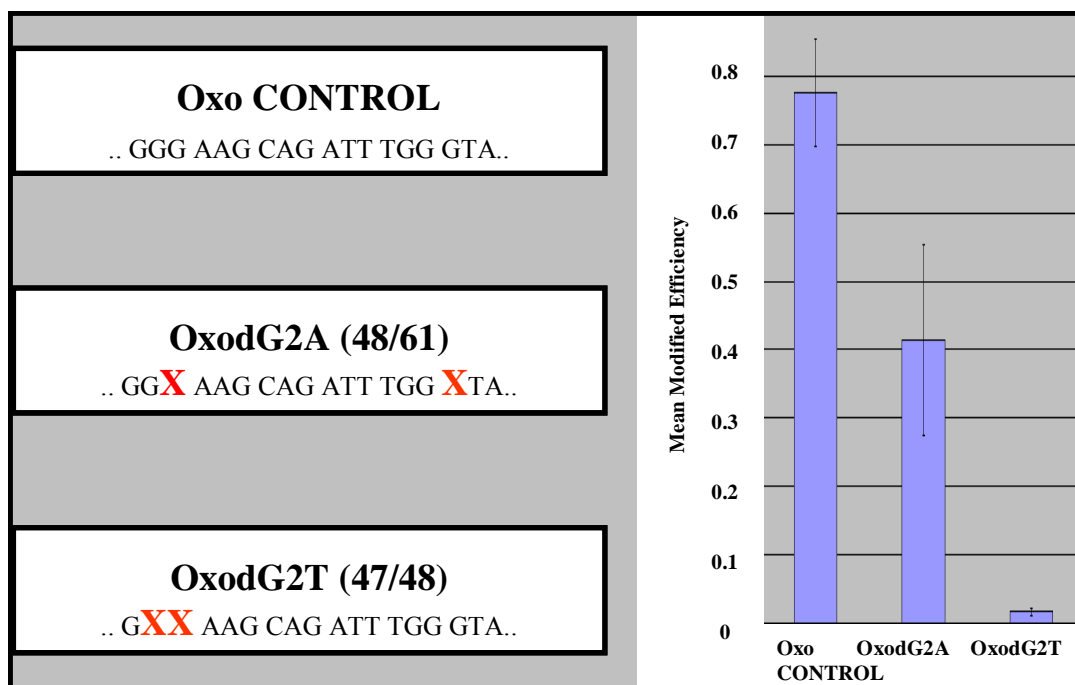


Figure 5.4. The positioning of multiple 8-oxodGs relative to one another significantly alters modified reaction efficiency. Placing two modifications adjacent one another results in a 96% decrease in modified amplification efficiency when compared to the MMEs from templates with two 8-oxodGs separated by 13 bases. Sites containing modified 8-oxodG bases are designated by (X).

The basis for QPCR methods of DNA damage detection is that the PCR is blocked by the presence of certain lesions in the DNA template which results in a decrease in amplification product (5, 8-11). These methods assume that each lesion blocks polymerase advancement to the same degree and that there are no positional effects (e.g. that two separate lesions would have the same effect as two tandem lesions). Observations that the type and position of base damage strongly influenced the PCR to differing degrees, suggest that some QPCR methods may underestimate or overestimate the amount of damage.

5.1.2. Calculation of lesion abundance

Current QPCR DNA damage assays rely on endpoint analysis and, in some instances, the incorporation of radiolabeled nucleotides in order to quantify PCR product from damaged or undamaged templates (5, 8-11). In addition, these methods require the independent establishment of exponential phase amplification for each DNA target (5, 8-

11). Adaptation of real-time PCR technology to DNA damage detection methods have allowed for rate-based determination of the extent of damage and obviated the need for radiolabeled nucleotides (151).

Most real-time PCR protocols require a short target DNA, usually less than one hundred fifty base pairs to insure high amplification efficiency. However, in order to achieve detection of biologically relevant levels of damage and estimate the sensitivity of the detection method, protocols for the real-time amplification of larger (1000-10,000 bp) target must be developed. In addition, development of formulae which calculate the probability of encountering a damaged base in cellular DNA containing both damaged and non-damaged template from changes in threshold cycle values was required.

To validate real-time PCR for detection of biologically relevant levels of UV induced photoproducts in cellular DNA, mtDNA fragments ranging from 600 bp to 2.25 kb (Amplicons 2-5; Figure 3.4) were amplified using the ABI 7000 sequence detection system from total cellular DNA stocks which had been previously determined to contain 0 L, 0.5 L, and 1.0 L per 10 kb by conventional QPCR methods (11). Significant differences in cycle threshold C_T values were observed and, in combination with equation 26, translated into lesion frequencies (Table 4.18). Significant levels of damage, ranging from 1 to 4 lesions per 10 kb, were consistently detected in amplicon sizes greater than 1.5 kb (Table 4.18).

Despite maintaining trends between both sample populations, real-time based polymerase stop assays estimated damage to be 1.9 to 4.8-fold higher than QPCR assays. This increase in frequency could be explained by differences in (1) amplification targets or (2) PCR protocols.

Previous studies comparing oxidative damage to nuclear and mitochondrial DNA suggest that mtDNA has a two to three fold higher lesion frequency than nuclear targets in the same sample (5, 11). It is reasonable to assume that UV damage would present with similar patterns and therefore the observed differences in lesion frequency would be expected. However, Kalinowski *et al.* (1992) see only marginal, although elevated, differences between lesion frequencies of nDNA and mtDNA from UV irradiated sample material (approximately 1.5-fold more in mtDNA (7)). In general, such discrepancies

may be caused by a difference in AT content. However, a review of the targets used in this study yielded no appreciable difference in sequence content. Therefore, at least in this case, AT content was not a likely cause in observed differences in lesion frequency (data not shown).

Shielding by nuclear chromatin may afford protection to nDNA, a mechanism not found in mitochondria and therefore can not be ruled out as a possible reason for lesion differences in mitochondrial and nuclear DNA. In addition, NER mechanisms which remove bulky adducts from DNA do not exist in the mitochondria and could inflate the proportion of mitochondrial versus nuclear lesions should damaged cells have time to initiate repair processes (9). Approximately 10% of UV induced blocking lesions are repaired after 4 hrs (7); making it highly unlikely that appreciable repair occurred between exposure and freezing in this current study.

QPCR employs *rTth* DNA polymerase XL and a protocol optimized to amplify long fragments of DNA. The real-time PCR assay described here uses *Taq* DNA polymerase and was adapted from protocols optimized to amplify short fragments (less than 150 bp). Despite a similarity in polymerases, differences in incorporation/extension kinetics past DNA modifications would result in changes in observed lesion frequencies. While certainly possible, the likelihood that these differences would impact lesion bypass to a degree significant enough to alter lesion frequencies is remote (as inferred by lesion bypass simulations; Table 4.20). QPCR measures lesion frequency based on the amplification of longer DNA targets (5, 11). It is possible that UV photoproducts impact the PCRs to a lesser degree in longer DNA target lengths and would, therefore, increase the observed lesion frequencies in shorter templates.

Even with observed differences in lesion frequency, these data implied that real-time PCR protocols could be adapted to estimate relevant amounts of UV damage in cellular DNA and may provide greater sensitivity than conventional QPCR protocols.

5.1.3. Matched controls are required for real-time PCR quantification

In order to prepare an appropriate control template for the TT Dimer1 oligonucleotide, several thymidine substitutions were made in the Oxo CONTROL

sequence (Table 3.1). The RTC and MMEs from this Dimer CONTROL (1.03 and 1.28; Tables 4.5, 4.10) were greater than those of Oxo CONTROL (0.544 and .776; Tables 4.3, 4.8). Theoretically, these values should have equaled 1.0; the differences represented shifts in the full-length amplification curves when compared with curves from the ICRs (Figure 4.6). Observed differences in control RTC and MMEs can be explained by a reduction in the stability of secondary structure in the Dimer CONTROL template which resulted in improved *Taq* progression (Figures 4.9, 4.10). These observations emphasize the need for matched controls in the RTC/MME methods and, for that matter, any real-time PCR protocol.

5.1.4. PCR efficiency during early amplification impacts real-time calculations

Nogva *et al.* (2004) present evidence that products produced in early rounds of amplification by the PCR form secondary structures that alter their respective replication efficiencies and impact real-time PCR based transcript abundance calculations (Figure 2.8; (145)). The work presented here is in agreement with these findings (Figures 4.9, 4.10); adding that DNA base lesions impact early rounds of the PCR and influence current real-time PCR mathematics (Tables 4.1, 4.2). Due to the decreased probability of encountering a damaged site in short targets (used in most real-time PCR assays; presented in *lesion frequency* results section 4.1.2.1.), attempts to correlate DNA amounts determined from short template amplification to those of larger targets should be done with great caution. An example of this would be the use of real-time PCR to determine DNA amounts in forensic science where the environmental assault on sample material is great; the amplification of 50 bp (real-time PCR target) may not translate into amplifiable DNA at 400 bp (largest target loci). In these cases, it would be more appropriate to define results obtained as amplifiable template at a particular target length than it would be to report template abundance from real-time data.

5.2. Lesion Induced PCR Mutation

5.2.1. PCR derived mutation as a consequence of lesion bypass

The generation of full-length products in PCRs with 8-oxodG, 8-oxodA, abasic, and TT dimer lesion containing oligonucleotide templates suggested that *Taq* DNA polymerase was not completely blocked by these base modifications. These observations are in accordance with lesion bypass studies using DNA polymerase I (2, 18, 51, 68, 73) and indicate the assumption that lesions block thermostable polymerase progression requires revision (5). Given that these lesions do not completely block *Taq*, the degree to which the fidelity of the PCRs was impacted was characterized.

From previous work done by others, in addition to influencing the rates of proper nucleotide insertion and extension, the capability to insert mismatched bases by many DNA polymerases is increased in the presence of base lesions (2, 18, 51, 68, 73). For example, Shibutani *et al.* (1991) report that dAMP is introduced opposite 8-oxodG and readily extended by both the Klenow fragment and intact DNA polymerase I; therefore, 8-oxodG is considered pre-mutagenic (17). Sequence data from PCR products obtained from reactions with 8-oxodG templates contained a mixture of dG and dT at the sites of modification suggesting that both dCMP and dAMP were incorporated by *Taq* DNA polymerase and, therefore, that the 8-oxodG base lesion was pre-mutagenic in the PCRs (Figure 4.18).

8-oxodA, on the other hand, is not mutagenic in the presence of all four dNTP promoting the insertion and extension of dTMP by DNA pol I opposite the site of damage (68). The authors point out, however, that if the concentration of the polymerase is reduced 100-fold, translesional synthesis past 8-oxodA by Klenow is retarded one base before and directly opposite the lesion (68). Guschlebauer *et al.* (1991) observe that, in the presence of all four dNTPs, *Taq* DNA Polymerase (1 U of enzyme) directs dTMP incorporation exclusively (67). In addition to the expected dTMP, n-1 deletions were observed in PCRs with 8-oxodA originating at the site of modification (Figure 4.19A). These findings were surprising as they aren't consistent with other reports of *Taq* polymerase bypass of this lesion (67). One possible explanation for this discrepancy is

that the amount of enzyme used in each study differed; while the amount of enzyme in the Applied Biosystems master mix used within is proprietary, the number of units of enzyme per reaction were estimated to be half of that used in the Guschlebauer *et al.* (1991) experiments (data not shown; (67)). Given, when in excess, Klenow is also not hindered at the site of modification (68), it is reasonable to assume that an excess amount of *Taq* would react in the same fashion and could explain why Guschlebauer and colleagues observed no 8-oxodA impact on *Taq* polymerase progression. In addition, the ABI master mix contains a dNTP mixture with dUTP; a measure used to decrease PCR carryover contamination. The insertion kinetics of an incoming dUMP opposite 8-oxodA has not been characterized and it is certainly possible that this could result in decreased polymerase fidelity and the observed n-1 deletion. This argument is strengthened by the apparent decrease in n-1 deletion products from the Restorase PCRs; containing dTTP rather than dUTP (Figure 5.5).

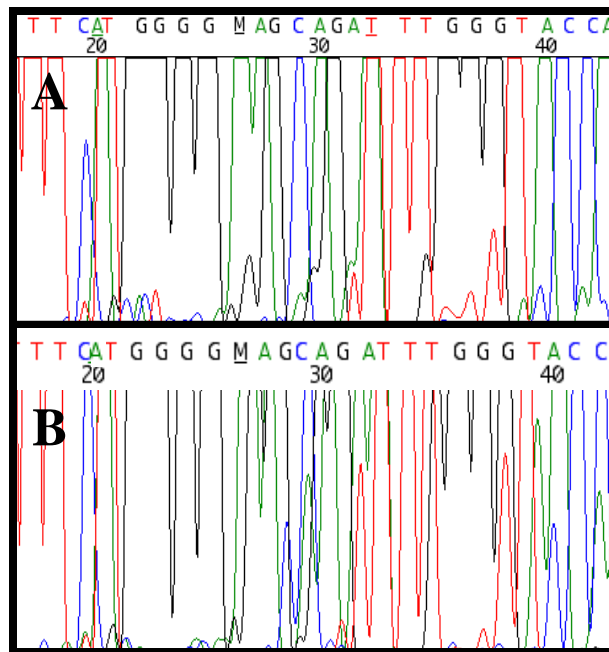


Fig. 5.5. Mutations opposite 8-oxodA lesions are reduced with Restorase. Black, green, red, and blue represent guanine, adenine, thymine, and cytosine bases respectively. The frequency of n-1 deletions appears to decrease in reactions with the A) Restorase polymerase mixture and dTTP in comparison to B) AmpiTaq Gold and dUMP.

Smith *et al.* (1998) report that both Klenow and *Taq* are able to bypass *cis-syn* dimers slowly (87). Data presented here are in agreement with these findings as the presence of the primer binding site required for the cycle sequencing reactions suggested that full-length products were generated. dCMP was the most incorporated dNTP opposite the modification and the lack of readable sequence post modification suggested the presence of multiple frameshifting mutations; originating at the site of damage (Figure 4.20B).

In reactions containing templates with single abasic sites, a stalling occurred during early amplification (as suggested by the RTC and MME data) and the resulting lesion bypass produced a mixture of n-1 deletions and n+1 insertions (Figure 4.19B). While data suggested the tetrahydrofuran analog in this *Taq* polymerase model didn't follow the A-rule proposed by Grollman and colleagues, a mechanistic deletion similar to that seen by Shibutani *et al.* (1997) with Klenow was observed (73). In this model, authors hypothesize that sequences flanking the absent base can mispair during the period in which the polymerase is stalled at the site of modification creating either insertions or deletions (73).

5.3. Future Directions

Polymerase stop based assays used to determine lesion frequencies assume that each DNA base lesion blocks polymerase advancement to the same degree and that there are no positional effects (e.g. two separate lesions would have the same effect as two tandem lesions). Since observations presented here implied that the type and position of base damage strongly influenced the PCR (presented as differences in RTC and MME), some polymerase stop assays may underestimate or overestimate the amount of DNA damage (151).

The rate of lesion bypass can be estimated using RTC or MME. These measurements can be determined and, using equation 27, incorporated into lesion frequency calculations (as presented as estimations in Table 4.20). In addition, novel formulae, presented in Appendix E, model the PCRs of mixed templates and report both lesion bypass rate and lesion frequency. Work to adapt lesion frequency measurements

to include rate of lesion bypass will increase precision and accuracy of lesion abundance measurements. However, instrument precision, in its current format, is insufficient to permit these types of calculations but may occur in the future as technology advances (Appendix E).

Real-time PCR based damage quantification methods presented here represent a stepping stone for the implementation of polymerase stop based assays as clinical tools to estimate DNA damage. Advancement of real-time PCR instrumentation and polymerase stop based protocols could present alternatives to current clinical monitoring assays of DNA intercalating drugs such as Cisplatin. In addition, screening aggregate levels of DNA damage and/or rates of DNA repair in age and cancer related disorders by PCR methods could become possible. Work to characterize the sensitivity limits of these assays is the next step in determining applicability of real-time PCR damage quantification methods in both research and clinical settings.

BIBLIOGRAPHY

- [1] Kunz, B., Straffon, A., and Vonarx, E. (2000) DNA damage-induced mutation: tolerance via translesion synthesis. *Mutat. Res.*, **451**, 169-185.
- [2] Wallace, S.S. (2002) Biological consequences of free radical-damaged DNA bases. *Free Radic. Biol. Med.*, **33**, 1-14.
- [3] Loft, S., and Poulsen, H. (1996) Cancer risk and oxidative DNA damage in man. *J. Mol. Med.*, **74**, 297-312.
- [4] Lu, C., Lee, H., Fahn, H., and Wei, Y. (1999) Oxidative damage elicited by imbalance of free radical scavenging enzymes is associated with large-scale mtDNA deletions in aging human skin. *Mutat. Res.*, **423**, 11-21.
- [5] Yakes, F.M., Chen, Y., and Van Houten, B. PCR-based assays for the detection and quantitation of DNA damage and repair, in: Pfeifer, G. (ed.) *Technologies for detection of DNA damage and mutations*, Plenum Press, New York, 1996, pp. 171-184.
- [6] Govan, H., Valles-Ayoub, Y., and Braun, J. (1990) Fine mapping of DNA damage and repair in specific genomic segments, *Nucleic Acids Res.*, **18**, 3823-3829.
- [7] Kalinowski, D., Illenye, S., and Van Houten, B. (1992) Analysis of DNA damage and repair in murine leukemia L1210 cells using a quantitative polymerase chain reaction assay, *Nucleic Acids Res.*, **20**, 3485-3494.
- [8] Salazar, J.J., and Van Houten, B. (1997) Preferential mitochondrial DNA injury caused by glucose oxidase as a steady generator of hydrogen peroxide in human fibroblasts. *Mutat. Res.*, **384**, 139-149.
- [9] Sawyer, D., and Van Houten, B. (1999) Repair of DNA damage in mitochondria, *Mutat. Res.*, **434**, 161-176.
- [10] Ayala-Torres, S., Chen, Y., Svoboda, T., Rosenblatt, J., and Van Houten, B. (2000) Analysis of gene-specific DNA damage and repair using quantitative polymerase chain reaction, *Methods*, **22**, 135-147.
- [11] Santos, J.H., Mandavilli, B.S., and Van Houten, B. (2002) Measuring oxidative mtDNA damage and repair using quantitative PCR. *Methods Mol. Biol.*, **197**, 159-76.
- [12] Halliwell, B. and Gutteridge, J. (1999) *Free Radicals in Biology and Medicine*: third edition, Oxford University Press, New York.

- [13] Mullis, K. (1990) The unusual origin of the polymerase chain reaction. *Scientific American*, **262**, 56-65.
- [14] Unified medical language system: National Library of Medicine, Bethesda, MD, <http://www.nlm.nih.gov/research/umls/>
- [15] Wang, D., Kreuzer, D., and Essigmann, J. (1998) Mutagenicity and repair of oxidative DNA damage: insights from studies using defined lesions. *Mutat. Res.*, **400**, 99-115.
- [16] Marnett, L. (2000) Oxyradicals and DNA damage. *Carcinogenesis*, **21**, 361-370.
- [17] Cooke, M., Evans, M., Dizdaroglu, M., and Lunec, J. (2003) Oxidative DNA damage: mechanisms, mutation, and disease. *FASEB J.*, **17**, 1195-1214.
- [18] Shibutani, S., Takeshita, M., and Grollman, A. (1991) Insertion of specific bases during DNA synthesis past the oxidation-damaged base 8-oxodG. *Nature*, **349**, 431-434.
- [19] Boer, J. (2002) Polymorphisms in DNA repair and environmental interactions. *Mutat. Res.*, **509**, 201-210.
- [20] Bohr, V. (2002) DNA damage and its processing. Relation to human disease. *J. Inherit. Metab. Dis.*, **25**, 215-222.
- [21] Cortopassi, G., and Arnheim, N. (1990) Detection of specific mitochondrial DNA deletions in tissues of older humans. *Nucleic Acids Res.*, **18**, 6927-6933.
- [22] Wei, Y. (1992) Mitochondrial DNA alterations as ageing-associated molecular events. *Mutat. Res.*, **275**, 145-155.
- [23] Hanukoglu, I., Rapoport, R., Weiner, L., and Sklan, D. (1993) Electron Leakage from the Mitochondrial NADPH-Adrenodoxin Reductase-Adrenodoxin-P450_{scc} (Cholesterol Side Chain Cleavage) System. *Archives Biochem. Biophys.*, **305**, 489-498.
- [24] Zhang, C., Linnane, A., and Nagley, P. (1993) Occurrence of a Particular Base Substitution (3243 A to G) in Mitochondrial DNA of Tissues of Ageing Humans. *Biochem. Biophys. Res. Comm.*, **195**, 1104-1110.
- [25] Melov, S., Shoffner, J., Kaufman, A., and Wallace, D. (1995) Marked increase in the number and variety of mitochondrial DNA rearrangements in aging human skeletal muscle. *Nuc. Acid Res.*, **23**, 4122-4126.

- [26] Melov, S., Hinerfeld, D., Esposito, L., and Wallace, D. (1997) Multi-organ characterization of mitochondrial genomic rearrangements in ad libitum and caloric restricted mice show striking somatic mitochondrial DNA rearrangements with age. *Nuc. Acid Res.*, **25**, 974-982.
- [27] Murdock, D., Christacos, N., and Wallace, D. (2000) The age-related accumulation of a mitochondrial DNA control region mutation in muscle, but not brain, detected by a sensitive PNA-directed PCR clamping based method. *Nuc. Acid Res.*, **28**, 4350-4355.
- [28] Kokoszka, J., Coskun, P., Esposito, L., and Wallace, D. (2001) Increased mitochondrial oxidative stress in the Sod2 (+/-) mouse results in the age-related decline of mitochondrial function culminating in increased apoptosis, *Proc. Natl. Acad. Sci. USA*, **98**, 2278-2283.
- [29] Harman, D. (1956) Role of free radical and radiation chemistry. *J. Gerontol.*, **11**, 298-300.
- [30] Harman D. (1993) Free radical involvement in aging. Pathophysiology and therapeutic implications. *Drugs Aging*, **3**, 60-80.
- [31] Sies, H. (1991) *Oxidative Stress II*. Oxidants and Antioxidants. Academic Press, London.
- [32] Henderson, L.M., and Chappell, J.B. (1996) NADPH oxidase of neutrophils *Biochim. Biophys. Acta*, **1273**, 87-107.
- [33] Segal A.W. (1995) The NADPH Oxidase of Phagocytic Cells is an Electron Pump that Alkalinizes the Phagocytic Vacuole. *Protoplasma*, **184**, 86-103.
- [34] Turrens, J.F. (1997) Superoxide production by the mitochondrial respiratory chain. *Biosci Rep.* **17**, 3-8.
- [35] Raha, S., McEachern, G., Myint, A. and Robinson, B. (2000) Superoxides from mitochondrial complex III: Role of manganese superoxide dismutase, *Free Rad. Biol. Med.*, **29**, 170-180.
- [36] Shull, S., Heintz, N., Periasamy, M., Manohar, M., Janssen, Y., Marsh, J., and Mossam, B. (1991) Differential Regulation of Antioxidant Enzymes in Response to Oxidants. *J. Biol. Chem.*, **266**, 24398-24403.
- [37] Sohal, R., and Brunk, U. (1992) Mitochondrial production of pro-oxidants and cellular senescence. *Mutat. Res.*, **275**, 295-304.

- [38] Giulivi, C., Boveris, A., and Cadenas, E. (1995) Hydroxyl Radical Generation during Mitochondrial Electron Transfer and the Formation of 8-Hydroxydesoxyguanosine in Mitochondrial DNA. *Arch. Biochem. Biophys.*, **316**, 909-916.
- [39] Richter, C. (1992) Reactive oxygen and DNA damage in mitochondria. *Mutat. Res.*, **275**, 249-255.
- [40] Stadtman, E. (1992) Protein oxidation and aging. *Science*, **257**, 1220-1224.
- [41] Schraufstatter, I.U., Hinshaw, D.B., Hyslop, P.A., Spragg, R.G., and Cochrane, C.G. (1986) Oxidant injury of cells. DNA strand-breaks activate polyadenosine diphosphate-ribose polymerase and lead to depletion of nicotinamide adenine dinucleotide. *J. Clin. Invest.*, **77**, 1312-20.
- [42] Schraufstatter, I.U., Hyslop, P.A., Hinshaw, D.B., Spragg, R.G., Sklar, L.A., and Cochrane, C.G. (1986) Hydrogen peroxide-induced injury of cells and its prevention by inhibitors of poly(ADP-ribose) polymerase. *Proc. Natl. Acad. Sci. USA.*, **83**, 4908-12.
- [43] McGregor, D., and Lang, M. (1996) Carbon tetrachloride: genetic effects and other modes of action. *Mutat. Res.*, **366**, 181-95.
- [44] Brent, J.A., and Rumack, B.H. (1993) Role of free radicals in toxic hepatic injury. I. Free radical biochemistry. *J. Toxicol. Clin. Toxicol.*, **31**, 139-71.
- [45] Brent, J.A., and Rumack, B.H. (1993) Role of free radicals in toxic hepatic injury. II. Are free radicals the cause of toxin-induced liver injury? *J. Toxicol. Clin. Toxicol.*, **31**, 173-96.
- [46] Michan, C., Manchado, M., Dorado, G., and Pueyo, C. (1999) In vivo transcription of the Escherichia coli oxyR regulon as a function of growth phase and in response to oxidative stress. *J. Bacteriol.*, **181**, 2759-64.
- [47] Barker, C.W., Fagan, J.B., and Pasco, D.S. (1994) Down-regulation of P4501A1 and P4501A2 mRNA expression in isolated hepatocytes by oxidative stress. *J. Biol. Chem.*, **269**, 3985-3990.
- [48] Wallace, D. (1999) Mitochondrial Disease in Man and Mouse. *Science*, **283**, 1482-1487.
- [49] Hampton, M.B., and Orrenius, S. (1997) Dual regulation of caspase activity by hydrogen peroxide: implications for apoptosis. *FEBS Lett.*, **414**, 552-556.
- [50] Breen, A.P., and Murphy, J.A. (1995) Reactions of oxyl radicals with DNA. *Free Radic. Biol. Med.*, **18**, 1033-77

- [51] Takeshita, M., Chang, C., Johnson, F., Will, S., and Grollman, A. (1987) Oligodeoxynucleotides containing synthetic abasic sites. *J. Biol. Chem.*, **262**, 10171-10179.
- [52] Taylor, J.S., Garrett, D.S., Brockie, I.R., Svoboda, D.L., and Telser, J. (1990) ¹H NMR assessment and melting temperature study of cis-syn and trans-syn thymine dimer containing duplexes of d)CGTATTATGC)*d(GCATAATACG). *Biochemistry*, **29**, 8858-8866.
- [53] Kasai, H., and Nishimura, S. (1984) *Nucleic Acids Res.*, **12**, 2137-2145.
- [54] Shigenaga, M.K., Gimenco, C.J., and Ames, B. (1989) *Proc. Natl. Acad. Sci. USA*, **8**, 9697-9701.
- [55] Kasai, H., Chung, M.H., Jones, D.S., Inoue, H., Ishikawa, H., Kamiya, H., Ohtsuka, E., and Nishimura, S. (1991) 8-Hydroxyguanine, a DNA adduct formed by oxygen radicals: its implication on oxygen radical-involved mutagenesis/carcinogenesis. *J. Toxicol. Sci.*, **16**, 95-105.
- [56] Cadet, J., Berger, M., Douki, T., Morin, B., Raoul, S., Ravanat, J.L., and Spinelli, S. (1997) Effects of UV and visible radiation on DNA-final base damage. *Biol Chem.*, **378**, 1275-86.
- [57] Cadet, J., Berger, M., Douki, T., and Ravanat, J.L. (1997) Oxidative damage to DNA: formation, measurement, and biological significance. *Rev. Physiol. Biochem. Pharmacol.*, **131**, 1-87.
- [58] Ames, B.N., Shigenaga, M.K., and Gold, L.S. (1993) DNA lesions, inducible DNA repair, and cell division: three key factors in mutagenesis and carcinogenesis. *Environ. Health Perspect.*, **101**, 35-44.
- [59] McAuley-Hecht, K. E., Leanoard, G. A., Gibson, N. J., Thomson, J. B., Watson, W. P., Hunter, W. N., and Brown, T. (1994) Crystal structure of a DNA duplex containing 8-hydroxydeoxyguanine-adenine base pairs. *Biochemistry*, **33**, 10266-10270.
- [60] Kouchakdjian, M., Bodepudi, V., Shibutani, S., Eisenberg, M., Johnson, F., Grollman, A. P., and Patel, D. J. (1991) NMR structural studies of the ionizing radiation adduct 7-hydro-8-oxodeoxyguanosine (8-oxo-7H-dG) opposite deoxyadenosine in a DNA duplex. 8-Oxo-7H-dG(syn).dA(anti) alignment at lesion site. *Biochemistry*, **30**, 1403-1412.
- [61] Oda, Y., Uesugi, S., Ikehara, M., Nishimura, S., Kawase, Y., Ishikawa, H., Inoue, H., and Ohtsuka, E. (1991) NMR studies of a DNA containing 8-hydroxydeoxyguanosine. *Nucleic Acids Res.*, **19**, 1407-1412.

- [62] Lipscomb, L. A., Peek, M. E., Morningstar, M. L., Verghis, S. M., Miller, E. M., Rich, A., Essignman, J. M., and Williams, L. D. (1995) *Proc. Natl. Acad. Sci. USA*, **92**, 719-723.
- [63] Lowe, L.G., and Guengerich, F.P. (1996) Steady-state and pre-steady-state kinetic analysis of dNTP insertion opposite 8-oxo7,8-dihydroguanine by *Escherichia coli* polymerases I exo⁻ and II exo⁻. *Biochemistry*, **35**, 9840-9849.
- [64] Mozzherin, D.J., Shibutani, S., Tan, C.K., Downey, K.M., and Fisher, P.A. (1997) Proliferating cell nuclear antigen promotes DNA synthesis past template lesions by mammalian DNA polymerase delta. *Proc. Natl. Acad. Sci USA.*, **94**, 6126-6131.
- [65] Einolf, H.J., and Guengerich, F.P. (2001) Fidelity of nucleotide insertion at 8-oxo-7,8-dihydroguanine by mammalian DNA polymerase delta. Steady-state and pre-steady-state kinetic analysis. *J. Biol. Chem.*, **276**, 3764-3771.
- [66] Bonicel, A., Mariaggi, N., Hughes, E., and Teoule, R. (1980) In vitro gamma irradiation of DNA: identification of radioinduced chemical modifications of the adenine moiety. *Radiat. Res.*, **83**, 19-26.
- [67] Guschlbauer, W., Duplaa, A.M., Guy, A., Teoule, R., and Fazakerley, G.V. (1991) Structure and in vitro replication of DNA templates containing 7,8-dihydro-8-oxoadenine. *Nucleic Acids Res.*, **19**, 1753-1758.
- [68] Shibutani, S., Bodepudi, V., Johnson, F., and Grollman A. (1993) Translesional synthesis on DNA templates containing 8-oxo-7,8-dihydrodeoxyadenosine. *Biochemistry*, **32**, 4615-4621.
- [69] Kamiya, H., Miura, H., Murata-Kamiya, N., Ishikawa, H., Sakaguchi, T., Inoue H., Sasaki, T., Masutani, C., Hanaoka, F., Nishimura, S., and Ohtsuka, E. (1995) 8-Hydroxyadenine (7,8-dihydro-8-oxoadenine) induces misincorporation in in vitro DNA synthesis and mutations in NIH 3T3 cells. *Nucleic Acids Res.*, **23**, 2893-2899.
- [70] Purmal, A.A., Kow, Y.W., and Wallace, S.S. (1994) Major oxidative products of cytosine, 5-hydroxycytosine and 5-hydroxyuracil, exhibit sequence context-dependent mispairing in vitro. *Nucleic Acids Res.*, **22**, 72-78.
- [71] Randall, S.K., Eritja, R., Kaplan, B.E., Petruska, J., and Goodman, M.F. (1987) Nucleotide insertion kinetics opposite abasic lesions in DNA. *J. Biol. Chem.*, **262**, 6864-6870.
- [72] Nakamura, J., Walker, V.E., Upton, P.B., Chiang, S.Y., Kow, Y.W., and Swenberg, J.A. (1998) Highly sensitive apurinic/apyrimidinic site assay can detect spontaneous and chemically induced depurination under physiological conditions. *Cancer Res.*, **58**, 222-225.

- [73] Shibutani, S., Takeshita, M., and Grollman, A. (1997) Translesional synthesis on DNA templates containing a single abasic site. *J. Biol. Chem.*, **272**, 13916-13922.
- [74] Gentil, A., Renault, G., Madzak, C., Margot, A., Cabral-Neto, J. B., Vasseur, J. J., Rayner, B., and Sarasin, A. (1990) Mutagenic properties of a unique abasic site in mammalian cells. *Biochem. Biophys. Res. Commun.* **173**, 704-710.
- [75] Gentil, A., Cabral-Neto, J. B., Mariage-Samson, R., Margot, A., Imbach, J. L., Rayner, B., and Sarasin, A. (1992) Mutagenicity of a unique apurinic/apyrimidinic site in mammalian cells. *J. Mol. Biol.* **227**, 981-984.
- [76] Cabral Neto, J. B., Gentil, A., Cabral, R. E. C., and Sarasin, A. (1992) Mutation spectrum of heat-induced abasic sites on a single-stranded shuttle vector replicated in mammalian cells. *J. Biol. Chem.* **267**, 19718-19723.
- [77] Cabral Neto, J. B., Cabral, R. E. C., Margot, A., Le Page, F., Sarasin, A., and Gentil, A. (1994) Coding properties of a unique apurinic/apyrimidinic site replicated in mammalian cells. *J. Mol. Biol.* **240**, 416-420.
- [78] Ling, H., Boudsocq, F., Woodgate, R., and Yang, W. (2004) Snapshots of replication through an abasic lesion: structural basis for base substitutions and frameshifts. *Mol. Cell*, **13**, 751-762.
- [79] Howe, H.L., Wingo, P.A., Thun, M.J., Ries, L.A., Rosenberg, H.M., Feigal, E.G., and Edwards, B.K. (2001) Annual report to the nation on the status of cancer (1973 through 1998), featuring cancers with recent increasing trends. *J. Natl. Cancer Inst.*, **93**, 824-42.
- [80] Armstrong, B.K., and Kricger, A. (1995) Skin cancer. *Dermatol. Clin.*, **13**, 583-94.
- [81] Armstrong, B.K., Kricger, A., and English, D.R. (1997) Sun exposure and skin cancer. *Australas. J. Dermatol.*, **38**, S1-6.
- [82] Jemal, A., Devesa, S.S., Hartge, P., and Tucker, M.A. (2001) Recent trends in cutaneous melanoma incidence among whites in the United States. *J. Natl. Cancer Inst.*, **93**, 678-683.
- [83] Bennett, J.P., and Hall, P. (1994) Moles and melanoma: a history. *Ann. R. Coll. Surg. Engl.*, **76**, 373-380.
- [84] Goldstein, A.M., and Tucker, M.A. (2001) Genetic epidemiology of cutaneous melanoma: a global perspective. *Arch. Dermatol.*, **137**, 1493-1496.

- [85] Jhappan, C., Noonan, F.P., and Merlino, G. (2003) Ultraviolet radiation and cutaneous malignant melanoma. *Oncogene*, **22**, 3099-3112.
- [86] You, Y.H., Lee, D.H., Yoon, J.H., Nakajima, S., Yasui, A, and Pfeifer, G.P. (2001) Cyclobutane pyrimidine dimers are responsible for the vast majority of mutations induced by UVB irradiation in mammalian cells. *J. Biol. Chem.*, **276**, 44688-44694.
- [87] Smith, C.A., Baeten, J., and Taylor, J.S. (1998) The ability of a variety of polymerases to synthesize past site-specific cis-syn, trans-syn-II, (6-4), and Dewar photoproducts of thymidyl-(3'-->5')-thymidine. *J. Biol Chem.*, **273**, 21933-21940.
- [88] Rosenstein, B.S., and Mitchell, D.L. (1987) Action spectra for the induction of pyrimidine(6-4)pyrimidone photoproducts and cyclobutane pyrimidine dimers in normal human skin fibroblasts. *Photochem. Photobiol.*, **45**, 775-80.
- [89] Linge, C. (1996) Relevance of in vitro melanocytic cell studies to the understanding of melanoma. *Cancer Surv.*, **26**, 71-87.
- [90] Cleaver, J.E., and Crowley, E. (2002)UV damage, DNA repair and skin carcinogenesis. *Front. Biosci.*, **7**, 1024-1043.
- [91] Matsumura, Y., and Ananthaswamy, H.N. (2002) Molecular mechanisms of photocarcinogenesis. *Front. Biosci.*, **7**,765-83.
- [92] Black, H.S., deGrujil, F.R., Forbes, P.D., Cleaver, J.E., Ananthaswamy H.N., deFabo E.C., Ullrich, S.E., and Tyrrell, R.M. (1997) Photocarcinogenesis: an overview. *J. Photochem. Photobiol. B.*, **40**, 29-47.
- [93] Washington, M.T., Prakash, L., and Prakash, S. (2003) Mechanism of nucleotide incorporation opposite a thymine-thymine dimer by yeast DNA polymerase eta (η). *Proc. Natl. Acad. Sci. USA.*, **100**, 12093-12098.
- [94] Wang, C.I., and Taylor, J.S. (1991) Site-specific effect of thymine dimer formation on dAn.dTn tract bending and its biological implications. *Proc. Natl. Acad. Sci. USA.*, **88**, 9072-9076.
- [95] Wang, C.I., and Taylor, J.S. (1993) The trans-syn-I thymine dimer bends DNA by approximately 22 degrees and unwinds DNA by approximately 15 degrees. *Chem. Res. Toxicol.*, **6**, 519-523.
- [96] Kim, J.K., Patel, D., and Choi, B.S. (1995) Contrasting structural impacts induced by cis-syn cyclobutane dimer and (6-4) adduct in DNA duplex decamers: implication in mutagenesis and repair activity. *Photochem. Photobiol.*, **62**, 44-50.

- [97] Tommasi, S., Swiderski, P.M., Tu, Y., Kaplan, B.E., and Pfeifer, G.P. (1996) Inhibition of transcription factor binding by ultraviolet-induced pyrimidine dimers. *Biochemistry*, **35**, 15693-15703.
- [98] Lewin, B. (2000) *Genes VII*. Oxford University Press Inc., New York.
- [99] Thoma, F. (1999) Light and dark in chromatin repair: repair of UV-induced DNA lesions by photolyase and nucleotide excision repair. *EMBO J.*, **18**, 6585-6598.
- [100] Ide, H., and Kotera, M. (2004) Human DNA glycosylases involved in the repair of oxidatively damaged DNA. *Biol. Pharm. Bull.*, **27**, 480-485.
- [101] Boiteux, S., Gajewski, E., Laval, J., and Dizdaroglu, M. (1992) Substrate specificity of the *Escherichia coli* Fpg protein (formamidopyrimidine-DNA glycosylase): excision of purine lesions in DNA produced by ionizing radiation or photosensitization. *Biochemistry*, **31**, 106-110.
- [102] Xu, J.F., Yang, Q.P., Chen, J.Y., van Baalen, M.R., and Hsu, I.C. (1996) Determining the site and nature of DNA mutations with the cloned MutY mismatch repair enzyme. *Carcinogenesis*, **17**, 321-326.
- [103] Tsai-Wu, J.J., Liu, H.F., and Lu, A.L. (1992) *Escherichia coli* MutY protein has both N-glycosylase and apurinic/apyrimidinic endonuclease activities on A.C and A.G mispairs. *Proc. Natl. Acad. Sci. USA.*, **89**, 8779-8783.
- [104] Radicella, J.P., Clark, E.A., Chen, S., and Fox, M.S. (1993) Patch length of localized repair events: role of DNA polymerase I in mutY-dependent mismatch repair. *J. Bacteriol.*, **175**, 7732-7736.
- [105] Michaels, M.L., Cruz, C., Grollman, A.P., and Miller, J.H. (1992) Evidence that MutY and MutM combine to prevent mutations by an oxidatively damaged form of guanine in DNA. *Proc. Natl. Acad. Sci. USA.*, **89**, 7022-7025.
- [106] Cunningham, R.P. (1996) DNA repair: how yeast repairs radical damage. *Curr. Biol.*, **6**, 1230-1233.
- [107] Asagoshi, K., Yamada, T., Terato, H., Ohyama, Y., Monden, Y., Arai, T., Nishimura, S., Aburatani, H., Lindahl, T., and Ide, H. (2000) Distinct repair activities of human 7,8-dihydro-8-oxoguanine DNA glycosylase and formamidopyrimidine DNA glycosylase for formamidopyrimidine and 7,8-dihydro-8-oxoguanine. *J. Biol. Chem.*, **275**, 4956-4964.
- [108] Rosenquist, T.A., Zharkov, D.O., and Grollman, A.P. (1997) Cloning and characterization of a mammalian 8-oxoguanine DNA glycosylase. *Proc. Natl. Acad. Sci. USA.*, **94**, 7429-7434.

- [109] Radicella, J.P., Dherin, C., Desmaze, C., Fox, M.S., and Boiteux, S. (1997) Cloning and characterization of hOGG1, a human homolog of the OGG1 gene of *Saccharomyces cerevisiae*. *Proc. Natl. Acad. Sci. USA.*, **94**, 8010-8015.
- [110] Slupska, M.M., Baikalov, C., Luther, W.M., Chiang, J.H., Wei, Y.F., and Miller, J.H. (1996) Cloning and sequencing a human homolog (hMYH) of the *Escherichia coli* mutY gene whose function is required for the repair of oxidative DNA damage. *J. Bacteriol.*, **178**, 3885-3892.
- [111] Sakumi, K., Furuichi, M., Tsuzuki, T., Kakuma, T., Kawabata, S., Maki, H., and Sekiguchi, M. (1993) Cloning and expression of cDNA for a human enzyme that hydrolyzes 8-oxo-dGTP, a mutagenic substrate for DNA synthesis. *J. Biol. Chem.*, **268**, 23524-23530.
- [112] Sancar, A. (1996) DNA excision repair. *Annu. Rev. Biochem.*, **65**, 43-81.
- [113] Goodman, M. F. (1997) *Proc. Natl. Acad. Sci. USA.*, **94**, 10493-10495.
- [114] Alba, M.M. (2001) Replicative DNA polymerases. *Genome Biol.* **2**, reviews3002.1-3002.4.
- [115] Moran, S., Ren, R.X., and Kool, E.T. (1997) A thymidine triphosphate shape analog lacking Watson-Crick pairing ability is replicated with high sequence selectivity. *Proc. Natl. Acad. Sci. USA.*, **94**, 10506-10511.
- [116] Ollis, D.L., Brick, P., Hamlin, R., Xuong, N.G., and Steitz, T.A. (1985) Structure of large fragment of *Escherichia coli* DNA polymerase I complexed with dTMP. *Nature*, **313**, 762-766.
- [117] Kelman, Z., Hurwitz, J., and O'Donnell, M. (1998) Processivity of DNA polymerases: two mechanisms, one goal. *Structure*, **6**, 121-5.
- [118] Krishna, T.S.R., Kong, X.P., Gary, S., Burgers, P.M. and Kuriyan, J. (1994) Crystal structure of the eukaryotic DNA polymerase processivity factor PCNA. *Cell* **79**, 1233-1243.
- [119] Bedford, E., Tabor, S., and Richardson, C.C. (1997) The thioredoxin binding domain of bacteriophage T7 DNA polymerase confers processivity on *Escherichia coli* DNA polymerase I. *Proc. Natl. Acad. Sci. USA.*, **94**, 479-484.
- [120] Minnick, D.T., Astatke, M., Joyce, C.M., and Kunkel, T.A. (1996) A thumb subdomain mutant of the large fragment of *Escherichia coli* DNA polymerase I with reduced DNA binding affinity, processivity, and frameshift fidelity. *J. Biol. Chem.*, **271**, 24954-24961.
- [121] Echols, H., and Goodman, M. F. (1991) Fidelity mechanisms in DNA replication. *Annu. Rev. Biochem.* **60**, 477-511.

- [122] Doubleie, S., and Ellenberger, T. (1998) The mechanism of action of T7 DNA polymerase. *Curr. Opin. Struct. Biol.*, **8**, 704-712.
- [123] Steitz, T. (1999) DNA polymerases: structural diversity and common mechanisms. *J. Biol. Chem.*, **274**, 17395-17398.
- [124] Patel, S.S., Wong, I., and Johnson, K.A. (1991) Pre-steady-state kinetic analysis of processive DNA replication including complete characterization of an exonuclease-deficient mutant. *Biochemistry*, **30**, 511-525.
- [125] Wong, I., Patel, S.S., and Johnson, K.A. (1991) An induced-fit kinetic mechanism for DNA replication fidelity: direct measurement by single turnover kinetics. *Biochemistry*, **30**, 526-537.
- [126] Washington, M.T., Prakash, L., and Prakash, S. (2001) Yeast DNA polymerase η utilizes an induced-fit mechanism of nucleotide incorporation. *Cell*, **107**, 917-927.
- [127] Plosky, B.S., and Woodgate, R. (2004) Switching from high-fidelity replicases to low-fidelity lesion-bypass polymerases. *Curr. Opin. Genet. Dev.*, **14**, 113-119.
- [128] Johnson, R.E., Washington, M.T., Prakash, S., and Prakash, L. (2000) Fidelity of human DNA polymerase η . *J. Biol. Chem.*, **275**, 7447-7450.
- [129] Washington, M.T., Johnson, R.E., Prakash, S., and Prakash, L. (1999) Fidelity and processivity of *Saccharomyces cerevisiae* DNA polymerase η . *J. Biol. Chem.*, **274**, 36835-36838.
- [130] Berneburg, M., and Lehmann, A.R. (2001) Xeroderma pigmentosum and related disorders: defects in DNA repair and transcription. *Adv. Genet.*, **43**, 71-102.
- [131] Sutton, M.D., and Walker, G.C. (2001) Managing DNA polymerases: coordinating DNA replication, DNA repair, and DNA recombination. *Proc. Natl. Acad. Sci. USA.*, **98**, 8342-8349.
- [132] Bohr, V., Smith, C., Okumoto, D., and Hanawalt, P. (1985) DNA repair in an active gene: removal of pyrimidine dimers from the DHFR gene of CHO cells is much more efficient than in the genome overall, *Cell*, **40**, 359-369.
- [133] Bohr, V. (1991) Gene specific DNA repair, *Carcinogenesis*, **12** 1983-1992.
- [134] Withrow, A.G., Sikorsky, J., Downs, J.C., and Fenger, T. (2003) Extraction and analysis of human nuclear and mitochondrial DNA from electron beam irradiated envelopes. *J. Forensic Sci.*, **48**, 1302-1308.

- [135] Perkin Elmer Corporation, USA. (1998) Perkin Elmer AmpF{STR}® Profiler Plus™ PCR Amplification Kit, user's manual.
- [136] Frégeau, C. J., Bowen, K. L., and Fournay, R. M. (1999) Validation of Highly Polymorphic Fluorescent Multiplex Short Tandem Repeat Systems Using Two Generations of DNA Sequencers. *J. Forensic Sci.*, **44**, 133-166.
- [137] Bustin, S.A., and Nolan, T. (2004) Pitfalls of quantitative real-time reverse-transcription polymerase chain reaction. *J. Biomol. Tech.*, **15**, 155-166
- [138] Freeman, W., Walker, S., and Vrana, K. (1999) Quantitative RT-PCR: pitfalls and potential, *Biotech.*, **26**, 112-125.
- [139] Bustin, S. (2002) Quantification of mRNA using real-time reverse transcription PCR (RT-PCR): trends and problems. *J. Mol. Endo.*, **29**, 23-29..
- [140] Livak, K. (1997) ABI Prism 7700 Sequence Detection System, User Bulletin 2, *PE Applied Biosystems*.
- [141] Livak, K. and Schmittgen, T. (2001) Analysis of relative gene expression data using real-time quantitative PCR and the $2^{-\Delta\Delta CT}$ Method, *Methods*, **25**, 402-408.
- [142] Liu, W. and Saint, D. (2002) A new quantitative method of real-time reverse transcription polymerase chain reaction assay based on simulation of polymerase chain reaction kinetics, *Anal. Biochem.*, **302**, 52-59.
- [143] Liu, W. and Saint, D. (2002) Validation of a quantitative method for real-time PCR kinetics, *Biochem. Biophys. Res. Commun.*, **294**, 347-353.
- [144] Rasmussen, R. (2001) Quantification on the LightCycler instrument, in: Meuer, S. Wittwer, C. and Nakagawara, K. (eds.) *Rapid Cycle Real-time PCR: Methods and Applications*. Springer Press, Heidelberg, pp. 21-34.
- [145] Nogva, H.K., and Rudi, K. (2004) Potential influence of the first PCR cycles in real-time comparative gene quantifications. *Biotech.*, **37**, 246-253.
- [146] Hogrefe, H.H., Hansen, C.J., Scott, B.R., and Nielson, K.B. (2002) Archaeal dUTPase enhances PCR amplifications with archaeal DNA polymerases by preventing dUTP incorporation. *Proc. Natl. Acad. Sci. USA*, **99**, 596-601.
- [147] Barnes, W.M. (1994) PCR amplification of up to 35-kb DNA with high fidelity and high yield from λ bacteriophage template. *Proc. Natl. Acad. Sci. USA*, **91**, 2216-2220.
- [148] Wallace, D. (1992) Mitochondrial Genetics: A paradigm of Aging and Degenerative Diseases? *Science*, **256**, 628-632.

- [149] Heales, S., Bolanos, J., Stewart, V., Brookes, P., Land, J., and Clark, J. (1999) Nitric oxide, mitochondria and neurological disease, *Biochimica et Biophysica Acta*, **1410**, 215-228.
- [150] Jun, A., Trounce, I., Brown, M., Shoffner, J., and Wallace, D. (1996) Use of Transmitochondrial Cybrids to assign a Complex I Defect to the Mitochondrial DNA-Encoded NADH Dehydrogenase Subunit 6 Gene Mutation at Nucleotide Pair 14459 That Causes Leber Hereditary Optic Neuropathy and Dystonia. *Mol. Cell Biol.*, **16**, 771-777.
- [151] Sikorsky, J.A., Primerano, D., Fenger, T., and Denvir, J. (2004) Effect of DNA Damage on PCR Amplification Efficiency with the Relative Threshold Cycle Method. *Biochem. Biophys. Res. Commun.*, **323**, 823-830.
- [152] Gait, M. (1991) DNA/RNA synthesis and labeling. *Curr. Opin. Biotechnol.*, **2**, 61-68.
- [153] Sproat, B. (1995) Chemistry and applications of oligonucleotide analogues. *J. Biotechnol.*, **41**, 221-238.
- [154] Anderson, S., Bankier, A., Barrell, B., de Bruijn, M. Coulson, A. Drouin, J. Eperon, I. Nierlich, D. Roe, B. *et al.* (1981) Sequence and organization of the human mitochondrial genome. *Nature*, **290**, 457-462.
- [155] Bodepudi, V., Shibutani, S., and Johnson, F. (1992) Synthesis of 2'-deoxy-7,8-dihydro-8-oxoguanosine and 2'-deoxy-7,8-dihydro-8-oxoadenosine and their incorporation into oligomeric DNA. *Chem. Res. Toxicol.*, **5**, 608-617.
- [156] Andrus, A. (1987) Evaluating and Isolating Synthetic Oligonucleotides: The Complete Guide, User Bulletin 13, *PE Applied Biosystems*.
- [157] Malins, D., Polissar, N., Ostrander, G., and Vinson, M. Single 8-oxo-guanine and 8-oxo-adenine lesions induce marked changes in the backbone structure of a 25-base DNA strand. (2000) *Proc. Natl. Acad. Sci. USA*, **97**, 12442-12445.
- [158] Levin B.C., Cheng H., and Reeder D.J. (1999) A human mitochondrial DNA standard reference material for quality control in forensic identification, medical diagnosis, and mutation detection. *Genomics*, **55**, 135-46.
- [159] Pfaffl, M. (2001) A new mathematical model from relative quantification in real-time RT-PCR. *Nucleic Acids Res.*, **29**, 2002-2007.
- [160] Tichopad, A., Dzidic, A., and Pfaffl, M. (2002) Improving quantitative real-time RT-PCR reproducibility by boosting primer-linked amplification efficiency, *Biotechnol. Lett.*, **24**, 2053-2056.

- [161] Ramakers, C., Ruijter, J., Lankanne Deprez, R., and Moorman, A. (2003) Assumption-free analysis of quantitative real-time polymerase chain reaction (PCR) data, *Neurosci. Lett.*, **339**, 62-66.
- [162] Peirson, S., Butler, J., and Foster, R. (2003) Experimental validation of novel and conventional approaches to quantitative real-time PCR data analysis, *Nucleic Acids Res.*, **31**, e73.
- [163] Rutledge, R., and Cote, C. (2003) Mathematics of quantitative kinetic PCR and the application of standard curves. *Nucleic Acids Res.*, **31**, e93.
- [164] Ticopad, A., Dilger, M., Schwarz, G., and Pfaffl, M. (2003) Standardized determination of real-time PCR efficiency from a single reaction set-up. *Nucleic Acids Res.*, **31**, e122.
- [165] Kayser, K. (2004) Personal correspondence. *Sigma-Aldrich Co.*
- [166] Amadio, M. (2001) TaqMan RNase P 96-well instrument verification plate (product insert). *Applera Corporation.*

APPENDIX A

PCR Primers

Primers were adapted from Levin *et al.* (1999), Ayala-Torres *et al.* (2000), or created using ABI primer express software to amplify fragments of mtDNA from cellular and synthetic samples (Table A.1; (10, 158)).

Table A.1. Oligonucleotide primer sequences.

Designation ^a	OLIGONUCLEOTIDE SEQUENCE	Function ^b
FWD#15912	5'-CCAGTCTTGTAACCGGAGATGA-3'	751 bp template
REV#93	5'-TCGCAATGCTATCGCGTG-3'	751 bp template
Oxo CONTROL	See Table 3.1	Modified Oligo ligation
FWD#12-B	5'-AGACCTGTGATCCATCGTGAT-3'	Modified Oligo ligation
REV#16090	5'-TATTTCTGAATTACTGCCAGCC-3'	Oligo ligation- ICR
FWD#16138^c	5'-CCCAAAGCTAAGATTCTAATTT-3'	90mer Oligo
REV#16053	5'-GGGTGAGTCAATACTTGGGT-3'	90mer Oligo-Full
REV#16095	5'-CATGAAAGAACAGAGAATAGT-3'	90mer Oligo- ICR
REV#14841	5'-TTTCATCATGCGGAGATGTTGGATGG-3'	Amplicons 1-7
FWD#14620	5'-CCCCACAAACCCCACTTACTAAACCCA-3'	Amplicon 1
FWD#14470	5'-TCCAAAGACAACCATCATTCC-3'	Amplicon 2
FWD#14148	5'-CCTATTCCCCCGAGCAATCTCAATTAC-3'	Amplicon 3
FWD#13899	5'-TTTCTCCAACATACTCGGATTC-3'	Amplicon 4
FWD#13188	5'-CACTCTGTTTCGCAGCAGTCTG-3'	Amplicon 5
FWD#12601	5'-TTCATCCCTGTAGCATTGTTCG-3'	Amplicon 6
FWD#11760	5'-ACGAACGCACTCACAGTCG-3'	Amplicon 7
FWD#14642	5'-CCCACACTCAACAGAAACAAAGC-3'	LX-ICR
REV#14693	5'-TGTAGTCCGTGCGAGAATAATGAT-3'	LX-ICR

a- Numerical designation is based on Anderson mtDNA reference sequence (154).

b- To create Amplicons 1-7, forward PCR primers were coupled with REV#14841.

c- Also used in combination with FWD#12 to amplify full-length ligated Oligo templates.

APPENDIX B

Amplicon Size Impacts Threshold Cycle Values

The real-time PCR assays presented here are based on the increase of excited fluorescent dye corresponding to an increase in PCR product formation during amplification. SYBR Green dye, used in these experiments, is an intercalating agent that can be excited when associated with double stranded DNA. It is reasonable to assume that larger amplicon target sizes will permit more dye incorporation.

To determine if increased dye incorporation translated into observed differences in C_T values, untreated cellular DNA stocks were amplified using LX-ICR primers (Appendix A) and then diluted to attain C_T values of 19.5 (based on direct $2^{-\Delta CT}$ comparison methods (141)). Diluted samples were then amplified using the primer walking strategy described above (Figures 3.4, 4.15) and C_T values obtained. As amplicon sizes increased from 51 bp to 693 bp, C_T values dropped from 19.61 to 17.83 (Table B.1). Further increases in amplicon size resulted in observed increases in C_T values (Table B.1). Given that $2^{-\Delta CT}$ comparison mathematics assumes that efficiency of the reaction is equal between templates (141), the observations above suggested that increased dye incorporation endured by larger amplicons decreased observed C_T values until the efficiency of large fragment amplification became low enough to ultimately mask any dye influences.

Table C.1. Amplicon sizes and threshold cycle values.

Amplicon	C_T	S. D. C_T	Efficiency
51 bp	19.61	0.291	1.000 ^a
221 bp	18.21	0.028	0.953
693 bp	17.83	0.100	0.891
942 bp	18.49	0.134	0.849
1654 bp	19.50	0.111	0.751
2241 bp	21.05	0.059	0.692

a- Estimate of efficiency based on short template assumptions (141).

APPENDIX C

Dissociation Curves and PCR Product Gels from Long Extension PCRs

Dissociation profiles can be used to determine homogeneity of PCR products and may suggest the presence of non-specific product formation during the PCRs (Figure 4.16). To generate these profiles, temperatures are increased to denature duplex DNA and therefore decrease the amount of SYBR incorporation and subsequent fluorescent intensity. With longer amplicon targets, the likelihood of encountering regions within an amplicon that have different denaturation kinetics increases.

To determine if increasing amplicon size impacted observed dissociation profiles, the primer walking strategy described above was again used (Figures 3.4, 4.15); by holding the reverse primer constant at all amplicon sizes, larger targets effectively contain the smaller ones (for example, the 693 bp amplicon is contained in the 2.25 kb amplicon; Figure 4.15). Five different targets were amplified, ranging from 221 bp to 2.25 kb, and the products were separated by agarose gel electrophoresis (Figure C.1). Single bands of expected sizes were observed in all cases suggesting unique product formation.

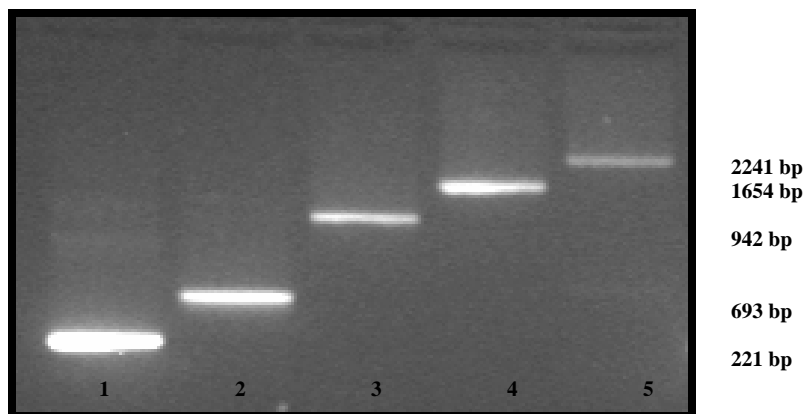


Figure C.1. Product gel of long templates PCRs. PCR products ranging from 221 bp to 2.25 kb were separated by agarose gel electrophoresis. The appearance of single bands suggested that unique products were generated by each primer set. Lanes 1-5 represent reaction products from Amplicons 1, 3, 4, 5, and 6, respectively.

Dissociation profiles for each sized amplicon were generated (Figure C.2). A unique peak with an approximate melting temperature of 75° C was observed in the 221 bp

products. When product size was increased to 693 bp, two peaks with equal amplitude could be distinguished. As product sizes increased from 900 to 2.25 kb the two peaks observed in the 693 bp profiles existed but the amplitude of the first peak decreased as product sizes increased. These observations, coupled with the unique bands on the PCR product gel (Figure C.1), suggested that two distinct melting domains existed in the PCR products larger than 693 bp; the impact of the first melting domain became less influential on product denaturation as amplicon size increased.

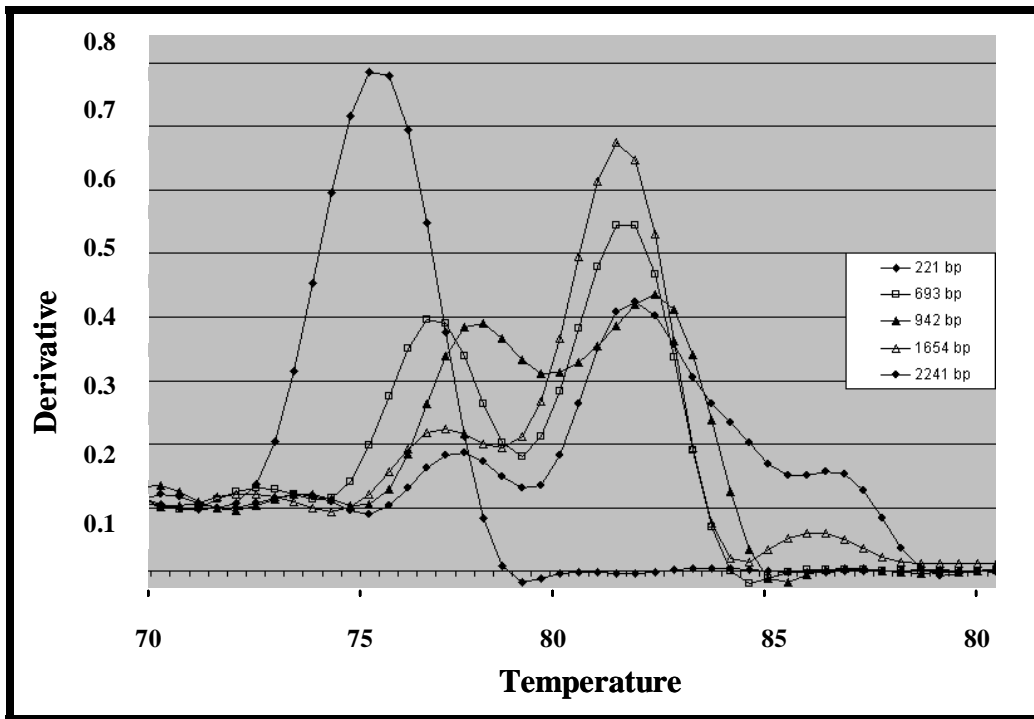


Figure C.2. Dissociation profiles of long PCR products. Melting curves of PCR products ranging from 221 bp to 2.25 kb were created by incrementally increasing temperature. Multiple peaks were present in dissociation profiles as PCR product size increased. The amplitude of the peaks shifted in larger products.

APPENDIX D

Simulated Lesion Bypass and Lesion Frequency Calculations

In developing equation **26** above (section 3.4.4.), the assumption was made that damaged input templates did not contribute to the reaction (11). It has been demonstrated that, for DNA damaged by UV radiation (specifically TT dimers), that such templates do contribute to the reaction but at a very low efficiency (of the order of 1%; (151)). In order to confirm that this does not invalidate the results presented in section 4.1.2.1., an additional mathematical model was developed which accounts for damaged templates participating in the reaction but at efficiencies different to the undamaged templates. This model was used to compute the lesion frequency over a range of simulated lesion bypass efficiencies and demonstrated that the assumption did not significantly affect the precision of the method (Table 4.20).

As before, let p be the proportion of damaged bases in the DNA (lesion frequency), x_0 be the number of input templates, x_n the total number of molecules present after n cycles of the PCR, and N be the number of base pairs in the target. Additionally, let y_n be the number of *undamaged* molecules present after n cycles of the reaction, and P be the proportion of input templates that are undamaged creating

$$P = (1 - p)^N,$$

$$x_n = y_n + (1 - P)x_0, \text{ and}$$

$$y_0 = Px_0.$$

Suppose now that in each cycle of the reaction, undamaged templates replicate with efficiency E_U , and damaged templates produce undamaged templates with efficiency E_D . Since the number of damaged templates is fixed at $(1 - P)x_0$, the following equation models each cycle of the reaction:

$$y_n = (1 + E_U)y_{n-1} + E_D(1 - P)x_0.$$

This equation has solution

$$y_n = (1 + E_U)^n y_0 + \frac{(1 + E_U)^n - 1}{E_U} E_D (1 - P) x_0, \text{ or}$$

$$y_n = (1 + E_U)^n P x_0 + \frac{(1 + E_U)^n - 1}{E_U} E_D (1 - P) x_0. \text{ Finally}$$

$$x_n = (1 + E_U)^n P x_0 + \frac{(1 + E_U)^n - 1}{E_U} E_D (1 - P) x_0 + (1 - P) x_0$$

is created.

For control input templates, $P=1$, and this reduces as usual to

$$x_n = (1 + E_U)^n x_0.$$

Again using the previous notation, where T denotes the common threshold value for both damaged and undamaged templates, C_U denotes the threshold cycle for undamaged (control) templates, and C_D denotes the threshold cycle for damaged templates, we have

$$T = (1 + E_U)^{C_D} P x_0 + \frac{(1 + E_U)^{C_D} - 1}{E_U} E_D (1 - P) x_0 + (1 - P) x_0$$

and

$$T = (1 + E_U)^{C_U} x_0$$

are produced.

Equating these two expressions for T and solving for P gives

$$P = \frac{E_U (1 + E_U)^{C_U} - E_D (1 + E_U)^{C_D} + E_D - E_U}{E_U (1 + E_U)^{C_D} - E_D (1 + E_U)^{C_D} + E_D - E_U}. \text{ Since } P = (1 - p)^N,$$

and

$$p = 1 - \left(\frac{E_U (1 + E_U)^{C_U} - E_D (1 + E_U)^{C_D} + E_D - E_U}{E_U (1 + E_U)^{C_D} - E_D (1 + E_U)^{C_D} + E_D - E_U} \right)^{1/N}.$$

27

APPENDIX E

Simultaneous Calculation of Lesion Frequency and Rate of Lesion Bypass

In theory, it is possible to compare ΔC_T values from reactions at two different amplicon lengths and simultaneously calculate both lesion frequency and lesion bypass rate.

By applying the equation described in the ABI RNaseP Specification Sheet (166), the instrument specification to “distinguish between 5,000 and 10,000 genomic equivalents with a 99.7% confidence level” can be converted to a C_T Standard Deviation of 0.16 (data not shown). At this time, these current limitations in instrumentation and fluorescent detection do not provide the precision necessary to perform these damage calculations. Below is a complete derivation of the formulae needed to simultaneously calculate LBR and LF in the event instrument precision is increased.

Starting with equation 27 from Appendix D:

$$p^N = \frac{1 - E_U(1 + E_U)^{C_U} - E_D(1 + E_U)^{C_D} + E_D - E_U}{E_U(1 + E_U)^{C_D} - E_D(1 + E_U)^{C_D} + E_D - E_U},$$

which can be rearranged to give

$$\frac{E_D}{E_U} = \frac{1 - (1 + E_U)^{C_U} - 1 - (1 + E_U)^{C_D} p^N + p^N}{(1 + E_U)^{C_D} - 1 - (1 + E_U)^{C_D} p^N + p^N}$$

or

$$\frac{E_D}{E_U} = \frac{1 - (1 + E_U)^{C_U} - 1 - p^N((1 + E_U)^{C_D} - 1)}{((1 + E_U)^{C_D} - 1)(1 - p^N)}.$$

For convenience, let

$$A = \frac{1}{E_U} - (1 + E_U)^{C_U} - 1 \quad \text{and}$$

$$B = (1 + E_U)^{C_D} - 1, \text{ giving}$$

$$\frac{E_D}{E_U} = \frac{A - Bp^N}{B(1 - p^N)}. \quad \mathbf{28}$$

Making the assumption that lesion bypass occurs at the same relative rate for all template length, in other words, assume that the quantity E_D / E_U is independent of template length N .

Consider two PCRs in the experiment, using template lengths M and N respectively (without loss of generality we may assume that $M > N$). Find E_U , C_U , and C_D in the usual manner (section 4.1.2.2.; Appendix E) for each and compute A and B from the formulae above. Denote by A_M and B_M the values of A and B computed for the PCR using templates of length M , and by A_N and B_N the values computed for the PCR using templates of length N . By assumption:

$$\frac{E_D}{E_U} = \frac{A_M - B_M p^M}{B_M (1 - p^M)} \quad \text{and}$$

$$\frac{E_D}{E_U} = \frac{A_N - B_N p^N}{B_N (1 - p^N)}. \quad \text{Hence}$$

$$\frac{A_N - B_N p^N}{B_N (1 - p^N)} = \frac{A_M - B_M p^M}{B_M (1 - p^M)}, \quad \mathbf{29}$$

which is simplified to

$$(B_N - A_N)B_M p^M - (B_M - A_M)B_N p^N + A_N B_M - A_M B_N = 0 \quad \mathbf{30}$$

Equation **29** can be solved for p ; in general, the equation cannot be solved algebraically (though it may be noted that if $M=2N$ it can be reduced to a quadratic equation), so a method for solving this numerically using Newton's method is presented.

First observe that there is a spurious solution at $p=1$ (this solution results from multiplying both sides of equation **29** by $(1-p^N)(1-p^M)$ to obtain equation **30**). Note also that the function

$$f(p) = (B_N - A_N)B_M p^M - (B_M - A_M)B_N p^N + A_N B_M - A_M B_N$$

has a single turning point at

$$p_* = \left(\frac{N(B_M - A_M)B_N}{M(B_N - A_N)B_M} \right)^{\frac{1}{M-N}}.$$

It follows that there is exactly one more zero of $f(p)$, corresponding to the solution to equation **(26)** (*the lesion frequency*).

In order to find this solution, Newton's method is employed. Choosing to start with the value $p_0=1-2p_*$, which will be close to the desired solution. Newton's method gives the iteration

$$p_{n+1} = p_n - \frac{f(p_n)}{f'(p_n)} = p_n - \frac{(B_N - A_N)B_M p_n^M - (B_M - A_M)B_N p_n^N + A_N B_M - A_M B_N}{M(B_N - A_N)B_M p_n^{M-1} - N(B_M - A_M)B_N p_n^{N-1}}.$$

This iteration can be repeated until convergence to any degree of precision is obtained: typically it will converge to a precision of $2n$ digits after n iterations.

APPENDIX G

Author's Curriculum Vitae

JAN A. SIKORSKY

930 Rutherford Ln. West Palm Beach, FL 33415
Home Phone: (561) 683-1882
Work Phone: -Na-
sikorsk1@marshall.edu

EDUCATION

- **Ph.D.** in Biomedical Sciences.
Joan C. Edwards School of Medicine
Marshall University
Date of Graduation: **May 2005**
Current G.P.A.: **3.75**
Dissertation Title: Effect of DNA base modification on polymerase chain reaction efficiency and fidelity.
Advisor: Terry W. Fenger, Ph.D.
- **M.S.** in Forensic Science.
Joan C. Edwards School of Medicine
Marshall University
Date of Graduation: May 1999
- **B.S.** in Medical Technology.
Michigan State University
Date of Graduation: August 1996

CONTINUING EDUCATION AND ADVANCED TRAINING

- *Bioinformatics Workshop (09/24/03-09/26/03).* Accelrys Inc.
-Theory and application behind use of bioinformatics to aid in scientific data analysis.
- *Death Investigation: A Training Course (03/20/00-03/21/00).* The Office of the Chief Medical Examiner, the State of West Virginia.
-Leading to certification in the practice of medicolegal death investigation for county coroners in the state of West Virginia (10hrs CME credit).

- *Advanced AmpFeSTR and ABI Prism 310 Genetic Analyzer Workshop*
(03/30/99-04/02/99)
- Theory behind multiplex amplification, capillary electrophoresis and the ABI 310 Genetic Analyzer.
- *AFIP/GMU Forensic DNA Training Course (11/02/98 – 11/12/98)*
-Introduction to and use of mitochondrial DNA sequencing as a tool for human identification; for forensic biologists.

AWARDS AND HONORS

- Member: Mitochondria Research Society (2000-present).
- **Best Graduate Student Presentation, Life Sciences Category (2004)** Sigma Xi Research Day- Marshall University.
- Anagene B. Heiner Memorial
Best Basic Science Poster Presentation Award (2004)
17th Annual Marshall University Research Day.
- Who's Who Among Students in American Universities and Colleges (2000)
- Forensic Science Masters Degree Program Award for **Academic Achievement (1999)**

PEER REVIEWED PUBLICATIONS

- **Sikorsky, J.**, Primerano, D., Fenger, T., and Denvir, J. (2005) Validation of real-time PCR for quantification of UV induced lesions in cellular DNA. (*In preparation*)
- **Sikorsky, J.**, Primerano, D., Fenger, T., and Denvir, J. (2005) DNA Lesions Alter Polymerase Chain Reaction Efficiency and Fidelity. (*In preparation*)
- **Sikorsky, J.**, Primerano, D., Fenger, T., and Denvir, J. (2004) Effect of DNA Damage on PCR Amplification Efficiency with the Relative Threshold Cycle Method. *Biochem. Biophys. Res. Commun.* **323**, 823-830.

- Withrow, A., **Sikorsky, J.**, Downs, J., and Fenger, T. (2003) Extraction and Analysis of Human Nuclear and Mitochondrial DNA from Electron Beam Irradiated Envelopes. *J. Forensic Sci.* **48**, 1302-1308.

PRESENTATIONS

- **Sikorsky, J.** (2005) The Exponential Rise of real-time PCR: Quantifying Nucleic Acid Using the Polymerase Chain Reaction. *Invited Speaker-* Palm Beach County Sheriffs Office Crime Lab: DNA/Serology section.
- **Sikorsky, J.**, Primerano, D., Fenger, T., and Denvir, J. (2004) Oxidative Modification to DNA Template Results in Decreased Amplification Efficiency and Alters Taq Polymerase Fidelity. *17th Annual Research Day and Sigma Xi Research Day 2004-* Joan C. Edwards School of Medicine, Marshall University.
- **Sikorsky, J.**, Primerano, D., Fenger, T., and Denvir, J. (2003) Determination of Amplification Efficiencies for DNA Templates with Oxidative Modification using Real-Time PCR. *16th Annual Research Day and Sigma Xi Research Day 2003-* Joan C. Edwards School of Medicine, Marshall University.
- Dice, A., **Sikorsky, J.**, Howard, K., and Primerano, D. (2002) Effects of Hydrogen Peroxide Treatment on Human Hepatocarcinoma Gene Expression. *WV-BRIN Summer Research Symposium-* Marshall University.
- **Sikorsky, J.** (2002) Mitochondrial DNA: A Designer DNA for the New Millennium. *Invited Speaker-* College of Allied Health Sciences, University of Cincinnati Medical Center.
- **Sikorsky, J.** and Fenger, T. (2001) Characterization of Mitochondrial DNA Heteroplasmy as a Means of Demonstrating the Confirmation of Genetic Mutation Utilizing Capillary Electrophoresis Sequencing Technologies. *14th Annual Research Day-* Marshall University.

ACADEMIC MEETINGS ATTENDED

- *4th Annual DNA Grantees' Workshop (2003)*. National Institute of Justice, U.S. Department of Justice.
- *New DNA Technology Expedition (2003)*. Promega Corporation.
- *Mitochondria 2001*: University of California, San Diego School of Medicine. (28hrs CME credit)
- *DNA Forensics 2000*: Cambridge Healthtech Institute (3 CFE credits).
- *Mitochondria: Interaction of Two Genomes (2000)*. National Institute of Health.

FUNDED GRANT ACTIVITY

- Grant **2001-RC-CX-K002**- Office of Justice Programs, National Institute of Justice (Principle Investigator- Terry W. Fenger, Ph.D.) Responsible for proposals, progress reports, and all subsequent research related to the efficiency and fidelity of Taq DNA polymerase.

TEACHING EXPERIENCE

- *FSC 603: Genetics- DNA Laboratory*.
Developed and team taught the course involving, but not limited to, topics such as basic laboratory skills, laboratory mathematics, amplifying DNA template using the PCR, fluorescent fragment analysis, and DNA sequencing.
- *FSC 604: Genetics and DNA Technologies*.
Lectured on the theory behind DNA sequencing, mtDNA haplotype analysis in Forensics, and the PCR.
- *BMS 670: Molecular Cloning*.
Presented lectures and associated labs involving the theory and basic applications of RT-PCR.

COMMUNITY WORKS AND SERVICES

- *Consultant/Volunteer- Palm Beach County Sheriff's Office Crime Lab: DNA/Serology section (Nov. 2004-present)*. Duties included aiding with validation of real-time PCR on an Applied Biosystems model 7000 sequence detection system for quantification of biological material in forensic casework.
- *Volunteer- Judge at West Virginia State High School Science Fair (2001-2004)*. Duties included critiquing research poster presentations awarding ribbons for outstanding research at the high school level.
- *Volunteer- Clandestine grave excavation unit, Office of the Chief Medical Examiner, state of West Virginia (1999-2000)*. Duties included aiding death investigators in the proper processing of multiple clandestine burials in remote areas of the state.
- *3rd Annual Mock Prison Riot: Moundsville, West Virginia (1999)*. Duties included the presentation of proper forensic investigation techniques to the corrections officer community.
- *West Virginia State CODIS Laboratory (1997-1999)*. Duties included ground work in converting the CODIS laboratory from RFLP to automated STR analysis.

INTERESTS & ACTIVITIES

- Avid fisherman, hiker, camper, white-water kayaker, and golfer.
- Traveled to forty-five out of the fifty states for observational and education purposes.